E-126
12/1/77

Experimental Study of Synchrotron-Čerenkov Radiation

SLAC Proposal E-126

Supplementary Information on Experimental Design

November 1977

Professor T. Erber
Department of Physics
Illinois Institute of Technology
Chicago, Illinois 60616
(312) 567-3382

Table of Contents

Table of Contents
(Continued)

2. Introduction

The conceptual and practical significance of synchrotron-Čerenkov radiation has been discussed in detail in the following papers:

[1] Inner Bremsstrahlung Processes; Acta Physica Austriaca 44, 315-336 (1976); 45, 29-64 (1976); T. Erber, D. White, H. G. Latal.

[2] Classical and Quantum Theory of Synergic Synchrotron-Čerenkov Radiation; Annals of Physics 96, 303-332 (1976); J. Schwinger, W-Y. Tsai, T. Erber.

[3] Experimental Aspects of Synchrotron-Čerenkov Radiation; Annals of Physics 102, 405-447 (1976); T. Erber, D. White, W-Y. Tsai, H. G. Latal.

Since the presentation of Proposal E-126 to the P.A.C. on 31 May 1977 two additional articles have become available:

[4] The Angular Distribution of Synchrotron-Čerenkov Radiation; Journal of Applied Physics (March, 1978; in press); T. M. Rynne, G. B. Baumgartner, T. Erber.

[5] Quantum Modifications in Magnetic Bremsstrahlung; Annals of Physics 108, 408-442 (October 1977); H. G. Latal, T. Erber.

The principal reasons for proposing an experimental study of synchrotron-Čerenkov radiation at SLAC can be summarized as follows [see Proposal E-126 for a full discussion]:

(a) Although the properties of synchrotron-Čerenkov radiation ("SC") have been derived by two independent classical

electrodynamic calculations and two distinct quantum electrodynamic calculations there may be conceptual errors involved in characterizing cooperative electrodynamic interactions in the keV-MeV range in terms of indices of refraction.

(b) The S-C synergism may be an inconsequent approximation instead of merely a first approximation to a still more comprehensive synergism uniting Coulomb bremsstrahlung, synchrotron radiation, and Čerenkov radiation. [A practical example of such an extended synergism is discussed in "Interference Between Transition and Čerenkov Radiation", Phys. Rev. D (in press, 1977); L. L. DeRaad, Jr., W-Y. Tsai, T. Erber.]

(c) All theoretical treatments of SC radiation indicate that in the vicinity of resonances in the index of refraction there should be corresponding resonances of the SC radiation --- in practice these would be manifested as enhancements in the SC spectrum, cf fig. 16; and also as drastic alterations in the angular distribution of the radiation, cf figs. 22, 23 [analogue of "glory" scattering]. These features should be useful in applying SC radiation to study the properties of matter and for the development of high energy "magnetic" Čerenkov counters. However in the x-ray region of the spectrum where the applications seem to be most promising there are large uncertainties in the dispersive and absorptive components of the dielectric functions. A clean measurement of the properties

of SC radiation in the vicinity of an isolated high energy atomic resonance, such as the K-edge of krypton, is absolutely essential for clarifying the experimental picture and a prerequisite for further theoretical studies of SC "resonance" radiation.

We propose to check on points (a) - (c) by carrying out the following specific experiments:

(A) A comparison of ordinary synchrotron radiation and SC radiation in N_2 at STP in the spectral range $4 \lesssim \omega \lesssim 15$ keV for $2 \lesssim H \lesssim 8$ kG and 20 GeV e^-.

(B) Measurement of the SC spectrum in N_2 at STP in the range $4 \lesssim \omega \lesssim 50$ keV for $2 \lesssim H \lesssim 8$ kG and 20 GeV e^-.

(C) Measurement of the SC spectrum in N_2 at various densities: $4 \lesssim \omega \lesssim 13$ keV; $H \simeq 8$ kG; $0 \leqslant \rho/\rho_0 \leqslant 3$ (ρ_0 = STP); and 20 GeV e^-.

(D) Study of the properties of SC radiation in the vicinity of the K-edge of krypton: $\omega \simeq 14.3$ keV; $0.5 \lesssim \rho/\rho_0 \leqslant 1.55$ (ρ_0 = STP); $2 \lesssim H \lesssim 16$ kG; and 20 GeV e^-.

The overall experimental designs for implementing (A) - (D) have already been discussed on pp. 11-26 of Proposal E-126. Further specific experimental details are provided in this " Supplement" [cf letter of 1 June 1977 from A. C. Odian, PAC Secretary]. In particular we have prepared 12 blueprints showing all components of the equipment: the proposed designs and their relation to experiments (A) - (D) are explained in the next Section "Comments on Blueprints". The count rates

for various phases of the experiments have been derived from computer simulations utilizing the SC theory. The anticipated spectra as well as the background estimates are discussed in detail in Section 4 "Specific Experiments".

3. Comments on Blueprints

0. Basic Experimental Configuration:

We propose to demonstrate the existence of SC radiation by utilizing a double scattering set-up: an incident electron beam is deflected by an 18D72 ($2 \lesssim H_1 \lesssim 8$ kG) while traversing scattering cells H and C each of which may be filled with gas (N_2,Kr,etc.). Each of the downstream absorption cells, nos. 1 and 2, may also be filled with gas. By running the experiment with appropriate gas and vacuum combinations in the scattering and absorption cells it is obviously possible to generate three spectra: (i) pure synchrotron radiation, (ii) synchrotron radiation sequentially filtered through a gas; (iii) SC radiation generated by the synergic interaction of the gas and a magnetic field. For instance Experiment (A) is equivalent to checking that spectrum (ii) $\neq$ spectrum (iii) in consonance with the simulations indicated on figs. 7 and 10.

The second 18D72 magnet is provided for two reasons: (1) synchrotron reference spectra can be generated at locations J and F; (2) by running both magnets at field levels satisfying the constraint $H_1 + H_2 \approx 16$ kG the variation in the location of the deflected electron beams can be held to a minimum. As indicated on Block no. 2 this arrangement provides clearance

for the detector electronics and should minimize background.

Block no. 2 of the blueprint also indicates the positions of the γ beams at the detector plane. The overall dimensions of the apparatus (circa 2m × 30m) have been chosen so as to provide adequate clearance between the counters [Si(Li) detectors mounted on Dewars]; and clearance between the "C", "H" spectra and the forward beam halo. Experience indicates that some halo will survive even if there is upstream bending in front of the set-up and shielding. The configuration has been designed to achieve a relative invariance in the detector positioning for signals originating from points C and H and F and J.

1A. Transverse Deflection of Particle Beams:

This figure shows a 12 ft. beam tracing --- approximately 1/8 scale --- of the electron trajectories through the experimental set-up. The deflections are derived from computer simulations which include the Lorentz force but neglect fringing fields and radiation reaction. In this configuration the field intensity in both 18D72 magnets is adjusted to be 8 kG. The fan out of the photon trajectories associated with SC radiation, synchrotron radiation, and Coulomb bremsstrahlung is indicated for a number of representative points A - G. The intrinsic photon beam divergence is determined by the electron beam spread (~200 μrad) and the divergence of synchrotron and SC radiation (~200 μrad). In this set-up (i.e. H_1 = 8 kG = H_2) the synchrotron spectra originating from positions H and J can be measured with Si(Li) detectors no. 1 and no. 2. This will provide a

relative calibration of the geometric factors and intrinsic efficiencies for the two detector channels. Experiments (A) - (D) can then be performed by supplying a gas fill in scattering cells H. Auxiliary calibrations of absorption effects in various gases and in the beryllium windows can be carried out with "target empty" runs utilizing absorption cells no. 1 and no. 2.

1B. Transverse Deflection of Particle Beams:

This figure shows the beam tracings corresponding to the magnetic configuration H_1 = 2 kG and H_2 = 14 kG, cf fig. 10. In this case γ spectra originating from scattering cell C and location F can be measured simultaneously in experiments (A) - (D).

2A and 2B. Photon and Electron Beam Trajectories:

These are enlargements of the beam tracings of figs. 1A and 1B showing the lateral deflections during the first 10 m [measured from point A on magnet no.1] at full scale. Inasmuch as it would be prohibitively expensive to build a vacuum system enclosing all the e^- and γ beams for all magnetic field configurations of interest, e.g. $2 \lesssim H_1 \lesssim 10$ kG, $6 \lesssim H_2 \lesssim 14$ kG; it is necessary to make provision for splitting the γ beams --- which will be observed by Si(Li) detectors nos. 1 and 2 --- and the e^- beams. These full scale tracings are helpful in indicating the optimum location for the beam splitting junctions --- "optimum" in this context means minimizing the obstructions opaque to x-rays between the detector plane and the sources of interest in the scattering cells. In our designs this leads

to a 1" blind spot between points B and C on fig. 2A: the corresponding hardware is shown in detail A of drawing 5B --- the blind spot is located between the junction of the 6" and 8" bellows sections.

3. Floor Plan of Experiment:

This is a 12 ft. overlay --- approximately 1/8 scale --- for figs 1A and 1B indicating the placement of vacuum system components around the electron and photon beams. In all cases (pace "blind spot") a minimum of 1" clearance has been provided between the walls, flanges, etc. and the beams of interest. The e^- beams are enclosed by vacuum because we wish to minimize all sources of background, e.g. soft x-ray albedo from e^- traversing aluminum or steel beam pipes. This feature will also be helpful for absolute calibration of the SC-rates. Note that the beam pipe between scattering cells H and C is off-center with respect to the 18D72's. The bellows section between the two 18D72's and the long vacuum box in the downstream 18D72 are slightly canted.

4A and 4B. Vacuum and Gas Handling System:

The synchrotron-Čerenkov experiment is designed for vacuum operation because (1) it is necessary to eliminate the absorption of soft x-rays by background gases (air) which can counterfeit or obscure the intrinsic quenching of SC radiation; (2) purity of the "target" gases is essential, e.g. the SC spectrum of air will differ from the SC spectrum of nitrogen because of the admixture of argon (K-edge at 3.2 keV); (3) it is desirable to reduce Coulomb bremsstrahlung from the electron beams as

much as possible --- of course some Coulomb background from scattering cells C and H is unavoidable in experiments where they are filled with gas; cf the estimates given in Section 4, Table 3.

Figs. 4A and 4B are essentially self-explanatory. Sufficient pumping capacity has been provided to evacuate the system on a time scale of hours rather than days. Pressure sensors have been arranged to give prompt indication of any leaks in the beryllium window inserts. Automatic pressure regulation for the gas filled portions has been provided.

5A. Mechanical Layout (0-9m):

Figs. 5A - C show a detailed mechanical layout of the beam enclosure indicated on overlay 3. The designs have been developed in concert with prospective vendors in order to minimize the number of custom made items. The construction is simple and modular --- the entire system can be disassembled in a matter of days. Flexibility has been provided in a literal sense with a number of bellows sections: this feature will be useful for rapid repositioning of the Si(Li) detectors, e.g. the upward tilt of γ line no. 1 when the nickel mirror is installed. In the present design the beryllium window between scattering cells H and C is relatively inaccessible; this defect could be eliminated by substituting two 18D36 magnets for the upstream 18D72 magnet.

5B. Mechanical Layout (9-19m):

This portion of the vacuum system contains the two "Y" sections corresponding to the splitting away of γ line no. 1

and the electron beam. Although these Y sections are not stock items, the fabrication methods indicated on details A - C are standard with several vendors.

5C. Mechanical Layout (19-30m):

This portion of the vacuum system contains the absorption cells and Si(Li) detectors. In order to avoid contamination of the Si(Li) elements the detector heads are usually fabricated with non-removable beryllium windows ($\gtrsim 25\,\mu$ thick). The interposition of additional beryllium windows can be minimized by combining the detector heads and absorption cells in integral units as shown on the detail inserts. The rest of the vacuum system can be assembled from stock components.

6. Block Diagram of Electronics:

The ADC and counting logic for these experiments has been designed to meet the following criteria: (i) Basically the shapes of two different kinds of x-ray spectra are to be determined: (a) the lower cut-off type shown on figs. 7 and 10, where the range $3 \lesssim \omega \lesssim 50$ keV is of principal interest, and energy resolutions of the order of 0.5 keV are adequate; and (b) a sharply peaked type of spectrum, of the kind expected for the krypton experiments, where a resolution of 0.3 keV for $\omega \sim 14.3$ keV is desirable, cf figs. 17 - 21. [Eventually the krypton experiments could be repeated with $\sim$ eV resolution x-ray monochromators of the kind under development at SSRP.] By appropriate choice of beam intensity, collimation, and counter acceptance the system can be tuned so that on the average one SC or synchrotron photon is incident on each of

the Si(Li) detectors during a 1.6 μsec beam pulse from the accelerator [see the discussion in Section 4 (A,B)]. We will nominally run until ~10^3 counts/0.5 keV channel ($\omega \gtrsim 10$ keV) have been accumulated. Energy calibration with an overall accuracy of $\lesssim 5\%$ can be provided with radioactive fiducial sources.

(ii) The signal patterns occurring during the operation of the experiment will be affected by statistics and background. Specifically: (a) The randomization introduced by Poisson statistics implies that in about 25% of the cases two SC or synchrotron "signal" photons will be incident on a Si(Li) within the 1.6 μsec time window. (b) Coulomb bremsstrahlung from the gas fill in a scattering cell is an intrinsic contaminant of the SC signals. It is evident from figs. 7 and 10, as well as the numerical estimates given in Table 3 of Section 4(A,B) that this contamination is usually of negligible significance. However if we wish to pin-point the cross-over between SC radiation and the Coulomb bremsstrahlung background --- especially to settle the important problem of the Ter-Mikaelian quenching --- then double or multiple photon signals may appear in the 1.6 μsec time window. (c) High energy radiation (electrons, muons, Coulomb bremsstrahlung, etc.) ranging up to ~25 GeV may be incident on the Si(Li) detectors during the 1.6 μsec accelerator pulse without the appearance of a 2-60 keV SC or synchrotron photon; i.e. ~30% of the time there will be no "signal" photon due to Poisson randomization. (d) Natural background in the $1 \lesssim \omega \lesssim 100$ keV range is roughly 0.2 counts per second as measured with a standard unshielded Si(Li) system

[G. Walford, ORTEC, private comm.]. Higher background rates have to be allowed for in a "hot" environment such as the SLAC experimental area.

The spectra of interest can be identified by minimizing the distortions caused by (a) - (d). In particular by gating the MCA logic in coincidence with the 1.6 μsec accelerator beam pulses background effects such as (d) can be reduced. Furthermore within the 1.6 μsec windows the output of the Si(Li)'s will be monitored by pile-up inspect/reject circuits with ~20 nsec resolution: most multiple pulses due to effects (a), (b) and (d) can therefore be blocked from the ADC. High energy background (c) does not have an unambiguous signature in solid state detectors [Landau tail]; however by running the Si(Li)'s in fast coincidence with the shower counters --- and the accelerator gate pulses --- spurious low energy signals due to high energy background can also be eliminated.

4. Specific Experiments

(A) Comparison of Synchrotron Radiation and Synchrotron-Čerenkov Radiation in Nitrogen:

(B) The Synchrotron-Čerenkov Spectrum in Nitrogen:

As indicated in Proposal E-126, Section 4(A) the existence of synchrotron-Čerenkov radiation can be demonstrated by differential comparisons which are essentially insensitive to absolute beam intensities, counter efficiencies, and geometrical effects. After alignment and checkout of the set-up [figs. 0-6] the existence of the effect could be established in three steps:

(1) Set the fields in both 18D72's at 8 kG; run the entire system without gas fill; record the synchrotron spectra originating from source points H and F, cf the synchrotron^{1,2} curve on fig. 7. This step yields a relative calibration of the two Si(Li) detector channels.

(2) Record the synchrotron spectra including nitrogen absorption by alternately filling absorption cells 1 and 2: this procedure yields the synchrotron^{1,2,3} curve on fig. 7. Since the ratio of the synchrotron to the filtered synchrotron spectrum is completely determined by the known x-ray transmissivity of N_2, this step is useful as a check on detection efficiency.

(3) Fill scattering cell H with N_2 and evacuate absorption cell no. 1 --- record the corresponding SC^{1,2,3} spectrum on Si(Li) no.1. Compare with the synchrotron^{1,2,3} spectrum [i.e. synchrotron radiation originating from point F filtered through absorption cell no. 2 filled with N_2] simultaneously recorded by Si(Li) no. 2. As is obvious from fig. 7 the ratio of the synchrotron^{1,2,3} to SC^{1,2,3} intensity for $\omega \sim 6$ keV should be a factor of ~15.

Clearly this procedure tests the essential synergic character of the radiation process: synchrotron radiation sequentially filtered through nitrogen yields a spectrum substantially different from synchrotron-Čerenkov radiation emitted in the nitrogen ambient! The relative calibration of the SC spectrum in terms of the synchrotron spectrum is simplified by the fact that for $\omega \gtrsim 45$ keV the two spectra essentially

coincide, cf fig. 7. It is also apparent from Table 1 that an absolute calibration is feasible: specifically if the primary beam were decreased to $\sim 10^2$ e^-/pulse, the electrons could be registered individually by the beam monitor ($\lesssim$ 15 nsec resolution); the corresponding synchrotron intensity would then be $\sim 1/5$ photons per pulse per Si(Li) channel. A one hour run at 120 pps should yield $\sim 10^5$ counts, and this is statistically adequate for a good ($\lesssim$ 5%) absolute determination of the efficiencies, cf eqs (4.2) - (4.8).

Additional information concerning the variation of the SC and synchrotron spectra is given on figs. 8 and 9. Since the low end of the SC spectrum has an extremely sensitive dependence on the magnetic field strength, it would be of great interest to measure SC radiation with the H_1 = 2 kG, H_2 = 14 kG configuration shown on figs. 1B and 2B. Results of detailed calculations of the anticipated spectra for this case are given on fig. 10.

The Si(Li) detector - ADC chain [fig. 6] requires ~30 μsec to process an individual photon signal in order to yield an 0.5 keV energy resolution in the spectral range of interest. This implies that the entire experiment should be tuned so that on the average one SC or synchrotron photon is incident on each of the Si(Li) detectors during a 1.6 μsec beam pulse from the accelerator. Since there is a direct relationship between e^-/pulse and counts/pulse, it is easy to estimate the nominal beam intensities appropriate for various phases of the experiment. As indicated in eq (4.9a) of Proposal E-126 the total photon counts per beam pulse are given by

$$M = \int d\omega\, \Delta N^*(\omega)[a \times b \times c \times d \times e \times f \times g], \tag{4.1}$$

where $\Delta N^*(\omega)$ denotes the theoretical SC or synchrotron radiation rate, and the alphabetical chain corresponds to the following factors:

$$a = \frac{\text{photon energy interval}}{\text{MCA - channel}} \simeq 0.5 \text{ keV/channel}; \tag{4.2}$$

$$b = \frac{\text{electronics pile-up rejection}}{\text{live time correction}} \sim 1 \quad (1 \text{ count per beam pulse}); \tag{4.3}$$

$$c = \text{Si(Li) detector efficiency [ORTEC data for Si(Li) type 7000; cf fig. 10 of E-126]}; \tag{4.4}$$

$$d = \text{Si(Li) detector geometrical efficiency} \sim \frac{\text{effective area of beam viewed by detector}}{\text{total area of beam}} \begin{cases} \sim 0.165 \text{ at H [fig.0,block 2];} \\ \sim 0.167 \text{ at C [fig.0,block 2].} \end{cases} \tag{4.5}$$

The geometrical assumptions are: electron beam diameter ~1 mm;

electron beam divergence ~200 μrad (half width);

photon beam divergence ~100 μrad (half width); see figs. 11, 12;

total photon beam divergence ~600 μrad (full width);

Si(Li) detector area ~12.5 mm^2.

$$e = \text{effective length of electron trajectory for synchrotron radiation [columns 3 and 4 of Table 1]}; \tag{4.6}$$

$$f = \text{electrons per pulse [columns 7 - 10 of Table 1]}; \tag{4.7}$$

g = optional factor for nitrogen absorption.

Imposing the constraint $M \sim 1$, leads to the results summarized in Table 1. It is apparent that all of these experiments can be done with about 5000 e^-/pulse in the beam line: the intensity can then be diminished with upstream bending and collimation.

The total number of pulses required for each experiment can be estimated on the basis of statistical criteria. Specifically in the $H_1 = H_2 = 8$ kG configuration [fig. 7] the disparity between synchrotron and SC radiation for $\omega \sim 6$ keV is a factor of 15. For "good" statistics we require a minimum of 200 counts in the SC spectral bin 6 - 7 keV; the corresponding synchrotron[1,2,3] spectrum would then have 3000 counts in the 6 - 7 keV bin. Clearly requiring 200 counts/channel in the spectral region where the intensity is <u>least</u> imposes the most severe restrictions on the <u>lower</u> limits for the total number of beam pulses. These worst-case estimates are summarized in Table 2. Evidently the most favored configuration is $H_1 = H_2 = 8$ kG [fig. 7]; in this case the essential "proof" of the existence of SC quenching could be obtained with 15 minutes of counting at 20 pps and 2×10^3 e^-/pulse. The $H_1 = 2$ kG, $H_2 = 14$ kG experiment is obviously somewhat more demanding in beam time but the physics yield is significantly greater: as indicated on fig. 10 the synchrotron[1,2,3]/SC[1,2,3] intensity ratio is amplified to $\sim 10^2$ for $\omega \sim 9$ keV, and the <u>non-existence</u> of a "knee" in the spectrum at this point is correlated with the Ter-Mikaelian form of the Coulomb bremsstrahlung spectrum.

Table 1. Electrons per pulse required for various phases of the synchrotron-Čerenkov experiment: E = 21.5 GeV.

Magnet field (kG)	Radius of curvature (m)	Effective length of e^- trajectory as seen by Si(Li) detectors (30m)		Synchrotron[1] photon counts per e^- per cm $1\ keV \leqslant \omega \leqslant 1\ MeV$	Synchrotron Čerenkov[1][2] photon counts per e^- per cm $1\ keV \leqslant \omega \leqslant 1\ MeV$	e^-/pulse for M ~ 1; eq.(4.1)			
		source point H(0.5m) (cm)	source point C(1.5m) (cm)			synchrotron H	synchrotron C	synchrotron-Čerenkov H	synchrotron-Čerenkov C
2	358.6	2.37	2.45	5.81×10^{-3}	5.23×10^{-4}	440	420	4889	4673
4	179.3	1.19	1.23	1.06×10^{-2}	2.05×10^{-3}	480	459	2484	2374
8	89.6	.59	.61	1.82×10^{-2}	5.56×10^{-3}	564	539	1847	1765

(1) Includes Si(Li) detector efficiency, (4.4), and geometrical factors (4.5).

(2) Includes absorption in 50 cm of nitrogen at STP.

Table 2. Number of beam pulses required to accumulate 200 counts in various MCA channels. Poisson statistics, Si(Li) efficiency and N_2 absorption included; E = 21.5 GeV.

Field (kG)	Channel (keV)	$\frac{\text{SC photons in channel}}{\text{Total number of SC photons in spectrum}}$ (1)	beam pulses required to accumulate 200 counts in channel (2)
2	9 - 10	1.26×10^{-3}	4.77×10^{5}
2	10 - 11	2.90×10^{-3}	2.07×10^{5}
4	6 - 7	4.15×10^{-4}	1.45×10^{6}
4	7 - 8	1.66×10^{-3}	3.61×10^{5}
8	5 - 6	1.70×10^{-3}	3.53×10^{5}
8	6 - 7	3.30×10^{-3}	1.82×10^{5}

(1) Total spectrum corresponds to range 1 keV $\lesssim \omega \lesssim$ 1 MeV (fig. 8).

(2) 20 pulses/sec $\times$ 10 hrs. of running $\sim 7.2 \times 10^{5}$ pulses.

Typical runs for these experiments would average 6 hours at 20 pps or 1 hour at 120 pps.

The background problems which may affect the interpretation of the experimental results have already been discussed in connection with the detector and signal processing layout [Section 3, comments on blueprint 6]. At present there is insufficient data on the natural γ background in the $1 \lesssim \omega \lesssim 100$ keV range that may be expected in a radioactively "hot" environment such as the SLAC experimental area. Accordingly we plan a background survey with unshielded as well as shielded (Heavimet) Si(Li) detectors before proceeding with the main SC experiments. The proposed electronics layout for the SC experiments can easily cope with background rates of 10^3 counts/sec --- this corresponds to a 10^4 fold increase over a normal "cold" environment, and still leaves an additional $\gtrsim 10^2$ safety factor for counter shielding.

The principal residual signal contamination is due to Coulomb bremsstrahlung [Section 3, blueprint 6 § (ii-b)]. Although it is overwhelmingly probable that our experiments will confirm that the appropriate description of coherent Coulomb bremsstrahlung is given by the Ter-Mikaelian spectrum, we consider it prudent to estimate this background on a "worst-case" basis with the Bethe-Heitler spectrum. One can then easily show that the number of Coulomb bremsstrahlung photons in the energy band 1 (keV) $\leqslant \omega \leqslant \omega_u$ (keV), radiated per cm per e^- in N_2 at STP is given by

$$\Delta N_0^{CB}(\omega_u) \cong 3.73 \times 10^{-5}\, \ell n[\omega_u(\text{keV})]. \qquad (4.9)$$

In order to correlate this estimate with the expected SC count rates, cf (4.1), it is useful to fold in the Si(Li) detector efficiency and allow for the effects of absorption in the beryllium windows (~ 5 mil). The "raw" signal estimate (4.9) can then be sharpened to

$$\Delta N_1^{CB}(\omega_u) \cong 3.73 \times 10^{-5} \int_1^{\omega_u} \frac{d\omega}{\omega}\, \epsilon(\omega), \qquad (4.10)$$

where ϵ represents the Be absorption and Si(Li) efficiency: In the energy range $\omega \lesssim 100$ keV we have used the manufacturer's data for the conversion efficiency of the solid state detectors [cf fig. 10 of E-126]; for $\omega > 100$ keV, we have estimated $\epsilon(\omega)$ on the basis of the data given by Storm and Israel [Nuclear Data Tables A7, 565-681 (1970)].

Finally it is useful to include the absorptive effects of the nitrogen. If $\tau_N(\omega)$ denotes the transmissivity of 50 cm of N_2, then the Si(Li) count rate in the energy band $1\ (\text{keV}) \leqslant \omega \leqslant \omega_u\ (\text{keV})$ per cm per e^- including detector efficiency and N_2 absorption is

$$\Delta N_2^{CB}(\omega_u) \cong 3.73 \times 10^{-5} \int_1^{\omega_u} \frac{d\omega}{\omega}\, \epsilon(\omega)\tau_N(\omega). \qquad (4.11)$$

The count rates (4.10) and (4.11) can then be evaluated by numerical integration. The results are summarized in Table 3.

Table 3. Cumulative Coulomb bremsstrahlung background rates.

ω_u (keV)	ΔN_0^{CB} (4.9)	ΔN_1^{CB} (4.10)	ΔN_2^{CB} (4.11)
10	8.6×10^{-5}	-	1.18×10^{-5}
10^2	1.72×10^{-5}	-	6.03×10^{-5}
10^3	2.58×10^{-5}	-	6.57×10^{-5}
10^4	3.44×10^{-4}	-	6.92×10^{-5}
10^5	4.30×10^{-4}	1.07×10^{-4}	7.07×10^{-5}
10^6(a)	5.16×10^{-4}	$< 1.16 \times 10^{-4}$	$< 7.93 \times 10^{-5}$
10^7	6.02×10^{-4}	$< 1.24 \times 10^{-4}$	$< 8.97 \times 10^{-5}$
2.15×10^7	6.31×10^{-4}	$< 1.27 \times 10^{-4}$	$< 9.08 \times 10^{-5}$

(a) In the energy range 100 MeV $< \omega <$ 2.15 GeV the Storm and Israel data are extrapolated by assuming ϵ [Si(Li)] $<$ 10%.

The entries in Table 3 are directly comparable to the total synchrotron-Čerenkov radiation rates given in column 6 of Table 1. In fact it is convenient to combine the two sets of data into two "signal/noise" ratios which indicate the (in)significance of the Coulomb bremsstrahlung background, cf Table 4. It should be possible to check the ratios given in column 3 of Table 4 by comparing the Si(Li) and shower counter rates. In any case it is clear that Coulomb bremsstrahlung background --- even allowing for the long high energy tail --- should not impair the measurement of SC radiation.

Table 4. Signal to noise estimates for SC radiation and Coulomb bremsstrahlung background.(a)

Signal / Noise — H (kG)	SC radiation ($1\ keV \leqslant \omega \leqslant 1\ MeV$) / Coulomb bremsstrahlung ($1\ keV \leqslant \omega \leqslant 1\ Mev$)	SC radiation ($1\ keV \leqslant \omega \leqslant 1\ MeV$) / Coulomb bremsstrahlung ($1\ MeV \leqslant \omega \leqslant 21.5\ GeV$)
2	8	~ 17
4	30	~ 70
8	85	~ 185

(a) Ratios computed with ΔN_2^{CB}; column 4 of Table 3.

(C) Variation of the Synchrotron-Čerenkov Spectrum as a Function of Nitrogen Density:

One of the basic features of SC radiation is its sensitive dependence on the environment. As pointed out in Proposal E-126, Section 4(C) one of the principal environmental parameters that can be conveniently controlled is the density. It appears in first approximation that the total emission due to Coulomb bremsstrahlung (Bethe-Heitler spectrum) and SC radiation can exhibit a minimum in certain spectral regions as the density of the gas is increased. This phenomenon is illustrated on fig. 13. In practice it will of course be most convenient to check on the existence of this effect by a series of differential comparisons --- beam intensity variations and counter efficiencies can then be essentially eliminated by relative normalizations. Specifically we will first evacuate the entire system; set the fields in both 18D72 magnets at 8 kG; and measure the synchrotron radiation originating from points H and J with Si(Li) counters

no. 1 and no. 2; cf figs. 0 and 7. Next we will slowly run up the N_2 density in absorption cell no. 2 --- recording the "absorption" curves shown on fig. 14 at several intermediate points. Finally, we will evacuate the entire system and then slowly fill scattering cell H as well as absorption cell no. 2 with N_2, being careful to run up the densities in tandem: With this arrangement Si(Li) no. 1 should record the SC + Coulomb bremsstrahlung (B.H.) spectra indicated on fig. 15, while the other detector channel, Si(Li) no. 2, retraces the corresponding curves on fig. 14. If sufficient beam time were made available at reduced intensities of the order of 200 e^-/pulse, absolute calibrations could be carried out [compare § A,B above]. In case the Coulomb bremsstrahlung follows the Ter-Mikaelian rather than the Bethe-Heitler curve (fig. 7), the divergence between the spectra shown of figs. 14 and 15 would be even more pronounced.

(D) Synchrotron-Čerenkov Radiation in the Vicinity of the K-edge of Krypton:

It has already been pointed out in the papers describing the properties of synchrotron-Čerenkov radiation [cf Section 2] that striking enhancements should occur in spectral regions where the index of refraction exhibits resonances. A rigorous treatment of "resonance" SC radiation, valid in the immediate vicinity of a resonance as well as within the resonance line itself, would require an extension of the theory which takes into account absorptive as well as dispersive effects in the dielectric function. However for purposes of numerical

orientation in designing experiments it should still be possible to utilize the existing SC theory if we excise a spectral region $\Delta\omega_K >> \Gamma_i$ centered on the resonance, where Γ_i denotes the width of the resonance, because the absorptive component of the complex index of refraction should then remain small in comparison with the dispersive part. In the x-ray region of the spectrum we anticipate this type of behavior in the vicinity of an isolated atomic resonance --- in particular just below the K-edge of a noble gas.

A survey of likely candidates has indicated that krypton is an optimum choice because the location of its K-edge approximates the ideal of an isolated resonance, and the associated SC resonance radiation can be generated and detected with the same experimental set-up that we propose to use for the nitrogen measurements; cf §§ (A) - (C) above. The relevant x-ray data for krypton including the location of the resonances (ω_i), the nominal widths (Γ_i), and oscillator strengths (g_i) are given in Table 5. Clearly there is a ~12 keV separation

Table 5. X-ray spectral parameters of krypton.

Shell	ω_i (eV)	Γ_i (eV)	g_i [b]
K_α	14325 [a]	3.1	1.26
L_I	1921	8.5	1.32
L_{II}	1727	1.45	1.64
L_{III}	1674	1.15	3.27

(a) The K-shell binding energy is 17.9 keV/electron.

(b) D.T. Cromer, Acta Cryst. 18, 17 (1965).

between the K-edge and the nearest L-resonance. From general dispersion arguments (Kramers-Kronig relations for the coherent Compton amplitude) we expect that in the spectral region $8 \lesssim \omega \lesssim 14$ keV the index of refraction is given by the simple asymptotic form (cf Section 2, reference [3])

$$2\Delta n(\omega) = - (\omega_p/\omega)^2, \tag{4.12a}$$

where ω_p corresponds to an effective plasma frequency

$$\hbar\omega_p = [(4\pi\alpha N_0 \lambda\!\!\!^{-}_c{}^3)(\rho[Z - g_K]/A)]^{1/2}\, mc^2 \tag{4.12b}$$

excluding the g_K oscillators associated with the K-edge, cf column 4 of Table 5. The SC radiation intensity then is linked to ω_p by a relativistic "boost", i.e.

$$\omega_0 \equiv (E/mc^2)\omega_p, \tag{4.13a}$$

which defines a characteristic "material" energy. For SLAC energies and krypton at densities $1.55\ \rho_0$ --- where ρ_0 denotes STP --- we find

$$\omega_0 \sim 70 \text{ keV} >> \omega_K \sim 14.3 \text{ keV}. \tag{4.13b}$$

Finally we note that the characteristic "magnetic" energy is given by

$$\omega_c(\text{keV}) = 6.65 \times 10^{-2}\, E^2(\text{GeV})\, H(\text{kG}); \tag{4.14a}$$

or under SLAC conditions

$$\omega_c(\text{keV}) \sim 30\, H(\text{kG}). \tag{4.14b}$$

Since it is well known that SC radiation becomes exponentially sensitive to variations in ω when $\omega_c \sim \omega_0$ and $\omega << \omega_0$,

the combination of 21.5 GeV electrons, gaseous krypton, and magnetic fields in the range $H \gtrsim 2$ kG, should favor the experimental detection of the SC intensity peak associated with the K-edge at 14.3 keV.

The total photoeffect cross-section in krypton is approximately 2470 barns just below the K-edge, and 18,600 barns just above the K-edge. Assuming a density of 4.18×10^{19} atoms/cm^3 ($\sim 1.5\ \rho_0$) the corresponding photon attenuation coefficients then are 0.12 cm^{-1} and 0.78 cm^{-1} respectively. In order to avoid appreciable attenuation of the SC signals in the vicinity of the K-edge we are therefore constrained to limit the lengths of the absorptive columns to a few centimeters --- in practice this means that Si(Li)'s no. 1 and no. 2 will be positioned to record the SC radiation emitted in the vicinity of the end windows of scattering cells H and C.

It is important to note that these attenuation length constraints do not clash with two additional length criteria which affect the net SC radiation rates: One of these is associated with the effective radiative path length as seen by the detectors --- the data given in column 4 of Table 6 indicate that these distances are $\lesssim 2.4$ cm and therefore do not cause any problems with absorption. The other characteristic length in the problem is the coherence length for the emission of an SC photon. This parameter plays a role analogous to the formation length in transition radiation and can be computed by similar methods. In first approximation we find

$$\ell_{coh} \simeq \lambda\!\!\!^{-}_{c} \frac{2mc^2}{\hbar\omega} \left[\left(\frac{mc^2}{E}\right)^2 - 2\Delta n(\omega) \right]^{-1}; \qquad (4.15)$$

and this implies that for the krypton experiments $\ell_{coh} \sim 0.2$ cm; this estimate is also consistent with the attenuation length constraints.

We have indicated previously that the published SC radiation formulas should be valid in the spectral regions

$$\omega_{L_I} << \omega \lesssim \omega_K - \Delta\omega_K;\ \omega_K + \Delta\omega_K \lesssim \omega: \qquad (4.16)$$

$$15 \text{ eV} \sim \Delta\omega_K > \Gamma_i \sim 3.1 \text{ eV}.$$

Since the Si(Li) detector resolution is $\gtrsim$ 300 eV, the excision of a 30 eV window centered on a 3 eV wide resonance is an excellent approximation in an experimental sense. A detailed estimate of the SC radiation expected in the vicinity of the krypton K-edge can then be made with the help of standard models for the index variations in the neighborhood of a resonance e.g. R. Glocker and K. Schäfer, Zeit. für Physik 73, 289 (1931): In this case it is assumed that the absorption edge can be represented by transitions from the K-shell to a set of continuum oscillators where the density of oscillators varies as ω^{-3} above the K-edge and vanishes below --- this ansatz leads to an ω^{-3} absorption law which is in good agreement with the observations for krypton above the K-edge. From a standard dispersion argument one can then obtain the corresponding index variation:

$$\Delta n(\omega) = 2\pi\alpha(g_K N \lambda_c^3)\left[\frac{mc^2}{\hbar\omega_K}\right]^2\left[\rho^2(\rho^2+r^2)\right]^{-1} \times$$

$$\times\left\{\tfrac{1}{2}(r^2-\rho^2)\ln\left[1+(r^2-2)\rho^2+\rho^4\right]-\rho^2(\rho^2+r^2)\right.$$

$$\left.+2r\rho\left[\frac{\pi}{2}-\tan^{-1}\left(\frac{1-\rho^2}{\rho r}\right)\right]\right\}, \qquad (4.17)$$

where, cf Table 5

$$r = \Gamma_K/\omega_K, \quad \rho = \omega/\omega_K.$$

The explicit radiation rates can then be computed by inserting this expression in the standard SC formulas. In order to allow some latitude for uncertainties in interpreting the experimental data currently available we have calculated the rates for $g_K = 1.26$ (Cromer) as well as $g_K = 2.00$. A synoptic view of the spectrum is shown of fig. 16. The spectacular variation of SC resonance radiation with magnetic field strength is indicated by the curves on figs. 17 and 18 which show the pertinent details in the vicinity of the K-edge. Finally figs. 19 - 21 display count-rate histograms which include the 0.3 keV Si(Li) resolution.

Unfortunately present experimental information is not adequate to determine precisely the superposition of the "background" term (4.12a) and the "resonance" term (4.17). An inventory of intensity and angular distributions (figs. 22 and 23) is therefore necessary to allow for reasonable contingencies in the nature of the experimental data. Most of this information

is summarized in Table 6. It is obvious from the entries in columns 5 and 7 that these experiments are feasible but basically inelegant since too much data is accumulated relative to the region of interest. For this reason we propose to improve the basic SC set-up with a spectral filtration device.

One practical means for accomplishing this spectral filtering is to use a flat nickel mirror near grazing incidence --- this technique is currently under development for x-ray astronomy applications. For example with a grazing angle of 4 mrad the upper cutoff frequency is about 15.0 keV. Fig. 24 is a counterpart to fig. 16 showing the enormous gains possible with the nickel cutoff: In particular with the great relative enhancement of the K-edge region of the spectrum, the number of beam pulses necessary to obtain good statistics in the 14.3 keV window is significantly reduced. Columns 8 and 9 of Table 6 show a number of representative cases: obviously experiments with good statistics can be done on time scales of the order of 1 - 2 hours with as few as 20 pps.

Finally we note that there is another bonus implicit in the use of an x-ray mirror since one can then automatically get rid of all photons with $\omega \gtrsim 15$ keV --- this voids the entire high energy Coulomb bremsstrahlung background (Table 3) as well as any other parasitic halo that has managed to follow the 18D72 beam deflections.

Table 6. Characteristics of SC resonance radiation in krypton: E = 21.5 GeV, $N \simeq 4.185 \times 10^{19}$ atoms/cm^3, $\omega \simeq 14.3$ keV.

H(kG)	(a) g_K	(b) I	(c) L(cm)	(d) $\frac{e^-}{\text{beam pulse}}$	(e) R	(f) beam pulses	(g) $\frac{e^-}{\text{beam pulse}}$	(h) beam pulses
2	1.26	3.28×10^{-5}	2.37	7.8×10^{4}	1.2×10^{-6}	5.0×10^{8}	7.6×10^{7}	5.0×10^{5}
2	2.00	3.24×10^{-5}	2.37	7.9×10^{4}	2.5×10^{-5}	2.4×10^{7}	-	-
4	1.26	3.05×10^{-4}	1.19	1.7×10^{4}	2.1×10^{-5}	2.9×10^{6}	4.6×10^{6}	1.1×10^{4}
4	2.00	3.03×10^{-4}	1.19	1.7×10^{4}	7.8×10^{-4}	7.7×10^{5}	-	-
8	1.26	1.50×10^{-3}	0.59	6.8×10^{3}	2.4×10^{-3}	2.5×10^{5}	3.1×10^{5}	5.6×10^{3}
8	2.00	1.50×10^{-3}	0.59	6.8×10^{3}	4.4×10^{-3}	1.4×10^{5}	-	-

(a) Oscillator strength for K-edge of krypton.

(b) Number of photons per e^- per cm with Si(Li) efficiency included; SC radiation integrated over energy band 1 keV $\leqslant \omega \leqslant$ 1 Mev.

(c) Effective path length seen by detectors viewing scattering cell H.

(d) Beam intensity computed from requirement of one SC photon per beam pulse, cf cols. 7-10 of Table 1.

(e) R = photons in SC peak (0.3 keV bin)/total number of photons in 1 keV - 1 MeV band.

(f) Number of beam pulses required to accumulate 200 counts in the SC peak (0.3 keV bin).

(g) Same as column 5 but includes nickel mirror system.

(h) Same as column 7 but includes nickel mirror system.

5. Beam Characteristics and Beam Time Requirements

As indicated in Proposal E-126 the synchrotron-Čerenkov experiment could be carried out at 12, 20 or 25 GeV; in the present "Supplement" we have assumed a nominal electron energy of 21.5 GeV for most of the design estimates. For experiments (A) - (C) beam currents of the order of 5×10^3 e^-/pulse would be adequate. The krypton resonance measurements (D) could most efficiently be performed at higher current levels, e.g. 10^5 e^-/pulse (Table 6). The ideal geometrical beam properties are similar to those established for E-97 --- this experiment was also carried out in beam line 19: angular divergence ~200 μrad half width, beam diameter circa 1 mm at point A on fig. 0. Since the SC experiment utilizes solid state detectors and "static" gas targets the beam pulse repetition rate is not critical --- the experiment can be run at 20 pps or at higher rates.

A generous estimate for the total number of pulses required for check out and test is 5×10^5. Experiments (A) - (B) could then be run with $\lesssim 10^6$ pulses (Table 2). A similar estimate applies to the variable density experiment (C). Column 9 of Table 6 indicates about $\lesssim 5 \times 10^5$ pulses for the krypton measurements --- on the other hand there is a trade-off with beam intensity (column 8) and 1.5×10^6 total beam pulses would be a more conservative estimate.

6. Summary of Arrangements with Host Laboratory

The principal points have been covered in E-126. The only significant modification is that we consider it advisable to carry out a preliminary experiment to measure the 1 - 100 keV photon background in the SLAC experimental area with a single Si(Li) detector assembly approximating part of the electronics layout on fig. 6. Before the krypton experiments are done, the nickel mirror technique should also be tested for spectral distortions in the 14.3 keV region --- these preliminary checks can be carried out at IIT.

7. Figures

Fig. 0-6 Blueprints - submitted separately.

Fig. 7 Characteristics of synchrotron-Čerenkov radiation by electrons in nitrogen at STP and a magnetic field of 8 kG. The spectra of synchrotron radiation (with and without N_2 absorption), and Coulomb bremsstrahlung (Bethe-Heitler and Ter-Mikaelian) are also indicated.

Fig. 8 Characteristics of synchrotron-Čerenkov radiation by electrons in nitrogen at STP for varying magnetic field strengths, $2 \leqslant H \leqslant 16$ kG.

Fig. 9 Synoptic view of the SC and synchrotron spectrum for 8 kG in the range 1 - 400 keV; the Coulomb bremstrahlung background is also indicated.

Fig. 10 Characteristics of SC radiation by electrons in nitrogen at STP and 2 kG.

Fig. 11 Comparison of the angular distribution of synchrotron and SC radiation.

Fig. 12 Variation of SC angular distribution with photon energy.

Fig. 13 Variation of SC radiation with density of N_2. The effect of Coulomb bremsstrahlung has been included.

Fig. 14 Synchrotron radiation sequentially absorbed by N_2 at varying densities.

Fig. 15 SC radiation + Coulomb bremsstrahlung (Bethe-Heitler) - self-absorption in N_2 at varying densities.

Fig. 16 Synoptic view of the krypton resonance SC spectrum.

Fig. 17 Details of the SC resonance spectrum at varying field intensities, $g_K = 1.26$.

Fig. 18 Details of the SC resonance spectrum at varying field intensities, $g_K = 2.00$.

Fig. 19 Histogram of the SC resonance spectrum with 0.3 keV bins, $g_K = 1.26$, H = 8 kG.

Fig. 20 Histogram of the SC resonance spectrum with 0.3 keV bins, $g_K = 1.26$, H = 2 kG.

Fig. 21 Histogram of the SC resonance spectrum with 0.3 keV bins, $g_K = 2.52$, H = 2 kG.

Fig. 22 Angular distribution of SC radiation $-8 \times 10^{-9} \leqslant \Delta n \leqslant 0$.

Fig. 23 Angular distribution of SC radiation $0 \leqslant \Delta n \leqslant 8 \times 10^{-9}$.

Fig. 24 SC resonance spectrum for krypton modified by grazing incidence mirror.

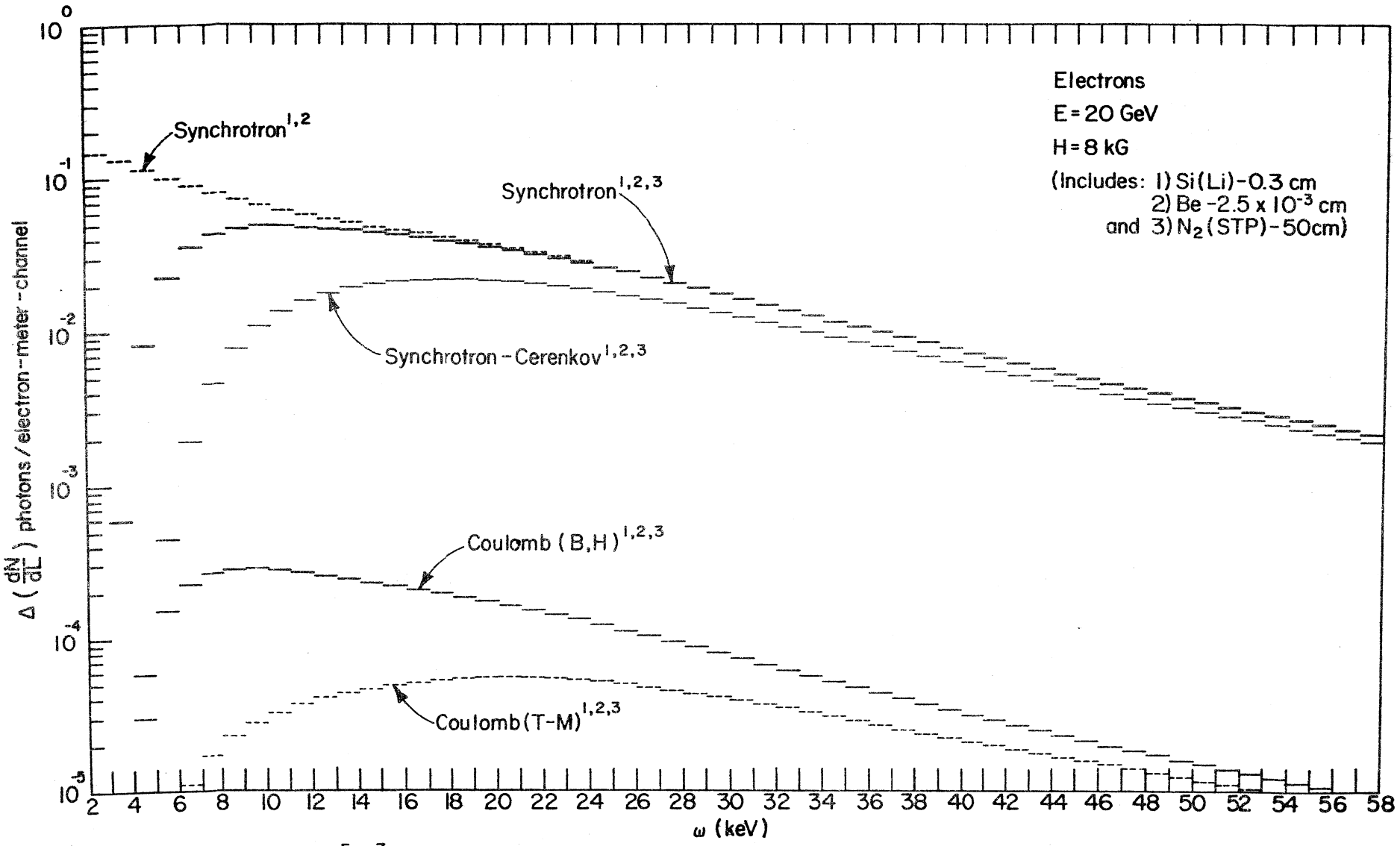
Electrons
E = 20 GeV
H = 8 kG
(Includes: 1) Si(Li) - 0.3 cm
2) Be - 2.5 x 10⁻³ cm
and 3) N₂ (STP) - 50cm)
Synchrotron 1,2
Synchrotron 1,2,3
Synchrotron - Cerenkov 1,2,3
Coulomb (B,H) 1,2,3
Coulomb (T-M) 1,2,3
Δ (dN/dL) photons / electron - meter - channel
ω (keV)

FIG. 7

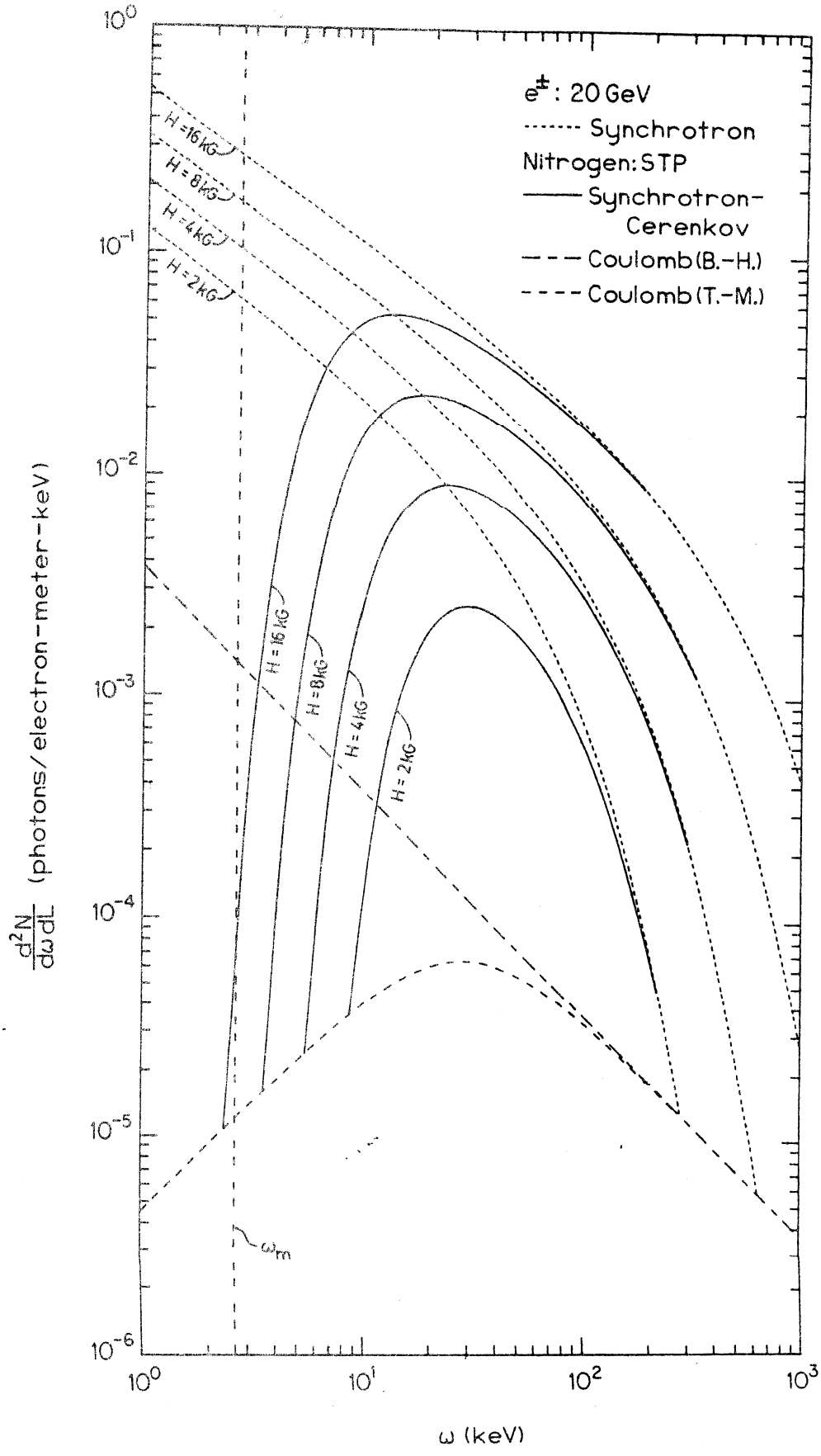
$e^{\pm}$: 20 GeV
Synchrotron
Nitrogen: STP
Synchrotron-Cerenkov
Coulomb (B.-H.)
Coulomb (T.-M.)
H = 16 KG
H = 8 KG
H = 4 KG
H = 2 KG
ω_m
$\frac{d^2N}{d\omega\, dL}$ (photons/electron-meter-keV)
ω (keV)
10^0
10^{-1}
10^{-2}
10^{-3}
10^{-4}
10^{-5}
10^{-6}
10^1
10^2
10^3

FIG. 8

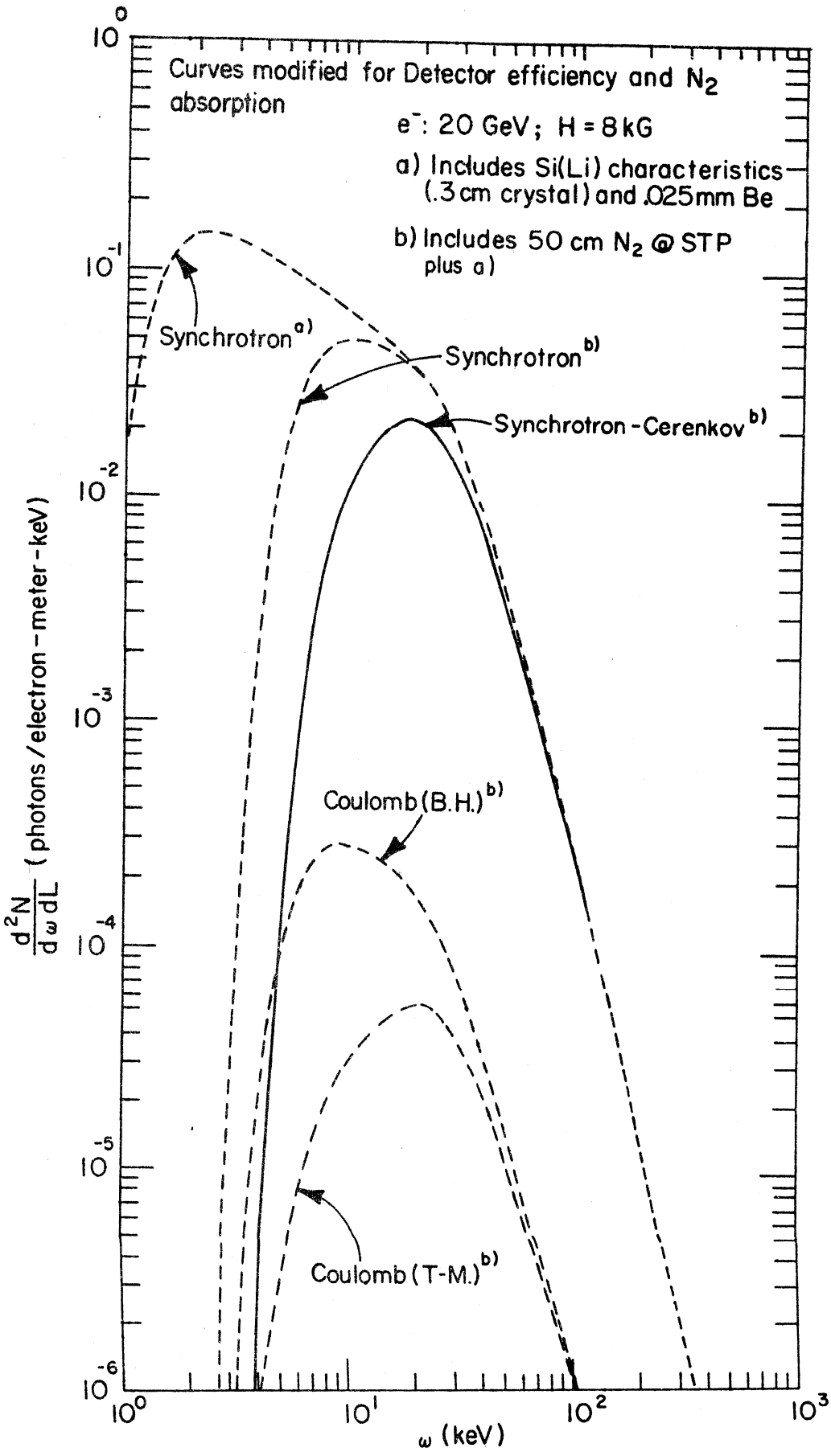
Curves modified for Detector efficiency and N_2 absorption
e^-: 20 GeV; H = 8 kG
a) Includes Si(Li) characteristics (.3 cm crystal) and .025 mm Be
b) Includes 50 cm N_2 @ STP plus a)
Synchrotron a)
Synchrotron b)
Synchrotron - Cerenkov b)
Coulomb (B.H.) b)
Coulomb (T-M.) b)
$\frac{d^2N}{d\omega dL}$ (photons / electron - meter - keV)
ω (keV)
10^0
10^{-1}
10^{-2}
10^{-3}
10^{-4}
10^{-5}
10^{-6}
10^1
10^2
10^3

FIG. 9

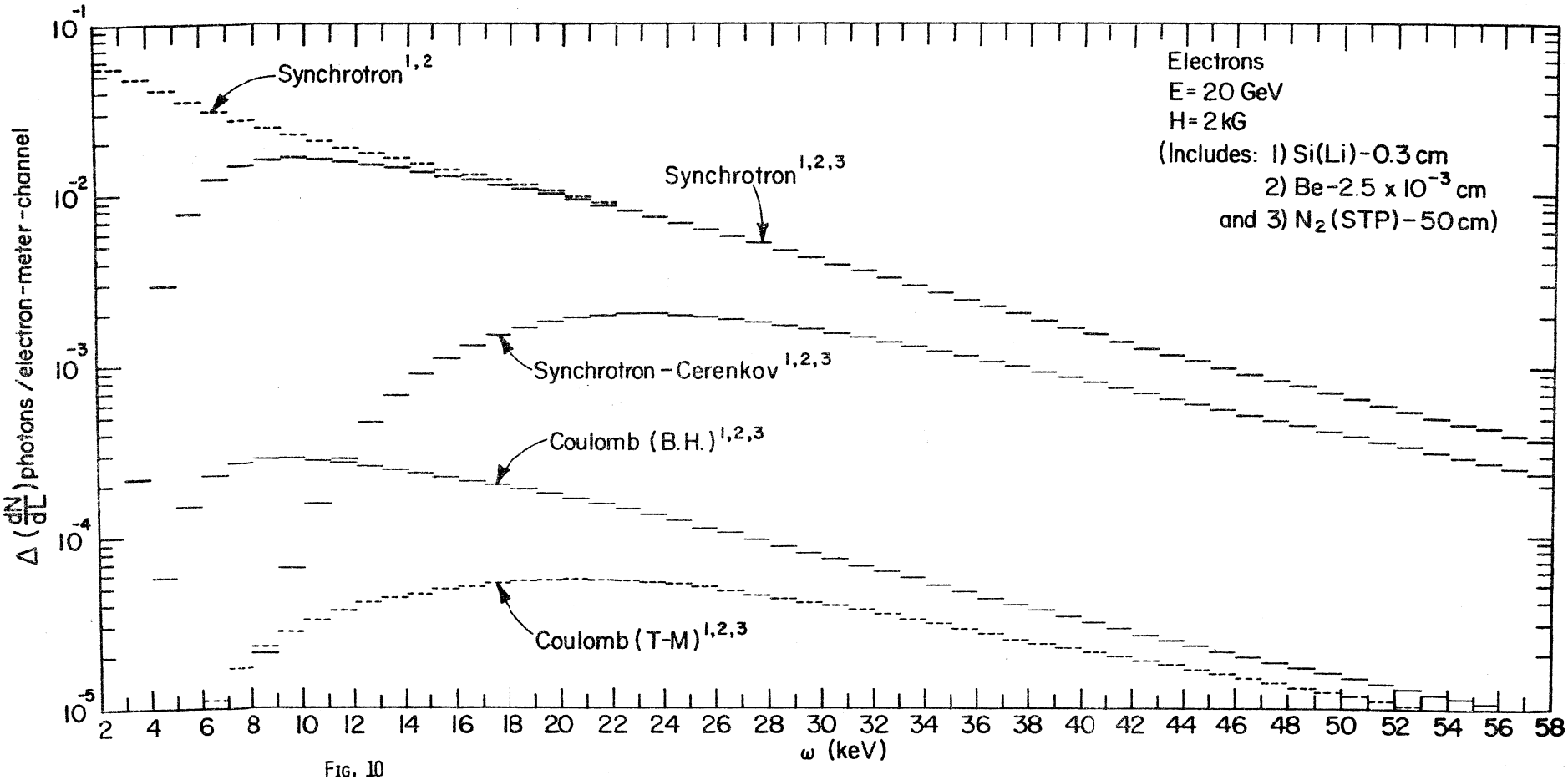
Synchrotron 1,2
Synchrotron 1,2,3
Synchrotron – Cerenkov 1,2,3
Coulomb (B.H.) 1,2,3
Coulomb (T-M) 1,2,3
Electrons
E = 20 GeV
H = 2 kG
(Includes: 1) Si(Li) – 0.3 cm
2) Be – 2.5 x 10⁻³ cm
and 3) N₂ (STP) – 50 cm)
Δ (dN/dL) photons / electron-meter-channel
ω (keV)
10⁻¹
10⁻²
10⁻³
10⁻⁴
10⁻⁵
2 4 6 8 10 12 14 16 18 20 22 24 26 28 30 32 34 36 38 40 42 44 46 48 50 52 54 56 58

FIG. 10

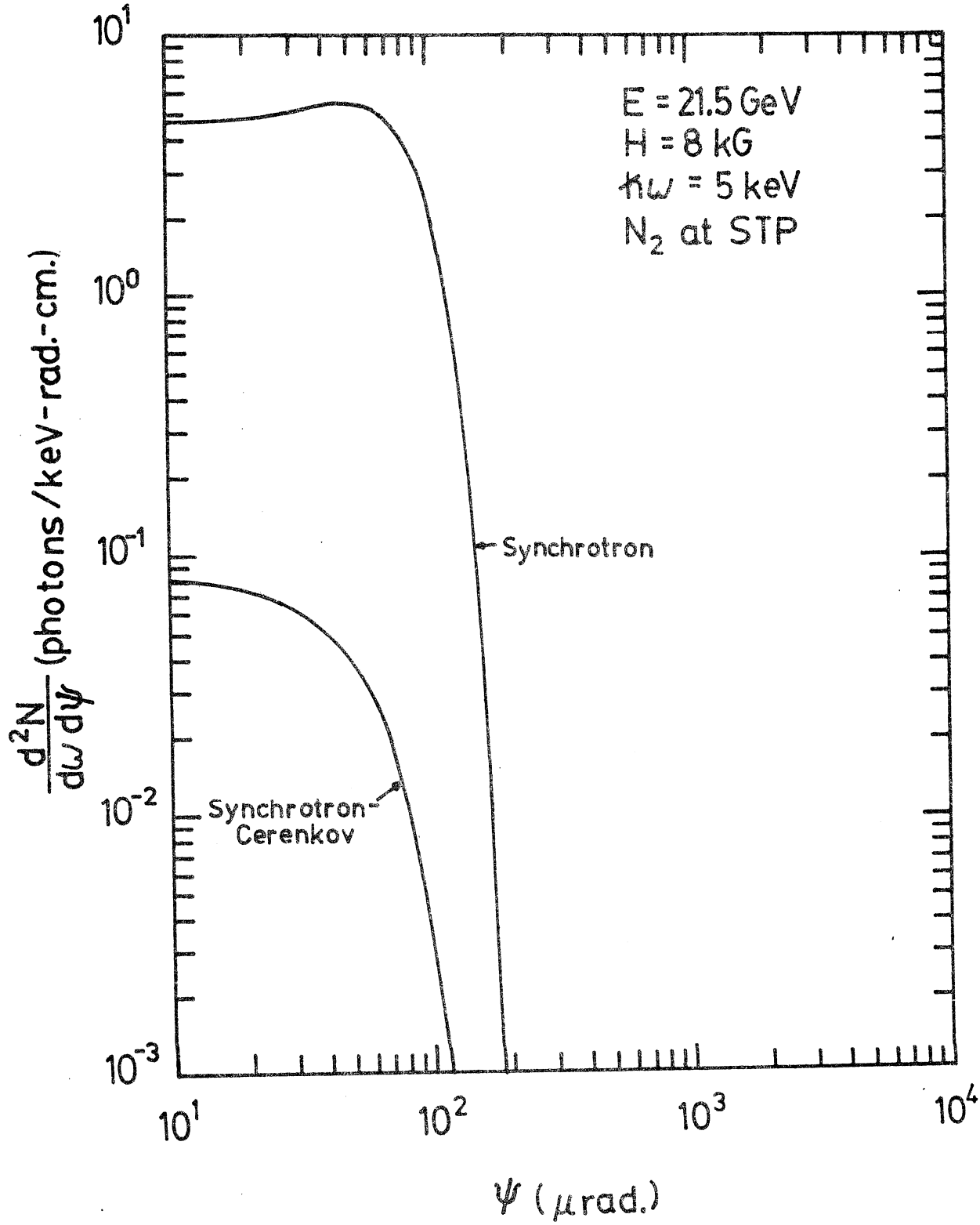
E = 21.5 GeV
H = 8 kG
ħω = 5 keV
N2 at STP
Synchrotron
Synchrotron-Cerenkov
d²N/dω dψ (photons/keV-rad.-cm.)
ψ (μrad.)
10¹
10⁰
10⁻¹
10⁻²
10⁻³
10¹
10²
10³
10⁴

FIG. 11

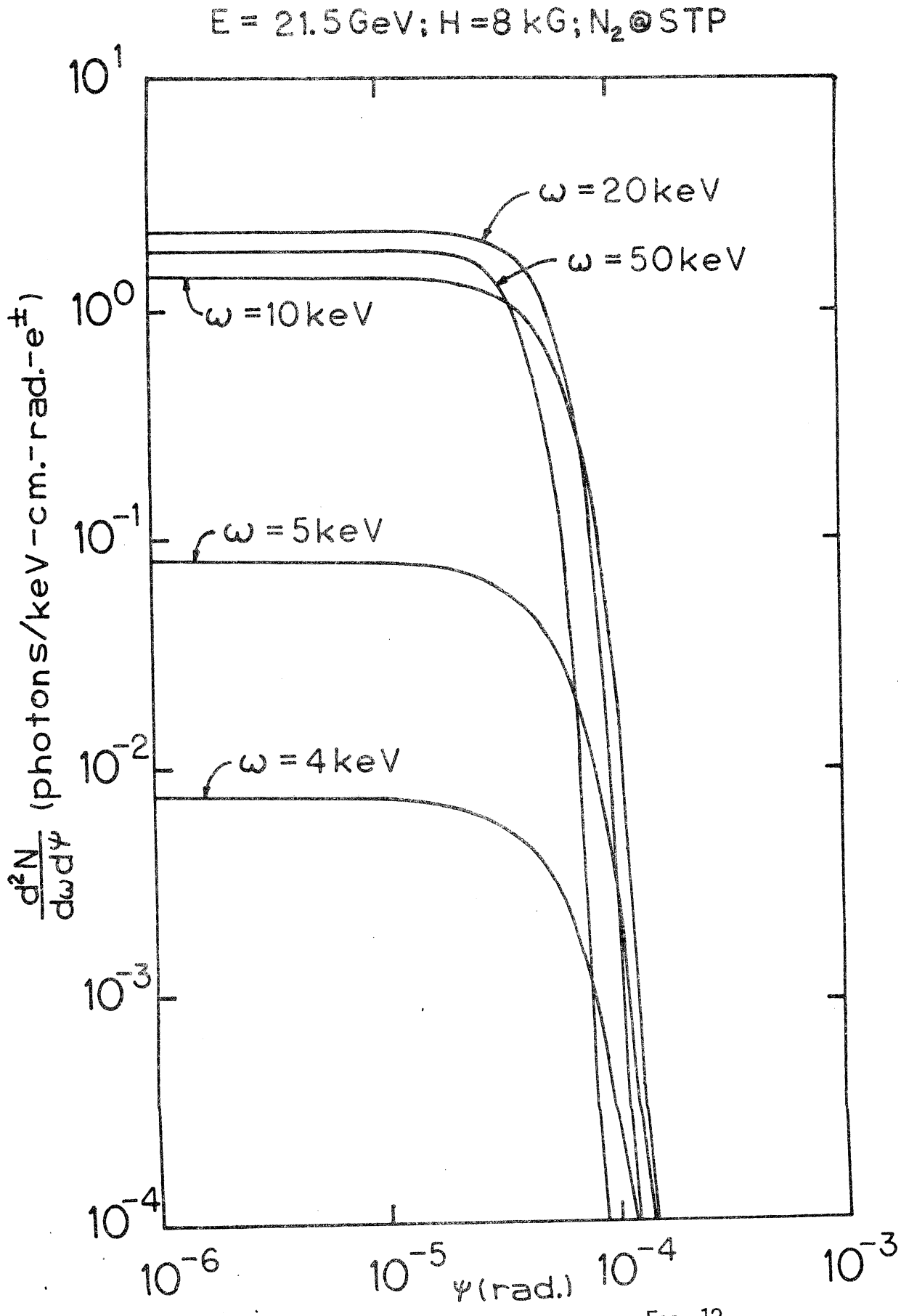
E = 21.5 GeV; H = 8 kG; N_2 @ STP
10^1
10^0
10^{-1}
10^{-2}
10^{-3}
10^{-4}
ω = 20 keV
ω = 50 keV
ω = 10 keV
ω = 5 keV
ω = 4 keV
$\frac{d^2N}{d\omega d\psi}$ (photons/keV-cm.-rad.-$e^{\pm}$)
10^{-6}
10^{-5}
ψ (rad.)
10^{-4}
10^{-3}

FIG. 12

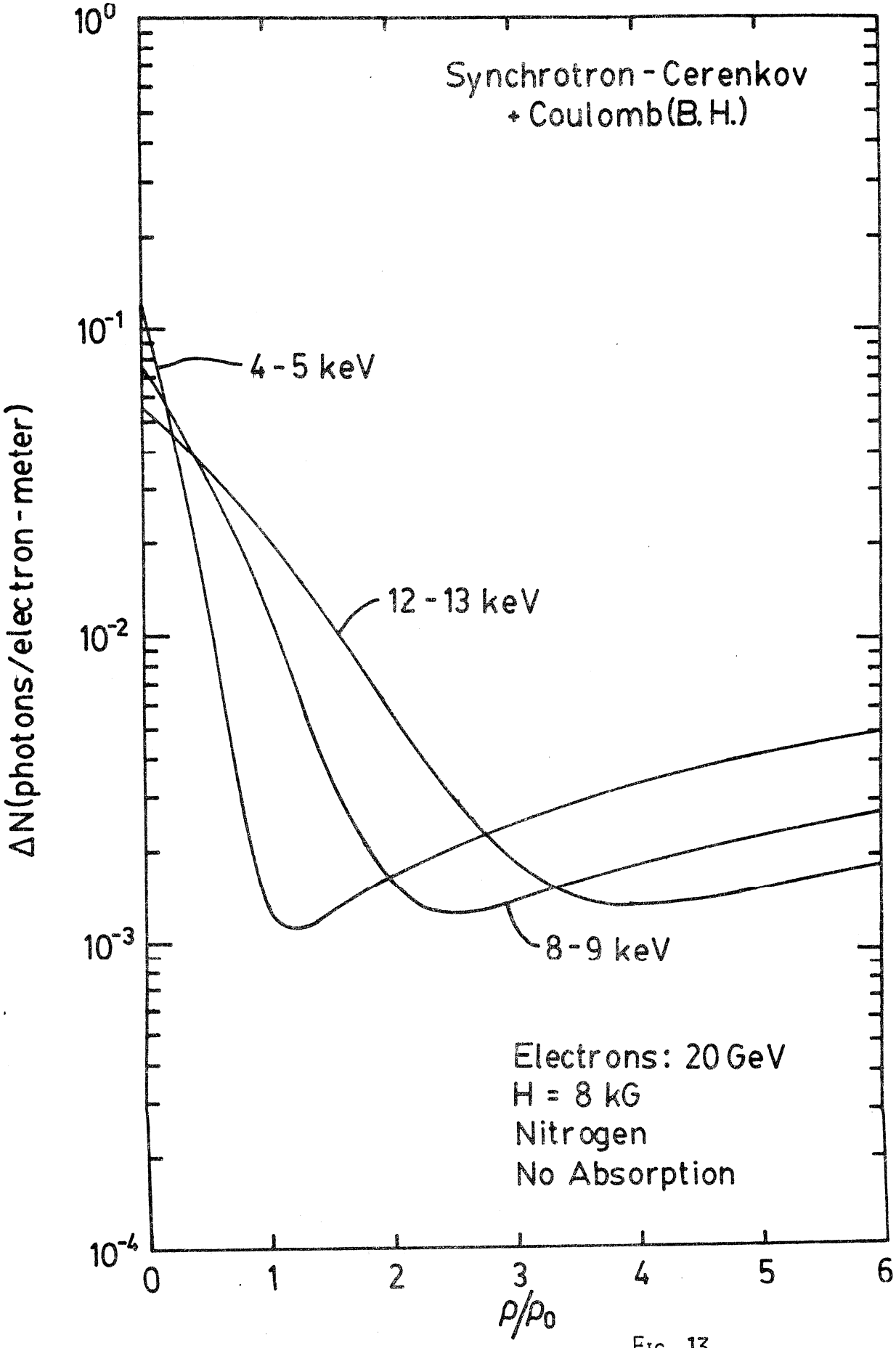
Synchrotron - Cerenkov
+ Coulomb (B. H.)
4 - 5 keV
12 - 13 keV
8 - 9 keV
Electrons: 20 GeV
H = 8 kG
Nitrogen
No Absorption
ΔN (photons/electron - meter)
10^{0}
10^{-1}
10^{-2}
10^{-3}
10^{-4}
0
1
2
3
4
5
6
ρ/ρ_0

FIG. 13

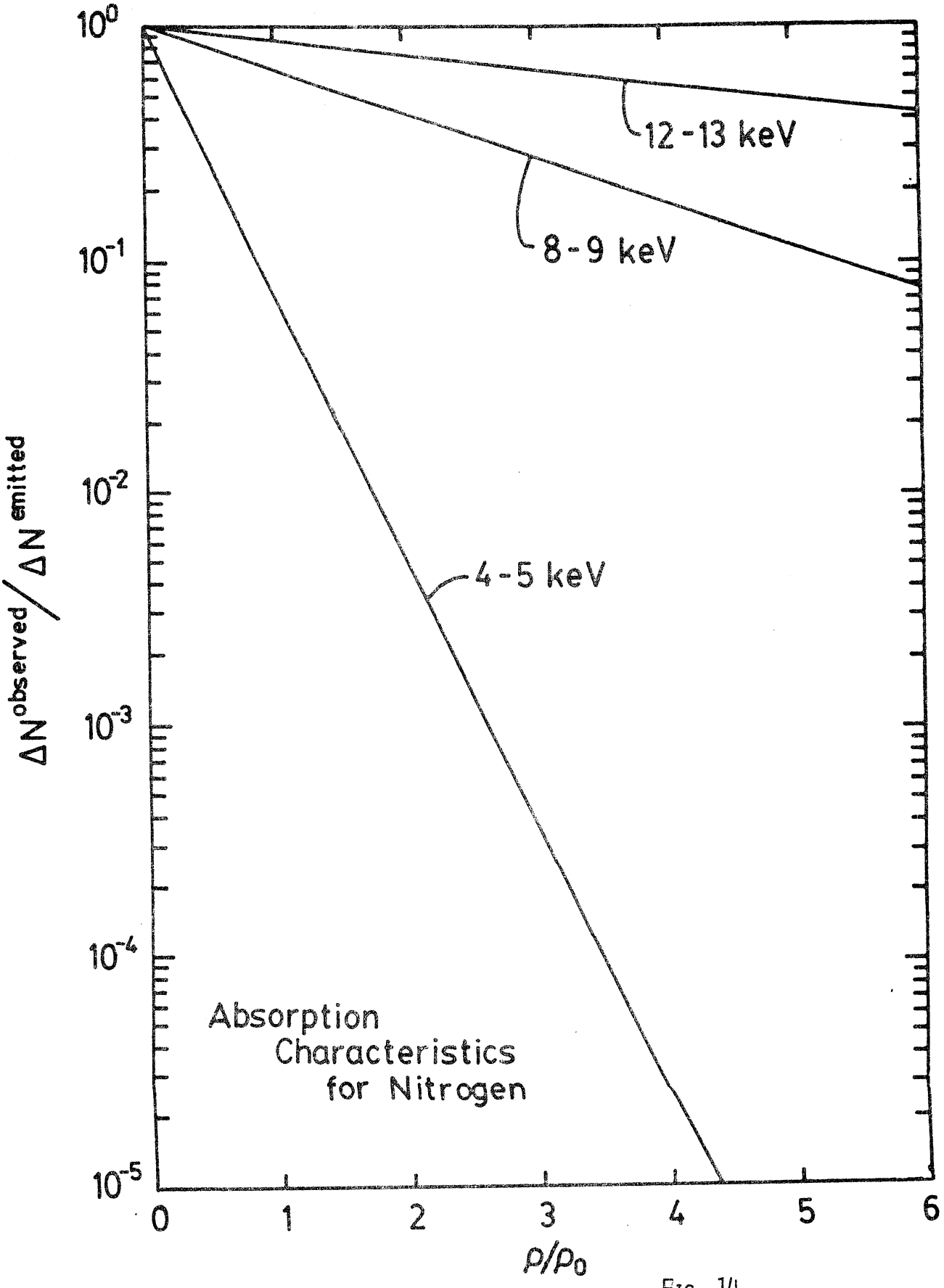
10^0
10^{-1}
10^{-2}
10^{-3}
10^{-4}
10^{-5}
$\Delta N^{observed} / \Delta N^{emitted}$
12 - 13 keV
8 - 9 keV
4 - 5 keV
Absorption
Characteristics
for Nitrogen
0
1
2
3
4
5
6
ρ/ρ_0

FIG. 14

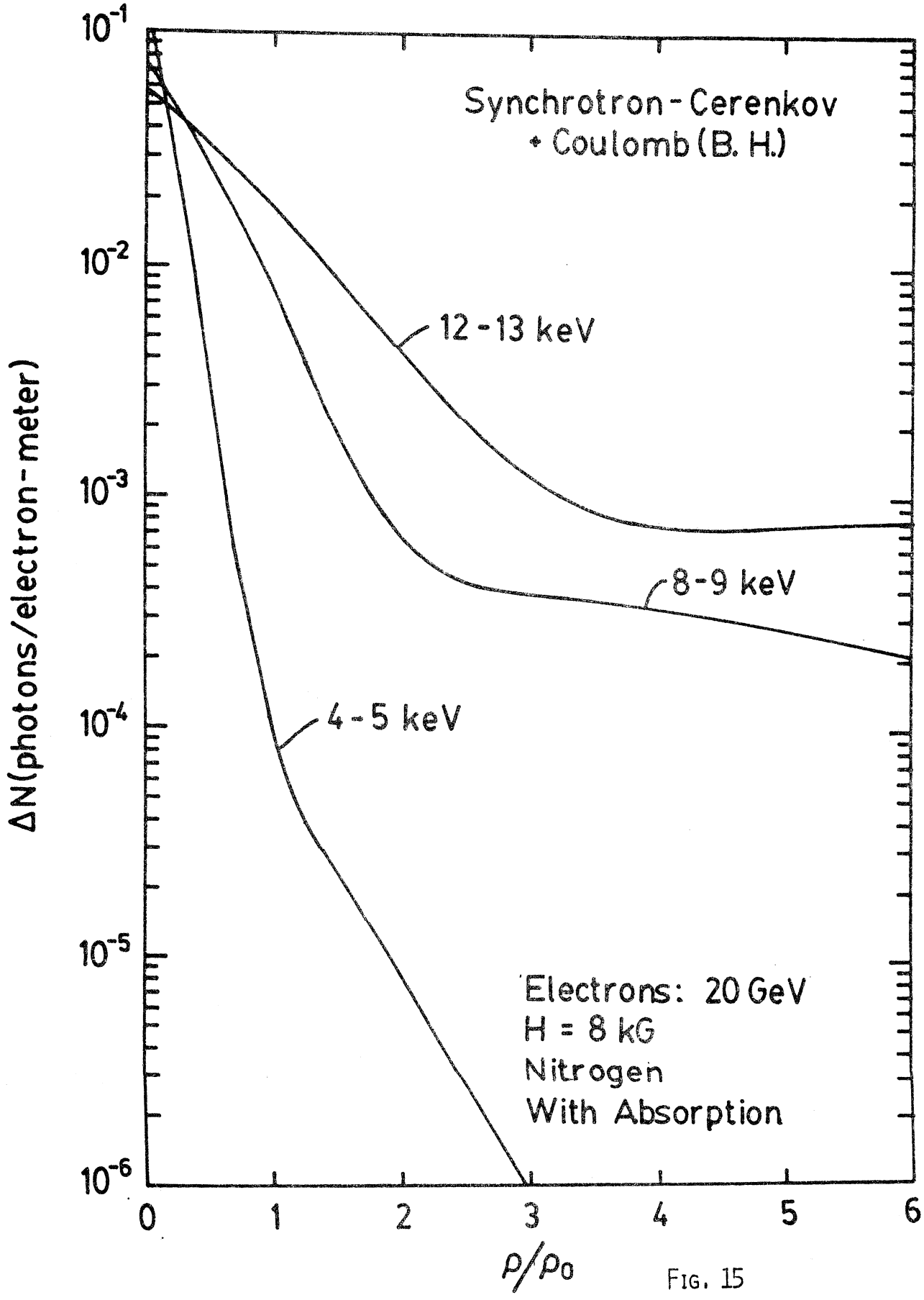
Synchrotron - Cerenkov
+ Coulomb (B. H.)
12 - 13 keV
8 - 9 keV
4 - 5 keV
Electrons: 20 GeV
H = 8 kG
Nitrogen
With Absorption
ΔN(photons/electron-meter)
10^{-1}
10^{-2}
10^{-3}
10^{-4}
10^{-5}
10^{-6}
0
1
2
3
4
5
6
ρ/ρ_0

FIG. 15

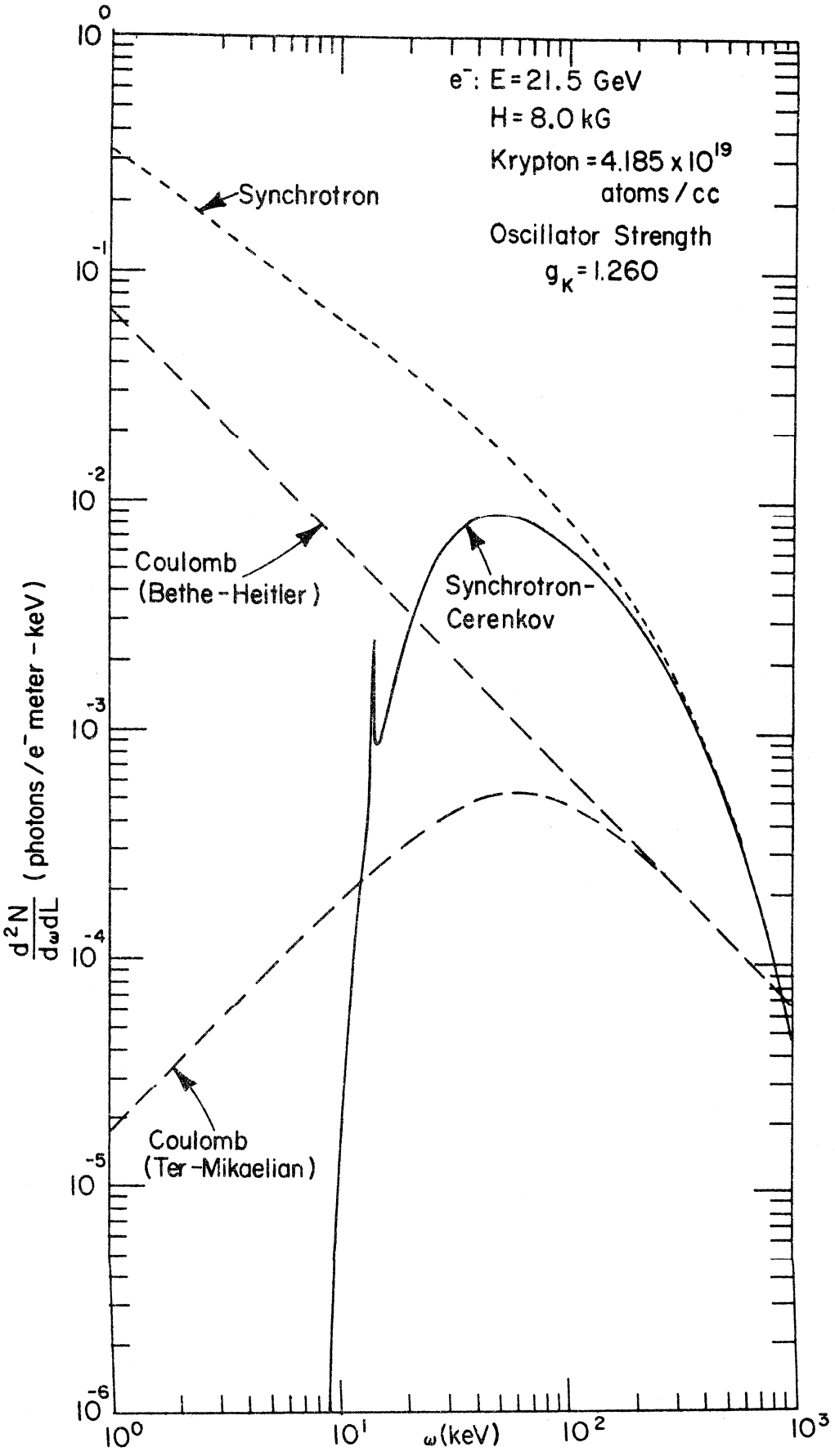
e⁻: E = 21.5 GeV
H = 8.0 kG
Krypton = 4.185 x 10^19 atoms / cc
Oscillator Strength
g_K = 1.260
Synchrotron
Coulomb (Bethe-Heitler)
Synchrotron-Cerenkov
Coulomb (Ter-Mikaelian)
d²N/dωdL (photons / e⁻ meter - keV)
ω(keV)
10^0
10^-1
10^-2
10^-3
10^-4
10^-5
10^-6
10^1
10^2
10^3

FIG. 16

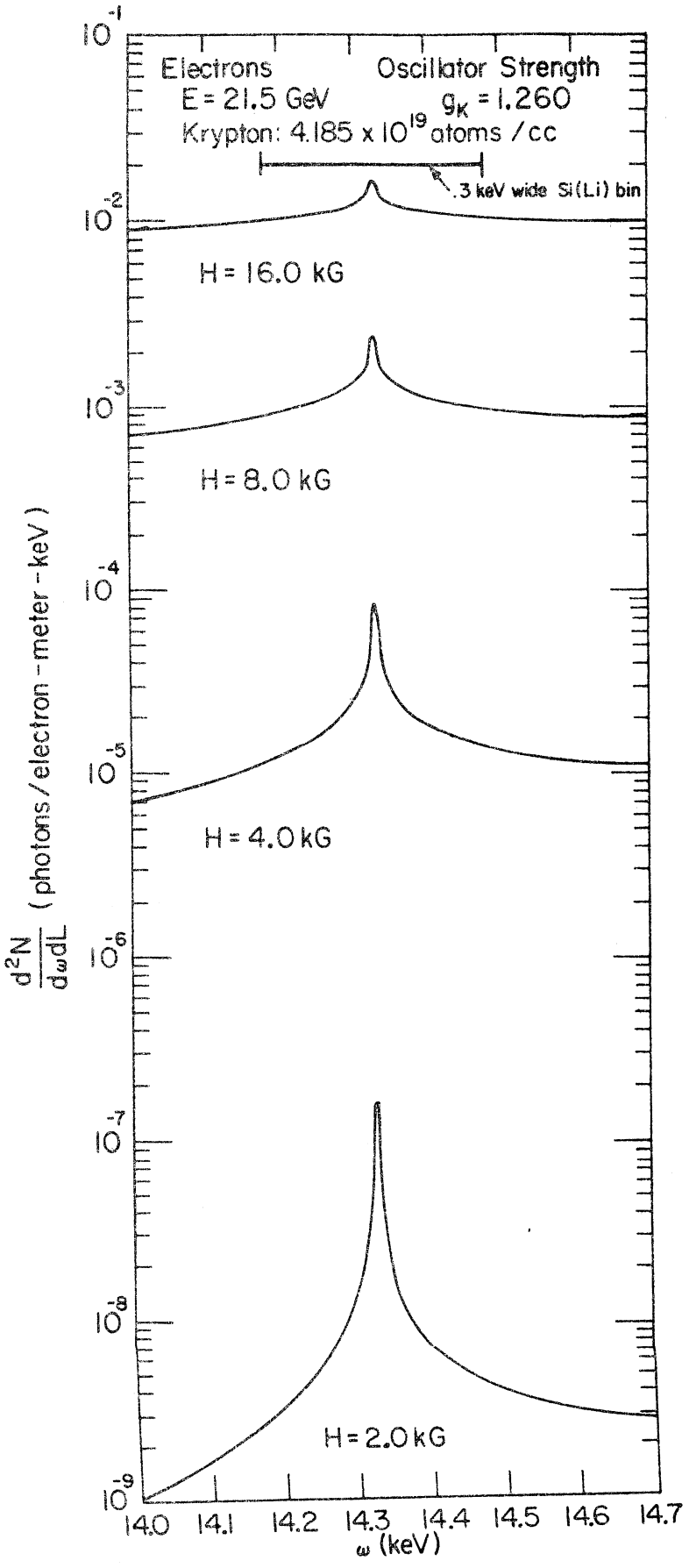
Electrons
E = 21.5 GeV
Oscillator Strength
g_K = 1.260
Krypton: 4.185 x 10^{19} atoms / cc
.3 keV wide Si(Li) bin
H = 16.0 kG
H = 8.0 kG
H = 4.0 kG
H = 2.0 kG
$\frac{d^2N}{d\omega dL}$ (photons / electron - meter - keV)
10^{-1}
10^{-2}
10^{-3}
10^{-4}
10^{-5}
10^{-6}
10^{-7}
10^{-8}
10^{-9}
14.0 14.1 14.2 14.3 14.4 14.5 14.6 14.7
ω (keV)

FIG. 17

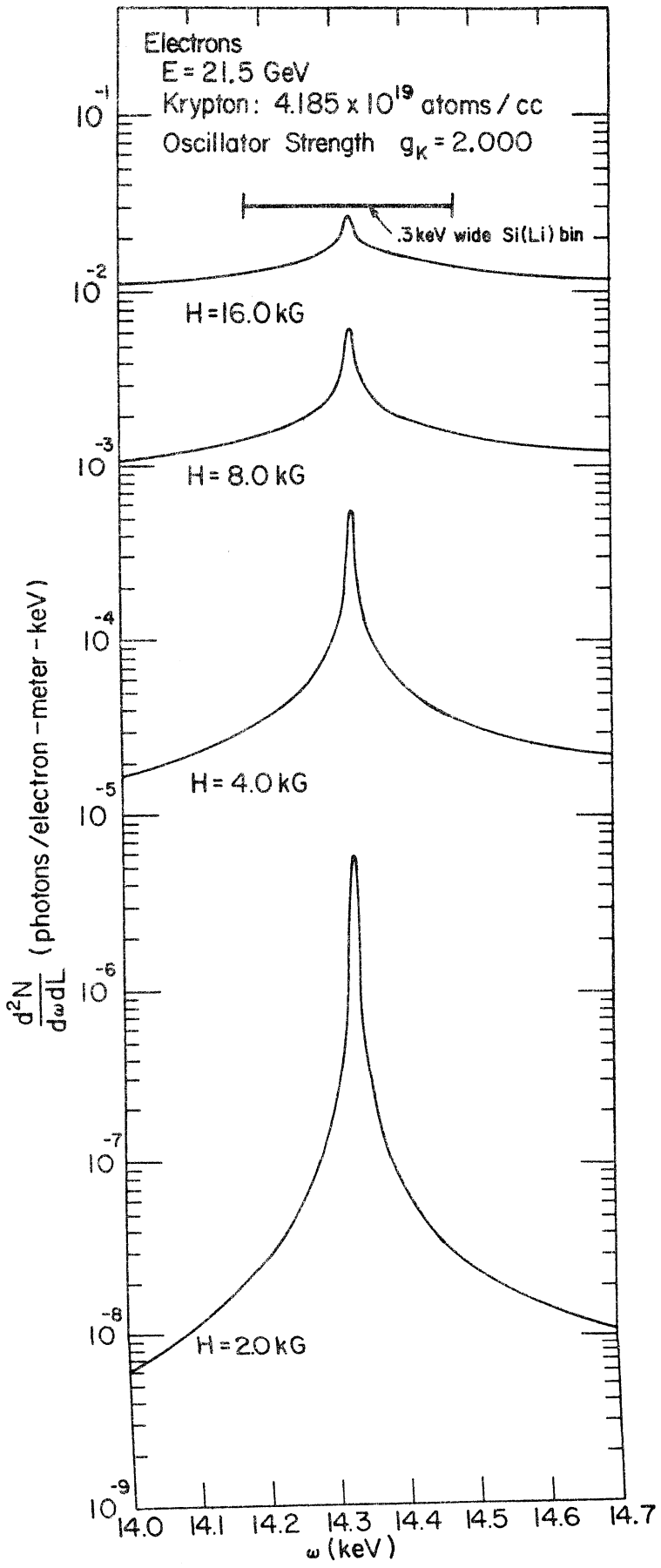
Electrons
E = 21.5 GeV
Krypton: 4.185 x 10^19 atoms / cc
Oscillator Strength g_K = 2.000
.3 keV wide Si(Li) bin
H = 16.0 kG
H = 8.0 kG
H = 4.0 kG
H = 2.0 kG
d²N/dωdL (photons/electron-meter-keV)
ω (keV)
14.0
14.1
14.2
14.3
14.4
14.5
14.6
14.7

FIG. 18

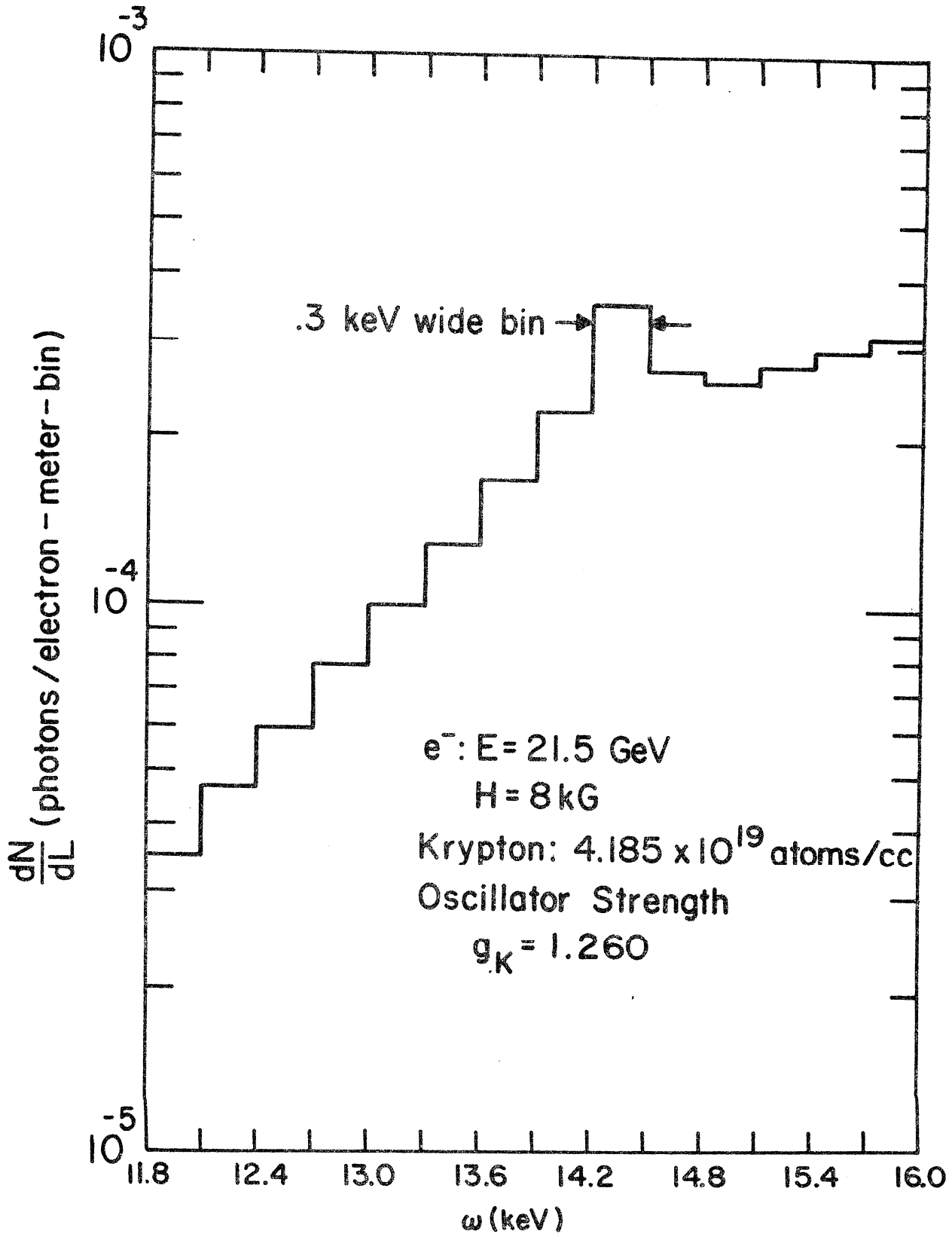
10^{-3}
10^{-4}
10^{-5}
$\frac{dN}{dL}$ (photons / electron - meter - bin)
.3 keV wide bin
e^-: E = 21.5 GeV
H = 8 kG
Krypton: 4.185×10^{19} atoms/cc
Oscillator Strength
$g_K = 1.260$
11.8
12.4
13.0
13.6
14.2
14.8
15.4
16.0
ω (keV)

FIG. 19

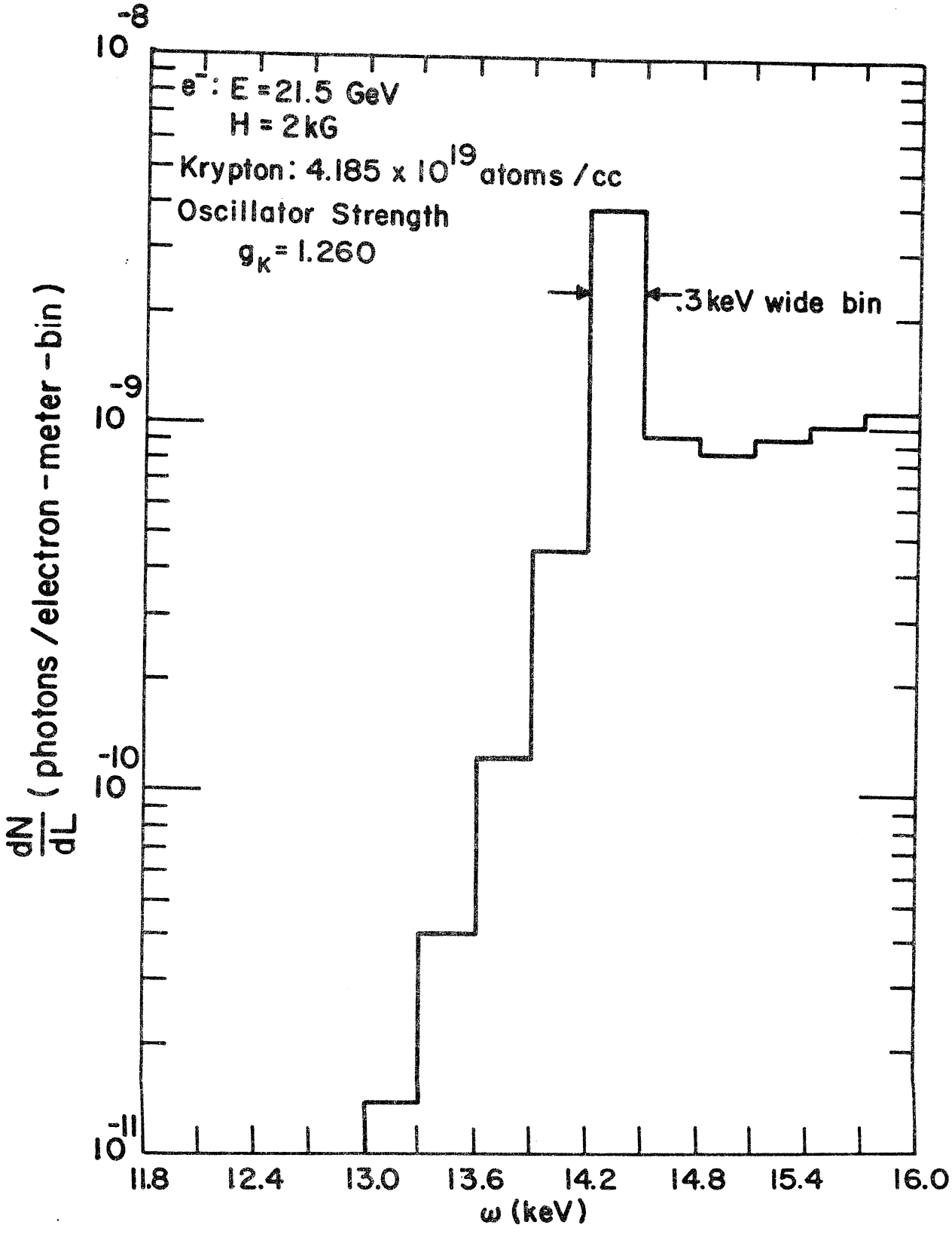
10^{-8}
10^{-9}
10^{-10}
10^{-11}
e^-: E = 21.5 GeV
H = 2 kG
Krypton: 4.185×10^{19} atoms / cc
Oscillator Strength
$g_K = 1.260$
.3 keV wide bin
$\frac{dN}{dL}$ (photons / electron - meter - bin)
11.8
12.4
13.0
13.6
14.2
14.8
15.4
16.0
ω (keV)

FIG. 20

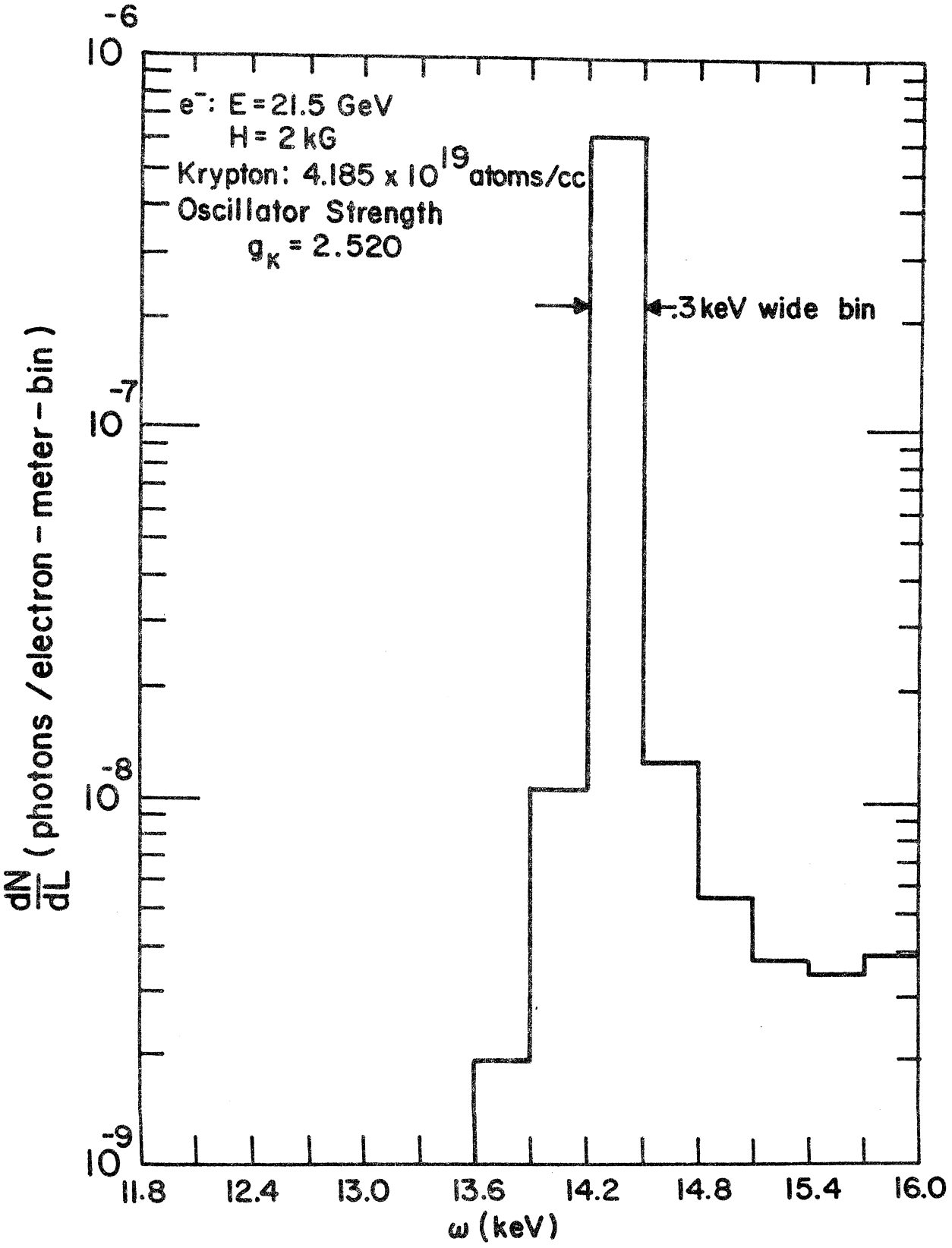
10^{-6}
10^{-7}
10^{-8}
10^{-9}
e^-: E = 21.5 GeV
H = 2 kG
Krypton: 4.185×10^{19} atoms/cc
Oscillator Strength
$g_K = 2.520$
.3 keV wide bin
$\frac{dN}{dL}$ (photons / electron - meter - bin)
11.8
12.4
13.0
13.6
14.2
14.8
15.4
16.0
ω (keV)

FIG. 21

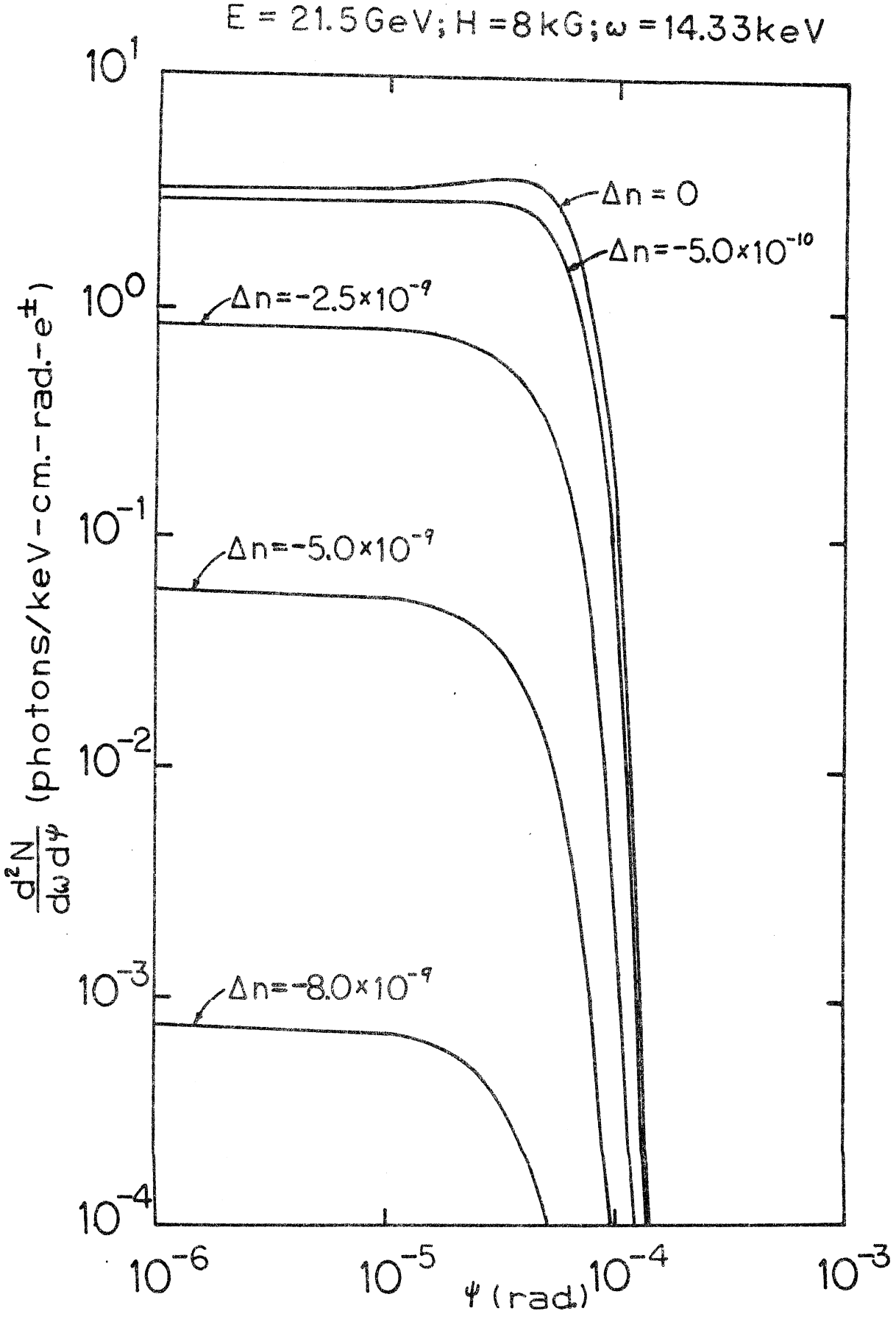
E = 21.5 GeV; H = 8 kG; ω = 14.33 keV
Δn = 0
Δn = -5.0×10⁻¹⁰
Δn = -2.5×10⁻⁹
Δn = -5.0×10⁻⁹
Δn = -8.0×10⁻⁹
d²N/dω dψ (photons/keV-cm.-rad.-e±)
ψ (rad.)
10¹
10⁰
10⁻¹
10⁻²
10⁻³
10⁻⁴
10⁻⁶
10⁻⁵
10⁻⁴
10⁻³

FIG. 22

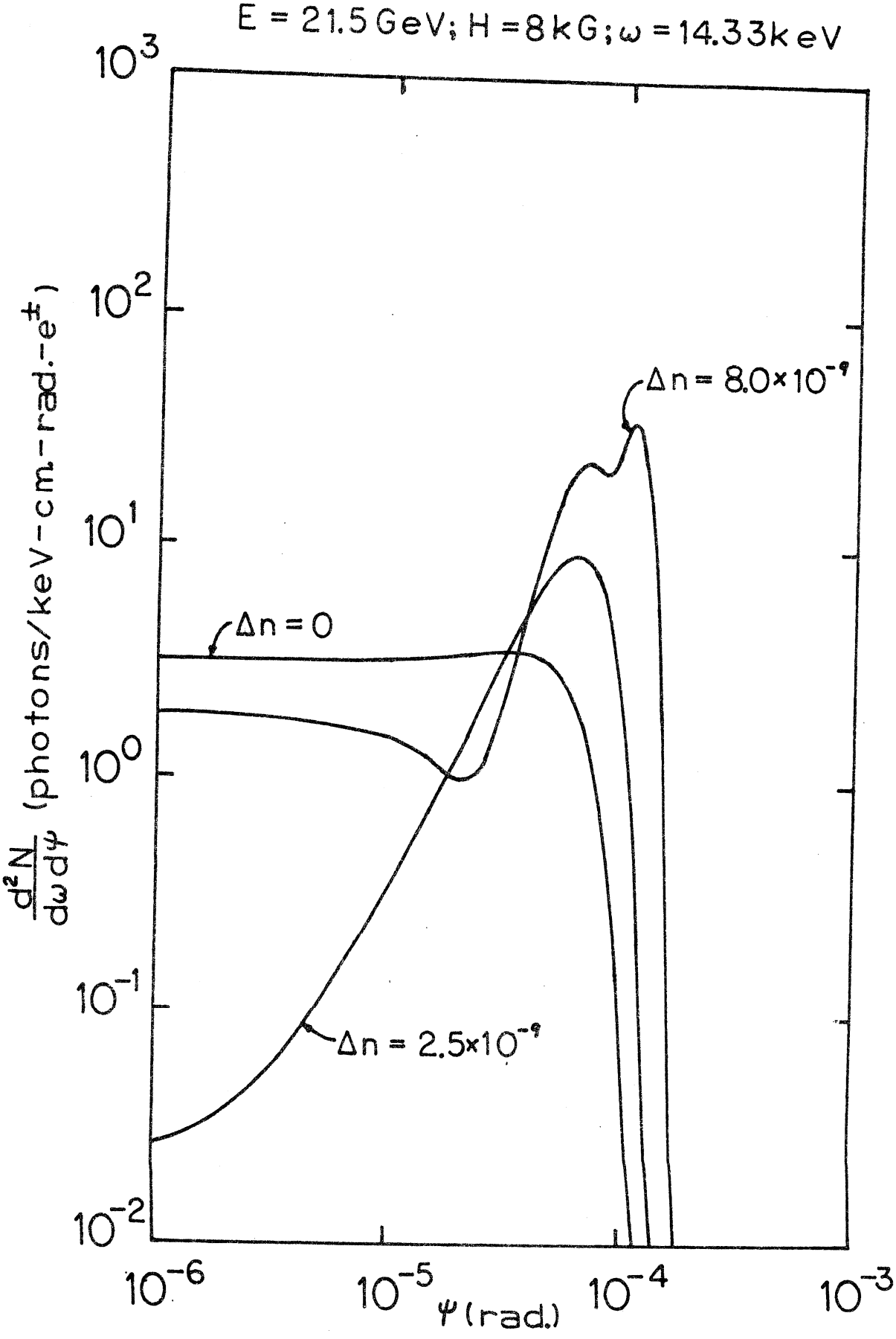
E = 21.5 GeV; H = 8 kG; ω = 14.33 keV
10^3
10^2
10^1
10^0
10^{-1}
10^{-2}
$\frac{d^2N}{d\omega d\psi}$ (photons/keV-cm-rad.-$e^{\pm}$)
Δn = 8.0×10⁻⁹
Δn = 0
Δn = 2.5×10⁻⁹
10^{-6}
10^{-5}
10^{-4}
10^{-3}
ψ (rad.)

FIG. 23

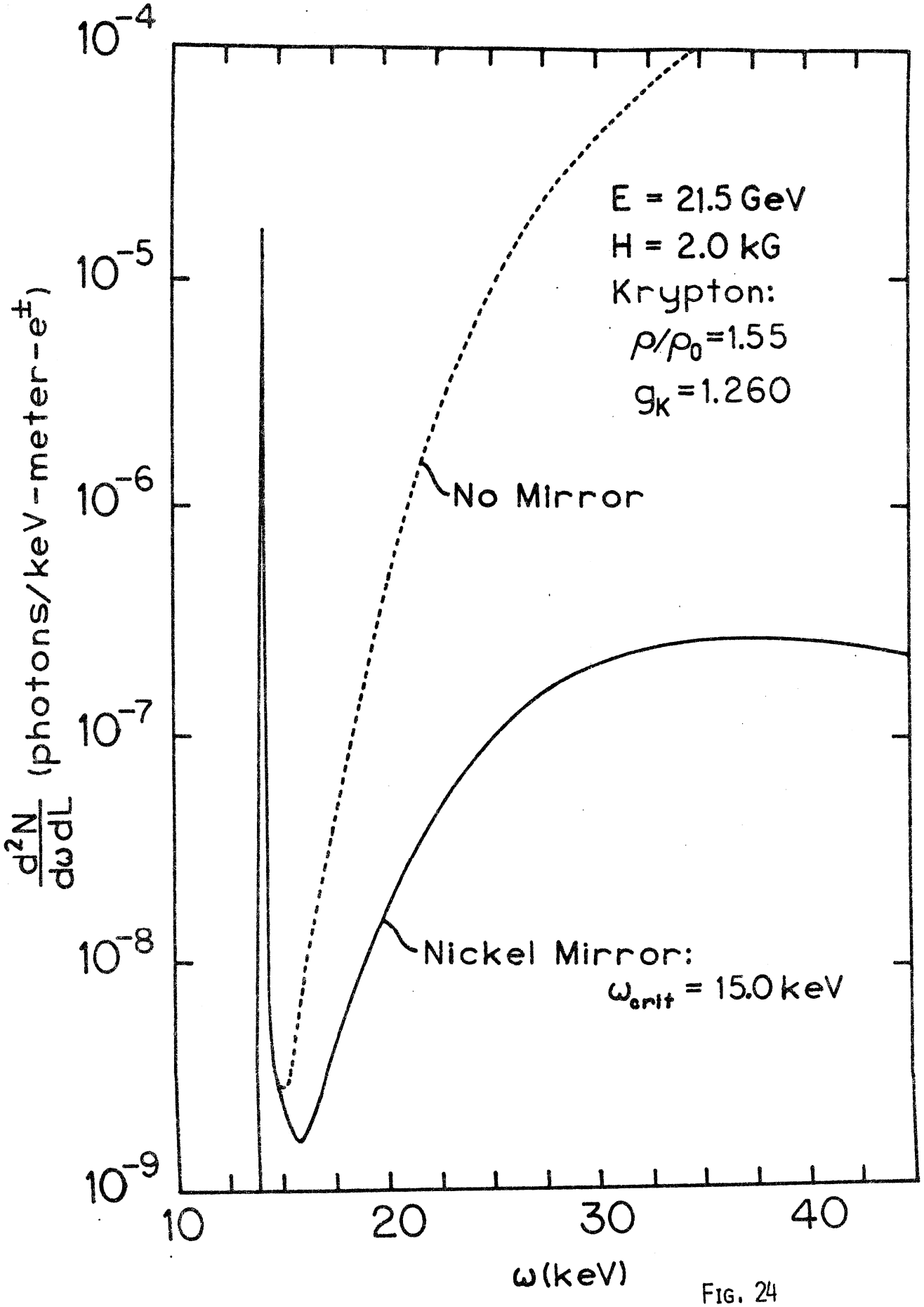
10^{-4}
10^{-5}
10^{-6}
10^{-7}
10^{-8}
10^{-9}
$\frac{d^2N}{d\omega dL}$ (photons/keV-meter-$e^{\pm}$)
E = 21.5 GeV
H = 2.0 kG
Krypton:
ρ/ρ_0=1.55
g_k=1.260
No Mirror
Nickel Mirror:
ω_{crit} = 15.0 keV
10
20
30
40
ω(keV)

FIG. 24

SLAC Proposal No. E-126
rec. August 9, 1976

EXPERIMENTAL STUDY OF SYNCHROTRON-ČERENKOV RADIATION

Proposal Submitted

to

Stanford Linear Accelerator Center

Stanford University

August 1976

Professor T. Erber
Department of Physics
Illinois Institute of Technology
Chicago, Illinois 60616
(312) 567-3382

1. Summary

It has recently been discovered that synchrotron radiation and Čerenkov radiation are limiting cases of a more pervasive radiation process which we call Synergic Synchrotron-Čerenkov Radiation [1,2,3,4,5]*. The synergism refers to the fact that in the limit of vanishing magnetic field intensity synchrotron-Čerenkov radiation (or "SC" for short) reduces to Čerenkov radiation, and in the complementary limit of vanishing material density SC reduces to synchrotron radiation; but the properties of SC radiation itself cannot be recovered by superposing these limits. An obvious analogy is the distinction between merely mixing hydrogen and oxygen and uniting them chemically to form water. Various applied features of SC radiation have already been considered in quantitative detail in reference [5] in the context of the following situations: (1) The passage of high energy electrons through gases, liquids, solids, and plasmas in the presence of magnetic fields. In these cases the properties of SC radiation lead to practical applications including the measurement of electron energies in the range 1 GeV-1 TeV; determinations of indices of refraction in the x-ray region; and the construction of peaked, tunable x-ray generators. (2) The suppression of synchrotron x-rays from high energy electrons in the earth's atmosphere and extra-terrestrial environs. (3) The detection of the real part of the Delbrück scattering amplitude. (4) Vacuum polarization effects on radiation by ultra high energy electrons in intense magnetic fields. (5) SC radiation by charged particles heavier than electrons. It is obvious from this list that SC radiation plays an important role in many areas of pure and applied physics.

The next logical step is to initiate an experimental study of the properties of synchrotron-Čerenkov radiation. Specifically we propose to perform a series of experiments with the following

Research Objectives

(1) The Demonstration of the Existence of Synergic Synchrotron-Čerenkov Radiation:

The properties of SC-radiation have been derived by two

*Bracketed numbers indicate papers cited in Section 6, "References".

independent but equivalent classical electrodynamic calculations [2,3] and a quantum electrodynamic calculation [3]. Accordingly there can only be a sliver of suspicion regarding the existence of SC-radiation as an observable natural phenomenon. Nevertheless an experimental check is essential because —

(a) There may be conceptual errors involved in characterizing cooperative electrodynamic interactions in the keV-MeV range in terms of indices of refraction.

(b) The synchrotron-Čerenkov synergism may be an inconsequent approximation instead of merely a first approximation to a still more comprehensive synergism uniting Coulomb bremsstrahlung, synchrotron radiation, Čerenkov radiation, and vacuum polarization phenomena [6].

An unambiguous and convenient method for verifying the existence of SC-radiation --- allowing for self-absorption, Coulomb bremsstrahlung (Bethe-Heitler, Ter-Mikaelian, or synergic [6]), and other background effects --- is to deflect 12 GeV electrons by means of 5 kG transverse fields in the presence of nitrogen at STP in a dual scattering set-up as shown on the blueprint. The essential point of this arrangement is that one scattering cell can be used to generate a photon number spectrum $N_S(\omega)$ corresponding to pure synchrotron radiation filtered through a downstream nitrogen absorber: The other scattering cell can be used to generate the spectrum $N_{SC}(\omega)$ corresponding to synchrotron-Čerenkov radiation + Coulomb bremsstrahlung - self-absorption. For instance in the energy range $5 \lesssim \omega \lesssim 5.5$ keV --- which is easily accessible with Si(Li) detectors --- the ratio of the photon counting rates associated with the two scattering cells should exhibit the radiation suppression

$$\frac{N_{SC}(5\ \text{keV})}{N_S\ (5\ \text{keV})} \approx 1/20, \qquad (1.1)$$

which is the salient feature of the synergic process. The experimental parameters may be adjusted so that an average beam intensity of the order of 10^6 e^-/sec --- corresponding to peak rates of 10^4 e^-/msec --- yields about 200 counts per channel per second in the 5 keV range. This is comfortably above the expected background limit of <1 count per channel per second. Shifting the incident electron energy from

12 GeV (Cornell) to 20 GeV (SLAC) and making allowance for the differences in pulse length and duty cycle does not significantly alter any of the basic experimental design parameters [compare Section 5].

(2) Measurement of the Principal Features of Synchrotron-Čerenkov Radiation:

If the experimental demonstration of the existence of SC-radiation is successful, then the next logical step is to check the detailed properties of the radiation against theoretical predictions. Specifically we propose to carry out the following measurements:

(a) SC spectrum in N_2 at STP for $5 \lesssim \omega \lesssim 30$ keV, e^- at 12/20 GeV, and $H \sim 5$ kG.

(b) Variation of the SC spectrum as a function of N_2 pressure in the range $0 \lesssim p \lesssim 2$ bar.

(c) Extinction of SC radiation with decreasing magnetic field strength.

(3) Measurements Utilizing Synchrotron-Čerenkov Radiation:

In the event that the program outlined in 2(a)-(c) yields good agreement between theory and experiment, it is possible to proceed with applications of SC-radiation. In particular the dual scattering set-up can be used to measure the dispersive and absorptive components of the indices of refraction of gases in the x-ray region, i.e. $5 \lesssim \omega \lesssim 40$ keV. We propose to study:

(a) Argon ($Z = 18$) at STP because the K edge (3.2 keV) is just at the lower limit of the Si(Li) detection system.

(b) Air at STP --- to check on the effects of the 1% argon component.

(c) Krypton ($Z = 36$) at 0.1 bar and STP because in these cases the K edge occurs at 14.3 keV and the L edge at 1.9 keV [compare 4(b)].

(4) Auxiliary Experiments; Future Research:

(a) The effect of the polarization of amorphous media on Coulomb bremsstrahlung, i.e. the Ter-Mikaelian modification of the Bethe-Heitler spectrum [6], is also a synergic radiation

process. It is in fact possible, as indicated in 1(b), that the synergism extends to synchrotron radiation. The single scattering cell modification of our experimental set-up [compare Section 4(E)] would be suitable for making measurements which would demonstrate the existence of the Ter-Mikaelian spectral modifications.

(b) The krypton index measurements of 3(c) should permit us to complete the design of magnetic Čerenkov counters which ought to be capable of distinguishing electron energies in the range > 100 GeV [7]. A (low energy) prototype counter could be built, tested, and calibrated.

(c) The synchrotron spectrum is drastically altered by quantum effects whenever the deflecting fields (H) and the incident electron energy (E) satisfy the constraint [2,8]

$$H(T) \gtrsim \frac{1150}{E^2(\text{GeV})} \, . \qquad (1.2)$$

Detectable effects occur under even more conservative conditions [9]; Fig. 11 shows the deviations for $E \sim 12$ GeV and $H = 10$ kG. These quantum modifications should be measurable with the double scattering set-up shown on the blueprint if Ge(Li) detectors were substituted for the Si(Li) detectors. Condition (1.2) could be satisfied at Cornell with 8T fields and at SLAC with 3T fields.

2. Table of Contents

3. Basic Properties of Synchrotron-Čerenkov Radiation

The general expressions derived in [3] describe the radiation emitted by particles with charge e, mass m, and energy E, traversing homogeneous and isotropic media --- with indices of refraction $n(\omega,H)$ --- in a direction perpendicular to the lines of flux of an externally applied magnetic field H. The validity of these formulas is constrained principally by the bound

$$H \ll H_{cr};\quad H_{cr} = \frac{m^2c^3}{e\hbar} \to 4.414 \times 10^{13}\ \text{G for } m = m_e; \tag{3.1a}$$

which in a practical sense is violated only under exotic astrophysical conditions (pulsars?) and in some nuclear interactions. Condition (3.1a) implies that radiation near the spectral tip may be ignored, i.e.

$$\hbar\omega \ll E. \tag{3.1b}$$

Additional simplifications follow from considering high energies

$$E \gg mc^2; \tag{3.1c}$$

and indices of refraction near unity, i.e. tenuous media or dispersion in the x-ray portion of the spectrum

$$n(\omega,H) \equiv 1 + \Delta n(\omega,H);\quad |\Delta n| \ll 1. \tag{3.1d}$$

Of course eqs. (3.1c & d) also imply

$$|1 - (n\beta)^2| = \left|1 - n^2\left(1 - \left[mc^2/E\right]^2\right)\right| \approx \left|\left[mc^2/E\right]^2 - 2\Delta n(\omega,H)\right| \ll 1, \tag{3.1e}$$

where $\beta = v/c$. It is now easy to check that in virtue of (3.1a-e) the general synchrotron-Čerenkov radiation rates for the number of photons dN, emitted in the frequency band $d\omega$, over a path length L, may be simplified as follows:

(i) "Synchrotron branch" $\quad 2\Delta n(\omega,H) - \left(\frac{mc^2}{E}\right)^2 < 0.$ (3.2a)

In this case eq. (3.49) of [3] becomes ($\mu = 1$)

$$dN = \frac{\alpha\sqrt{3}}{2\pi}\ \frac{L}{\lambda\!\!\!^{-}_c}\ \frac{H}{H_{cr}}\ \tilde{I}(\omega,E,H,\Delta n(\omega,H))\ \frac{d\omega}{\omega}, \tag{3.2b}$$

where $\alpha = e^2/\hbar c$, $\lambda\!\!\!^{-}_c = \hbar/mc$, and

$$\tilde{I} = \frac{\varkappa\left(\frac{\omega}{\omega_c}\left[1 - 2\Delta n\left(\frac{E}{mc^2}\right)^2\right]^{3/2}\right)}{\left[1 - 2\Delta n\left(\frac{E}{mc^2}\right)^2\right]^{1/2}}, \tag{3.2c}$$

with

$$\hbar\omega_c = \frac{3}{2} E\left(\frac{E}{mc^2} \; \frac{H}{H_{cr}}\right). \tag{3.2d}$$

The synchrotron function $\mathcal{K}$ is defined by the integral representation

$$\mathcal{K}(z) \equiv z \int_z^\infty dx \; K_{5/3}(x), \tag{3.2e}$$

where $K_{5/3}(x)$ is a modified Bessel function. In case the medium is "switched off", i.e. $\Delta n \to 0$, we have the limiting case

$$\tilde{I} \to \tilde{I}^s = \mathcal{K}\left(\frac{\omega}{\omega_c}\right), \tag{3.2f}$$

and (3.2b) reduces to the ordinary synchrotron spectrum.

For practical applications involving electrons, i.e. $m \to m_e$, it is convenient to rewrite eq. (3.2b) as

$$dN = 0.118 \; L \left\{\begin{matrix} mm \\ n \end{matrix}\right\} \; H \left\{\begin{matrix} MG \\ kG \end{matrix}\right\} \; \tilde{I} \; \frac{d\omega}{\omega}, \tag{3.2g}$$

where 'millimeters X megagauss' is equivalent to 'meters X kilogauss'. Similarly (3.2d) becomes

$$\omega_c(\text{keV}) = 6.65 \times 10^{-2} \; E^2(\text{GeV}) \; H(\text{kG}). \tag{3.2h}$$

Extensions to heavier particles are discussed in reference [5].

(ii) <u>"Čerenkov branch"</u> $\qquad 2\Delta n(\omega, H) - \left(\frac{mc^2}{E}\right)^2 > 0. \tag{3.3a}$

In this case eq. (3.50) of [3] can be recast in the simplified form ($\mu = 1$)

$$dN = \alpha \; \frac{L}{\lambda_c} \left[2\Delta n - \left(\frac{mc^2}{E}\right)^2\right] \Lambda\left(\frac{\omega}{\omega_c}\left|1 - 2\Delta n\left(\frac{E}{mc^2}\right)^2\right|^{3/2}\right) \frac{d(\hbar\omega)}{mc^2}, \tag{3.3b}$$

where

$$\Lambda(z) \equiv 1 - \frac{1}{3} \int_z^\infty dx \left\{J_{5/3}(x) + J_{-5/3}(x)\right\}, \tag{3.3c}$$

and the $J_{\pm 5/3}$ denote Bessel functions. In this case when the field is switched off, i.e. $H \to 0$, we have

$$\Lambda(z) \to \Lambda(\infty) = 1, \tag{3.3d}$$

and (3.3b) reduces to the ordinary Čerenkov spectrum:

$$dN = \alpha \frac{L}{\lambda_c}\left[2\Delta n - \left(\frac{mc^2}{E}\right)^2\right] \frac{d(\hbar\omega)}{mc^2}. \tag{3.3e}$$

For practical applications involving electrons the relation corresponding to (3.2g) is

$$dN = 3.70\times 10^4\ L(m)\left[2\Delta n - \left(\frac{mc^2}{E}\right)^2\right] \Lambda d[\omega(eV)]. \tag{3.3f}$$

The "Research Objectives" of the present proposal are essentially all concerned with the experimental study of eqs. (3.2b-c); see Section 1, §§ (1)-(3). The "Čerenkov branch" formulas are relevant to the construction of ultra-high energy "magnetic" Čerenkov counters [5,7]. The measurement of the index of refraction of krypton in the x-ray region $5 \tilde{<} \omega \tilde{<} 40$ keV is a preliminary step in the experimental realization of such devices [see Section 1, §§ 3(c) and 4(b); Section 4(D-C)].

We have assumed that the index of refraction for gaseous media in the x-ray region above the absorption edges is given by [2,3,5]

$$n(\omega) - 1 = \Delta n = -\frac{1}{2}\left(\frac{\omega_p}{\omega}\right)^2, \tag{3.4a}$$

where

$$\hbar\omega_p = \left[(4\pi\alpha N_o\ \lambda_c^{\,3})(\rho\ Z/A)\right]^{1/2} mc^2. \tag{3.4b}$$

or

$$\omega_p(eV) = 28.82\ (\rho\ Z/A)^{1/2}. \tag{3.4c}$$

As usual ρ denotes density (gms/cm^3), N_o is Avogadro's number, and A is atomic number.

We may now combine the general expression for synchrotron-Čerenkov emission (3.2b,c) with (3.4a) to obtain an explicit form for the radiation spectrum valid in the range $\omega(keV) > 0.054\ Z^2$ [5]. It is convenient to write this as

$$\tilde{I} = \frac{\chi\left(\frac{\omega_o}{\omega_c}\left\{\frac{\omega}{\omega_o}\left[1+\left(\frac{\omega_o}{\omega}\right)^2\right]^{3/2}\right\}\right)}{\left[1+\left(\frac{\omega_o}{\omega}\right)^2\right]^{1/2}}, \tag{3.5}$$

where

$$\omega_o = \frac{E}{mc^2}\,\omega_p, \tag{3.6a}$$

or, in practical units,

$$\omega_o(\text{keV}) = 56.40\ E(\text{GeV})\ [\rho\ Z/A]^{1/2}. \tag{3.6b}$$

Clearly all the essential features of $\tilde{I}$ are controlled by the relative magnitudes of ω_o and ω_c. In particular since there is a unique minimum

$$\text{Min}\left\{\frac{\omega}{\omega_o}\left[1+\left(\frac{\omega_o}{\omega}\right)^2\right]^{3/2}\right\} \cong 2.60, \text{ for } \omega = \sqrt{2}\,\omega_o; \tag{3.7a}$$

the condition

$$\frac{\omega_o}{\omega_c} \gtrsim 0.11, \quad \text{or} \quad \frac{[\rho\ Z/A]^{1/2}}{E(\text{GeV})\ H(\text{kG})} \gtrsim 1.3 \times 10^{-4}, \tag{3.7b}$$

implies that $\tilde{I}$ has a maximum in the vicinity of $\omega \simeq \sqrt{2}\,\omega_o$. According to (3.6b) the position of this spectral peak then is <u>independent</u> of the intensity of the magnetic field [see Fig. 2]. On the other hand when $\omega_c >> \omega_o$, the maximum of $\tilde{I}$ occurs at $\omega = 0.29\ \omega_c$, and this coincides with the usual synchrotron spectral peak.

Another distinctive feature of SC-radiation appears when (see (2.9b) and (3.2a,b) of [5])

$$\omega_m < \omega << \omega_o, \tag{3.8a}$$

since (3.5) in this case reduces to

$$\tilde{I} \to \frac{\omega}{\omega_o}\ \pi\left(\left[\frac{\omega_L}{\omega}\right]^2\right), \tag{3.8b}$$

where

$$\omega_L = \left[\frac{\omega_o^3}{\omega_c}\right]^{1/2}, \text{ or } \omega_L(\text{keV}) = 1642\left[\frac{E(\text{GeV})}{H(\text{kG})}\right]^{1/2}\left[\rho\,\frac{Z}{A}\right]^{3/4}. \tag{3.8c}$$

This leads to the characteristic <u>quenching</u> of SC-radiation in the spectral region $\omega < \omega_L$, i.e.

$$\tilde{I} \to 1.25\left[\frac{\omega_o}{\omega_c}\right]^{1/2}\exp\left\{-\left[\frac{\omega_L}{\omega}\right]^2\right\}. \tag{3.8d}$$

Many of the experiments we shall discuss later (Section 4) are concerned with measuring the sensitive variation of SC-radiation in this region.

All of the characteristics of SC-radiation are also manifest in the photon number spectrum; in fact this is the spectrum which is directly measurable with Si(Li) devices. It is convenient to specify this in terms of $N(\omega', \omega'')$, the number of photons in the frequency band $\omega' \leqslant \omega \leqslant \omega''$, radiated over path length L, per electron:

$$N(\omega', \omega'') = L(m) \int_{\omega'}^{\omega''} \frac{d\omega}{\omega} I, \tag{3.9a}$$

where

$$I = 0.118\ H(kG)\ \tilde{I}, \tag{3.9b}$$

and $\tilde{I}$ is given in (3.5). Since the energy resolution of the Si(Li) detection systems we plan to utilize is < 0.3 keV, we consider the increment

$$\omega'' - \omega' = 0.5 \text{ keV} \tag{3.10}$$

a conservative choice for the design of experiments. In particular the "count rate per channel per second" estimates given in Sections 4 and 5 are practically all based on the incremental photon number

$$\Delta N^*(\omega) \equiv N(\omega, \omega + 0.5\,\text{keV}) = \int_{\omega}^{\omega + 0.5} \frac{d\omega}{\omega} I \tag{3.11}$$

which represents the number of photons in the frequency band $\omega' \leqslant \tilde{\omega} < \omega + 0.5$ keV, radiated per meter per electron.

The experimental study of synchrotron-Čerenkov radiation is of course only possible under conditions where it can be reliably distinguished from other radiation processes by virtue of its angular distribution or dominant intensity [5,10]. On the "synchrotron branch", in the soft x-ray region and beyond, the principal competing process is Coulomb bremsstrahlung. In first approximation the photon number spectrum is given by

$$dN_c \simeq \frac{8\alpha}{9} L N_o \lambda_c^2 h(Z) \frac{d\omega}{\omega} \simeq 0.58\ L(mm)\ h(Z) \frac{d\omega}{\omega} \tag{3.12a}$$

where the auxiliary function h(Z) includes screening effects and Coulomb corrections

$$h(Z) = 6(\rho/A)(\alpha Z)^2\left[\ln(183\, Z^{-1/3}) + 0.083 - 1.20(\alpha Z)^2\{1-0.86(\alpha Z)^2\}\right]. \tag{3.12b}$$

Numerical values for representative cases are listed in Table 1 of reference [5].

If we restrict the energies of the incident particles to the range

$$E/mc^2 \gg 1600/Z, \tag{3.12c}$$

ionization losses which complicate the situation at lower energies may be ignored. The Bethe-Heitler spectrum (3.12a) then furnishes an essentially complete description of the Coulomb bremsstrahlung associated with the collision of ultra-relativistic particles with a single nucleus. However in condensed media a number of spectral modifications stemming from polarization and multiple scattering effects need to be taken into account [6]. For our present purposes the most important of these is a quenching of the Bethe-Heitler spectrum for frequencies in the range $\omega \lesssim \omega_o$, where ω_o is given by (3.6a & b). Specifically when $\hbar\omega_o \ll E$ the Bethe-Heitler expression (3.12a) goes over into the Ter-Mikaelian spectrum [6]

$$dN_c' \simeq \left(1 + \left[\omega_o/\omega\right]^2\right)^{-1} dN_c. \tag{3.13}$$

With the exception of a few experiments which are specifically intended for identifying background effects, e.g. the extinction of SC-radiation at low field levels and the Ter-Mikaelian modifications (3.13), all of the experimental design parameters given in Sections 4 and 5 have been chosen so that the SC-radiation effects exceed the Coulomb bremsstrahlung background by at least a factor of 5.

4. Experiments

Extensive surveys of the properties of SC-radiation in gases, liquids, and solids emitted by electrons in the energy range $0.5\ \text{GeV} \lesssim E \lesssim 1\ \text{TeV}$ with ambient field intensities $0.1\ \text{kG} \lesssim H \lesssim 2\ \text{MG}$ have been carried out. Some of these results have been reported in [5]. The specific experiments we propose to perform have been selected from this large inventory on the basis of the following criteria:

i) In order to establish the existence of SC-radiation it is essential to create experimental conditions in which there is a clear-cut correspondence between computations and measurements --- specifically the low energy quenching of SC-radiation should not be obscured or mimiced by other effects. It is for example clear from Fig. 5 that 12 GeV electrons radiating in N_2 at STP with an ambient field of 5 kG satisfy this criterion: The quenching region 5 keV $\tilde{<}$ ω $\tilde{<}$ 20 keV is situated far above the K-shell electron binding $\sim$0.6 keV, which is the largest characteristic energy that appears in the index of refraction. As a consequence the SC expression (3.5) should be valid, and the corresponding x-ray absorption in N_2 is small and slowly varying [see Figs. 6(a,b), 10]. Furthermore, as shown on Fig. 10, the quench region coincides with an essentially flat response region of the Si(Li) photon detector. Finally, as indicated on Figs. 5 & 6(a), the Coulomb bremsstrahlung background should not distort the spectra significantly.

ii) It is preferable that the experimental designs be matched to an energy range where electron beams with convenient features are available; for example easy beam deflection, alternate methods of energy calibration, and flexibility with respect to beam intensity and pulse structure. Beams at Cornell ($\sim$ 12 GeV) and SLAC ($\sim$ 20 GeV) appear to be suitable [compare Section 5(c)].

iii) The magnetic field requirements should be modest so that the construction of exotic and expensive high field devices (megagauss generators!) can be avoided. Our present experimental designs are restricted to field strengths of the order of 1 kG $\tilde{<}$ H $\tilde{<}$ 6 kG. Transverse field configurations in this range can presumably be furnished by standard dipoles and power supplies from laboratory inventory.

iv) The overall experimental designs should be as simple as possible: Economic realities dictate minimal budgets; and uncluttered experimental configurations tend to bolster confidence in the interpretation of the results.

Using these guidelines we have developed the experimental layout shown on the blueprint; this configuration is sufficiently flexible to carry out all the measurements corresponding to the "Research Objectives" stated in §§(1)-(3) of Section 1 --- the sole exception is the extinction measurement §(2-c) which is discussed in sub-section (E) below. The "layout drawn to scale" portions of the blueprint (III & III(a)) have been designed for an electron beam energy of 12 GeV and deflecting fields of 5 kG; these nominal dimensions can easily be modified for higher energies ($\sim$ 20 GeV) and corresponding field variations [compare Figs. 2, 3 & 5].

(A) Demonstration of the Existence of Synergic Synchrotron-Čerenkov Radiation:

We propose to demonstrate the existence of SC-radiation by utilizing the double scattering set-up shown on part I of the blueprint: An incident electron beam is deflected in two sequential scattering cells (#1 & 2) by transverse magnetic fields of 5 kG. Initially both cells are evacuated to $\tilde{<} 10^{-3}$ Torr (forepump vacuum). The electrons will emit synchrotron radiation [topmost curve on Figs. 6(a & b)] and the corresponding spectra will be detected and registered by the Si(Li)-multichannel analyzer system shown in part II of the blueprint. Next, one of the absorption cells --- for instance the cell downstream from scattering cell #2 --- is filled with N_2 at STP. The Si(Li) associated with scattering cell #1 should then continue to register the synchrotron spectrum, while the other Si(Li) detector should exhibit a synchrotron spectrum filtered through N_2 --- this corresponds to the dashed curve on Figs. 6(a) & (b); the transmissivity variation of the N_2 is given on Fig. 10. Of course the ratio of the synchrotron to the filtered synchrotron spectrum is completely determined by the (known) x-ray transmissivity of N_2, and this experiment serves as a check of the detection efficiency etc. of the dual scattering set-up. Now the decisive step is to fill scattering cell #1 with N_2 at STP --- the resulting spectrum registered by Si(Li) #1 should then correspond to the dashed red line indicated on Figs. 6(a) & (b). In other words, by physically changing the location of the N_2, we should be able to check directly on the essential characteristic of the synergism: synchrotron radiation

sequentially filtered through nitrogen yields a spectrum substantially different from synchrotron-Čerenkov radiation emitted in a nitrogen ambient.

The virtue of the dual scattering set-up is that the multiple options available in running the experiment with various N_2 and vacuum combinations in the scattering and absorption cells permit relative calibrations. This can be extended to sequences of relative calibrations linking synchrotron and SC radiation in N_2 at STP; SC radiation in N_2 at varying pressures; and SC radiation in a variety of other gases [compare §§(B)-(E) below].

It is clear from Figs. 6(a) & (b) etc. that the predictions of the synchrotron-Čerenkov theory have been presented in terms of the incremental photon spectrum $\Delta N^*(\omega)$ defined in (3.11). However the basic quantity which is determined experimentally is the photon count rate per channel in the multi-channel analyzer [see blueprint, part II]. If we denote this by ΔM, with units "counts/channel-sec", then theory and experiment are linked by

$$\Delta M = \Delta N^*(\omega)\ [a \times b \times c \times d \times e \times f \times g], \tag{4.1}$$

where the alphabetical chain corresponds to the following factors:

$$a = \frac{\text{photon energy interval}}{\text{MCA - channel}} \sim \frac{0.5\ \text{keV}}{\text{channel}}; \tag{4.2}$$

b = electronics pile-up rejection/live time correction ~ 1 for total count rates $< 10^5$/sec, or $> 10\,\mu$sec intervals between counts; (4.3)

c = Si(Li) detector energy efficiency ~ 1 for $\omega \gtrsim 3$ keV [see Fig. 10]; (4.4)

$$d = \text{Si(Li) detector geometrical efficiency} \sim \frac{\text{effective area of beam viewed by detector}}{\text{total area of beam}} \sim \frac{40\ \text{mm}^2}{80\ \text{mm}^2} \sim \frac{1}{2}; \tag{4.5}$$

e = effective length of electron trajectory for synchrotron radiation $\sim$0.022 meters (at Cornell); (4.6)

f = electrons per pulse [see (4.9d) et seq]; (4.7)

$$g = \text{pulses per second} \begin{cases} 60 - \text{Cornell;} \\ 360 - \text{SLAC.} \end{cases} \tag{4.8}$$

The beam intensity and beam time requirements [Section 5(c)] are of course compounded from the values chosen for the parameters f and g; where the latitude in adjusting f is constrained principally by the maximum count rate tolerated by the Si(Li)-MCA detection system. The nominal values suitable for various experiments can be obtained by considering the total photon counts per pulse. If we denote this parameter by M, then obviously (4.1) implies

$$M = \int d\omega \; \Delta N^*(\omega) \; [a \times b \times c \times d \times e \times f], \tag{4.9a}$$

where the integral in principle extends over the entire spectrum (or all MCA channels). In our "canonical" example [E ~ 12 GeV, H ~ 5 kG, N_2 at STP] the SC spectrum [Fig. 6(a)] roughly coincides with the flat portion of the Si(Li) energy efficiency c [Fig. 10 and (4.4)], and so we can approximate (4.9a) by

$$M \approx \frac{f}{2} \times 0.022 \times \int d\omega \; \Delta N^*(\omega). \tag{4.9b}$$

The total number of SC photons for our "canonical" example is (compare (3.16c) of [5])

$$\int d\omega \; \Delta N^*(\omega) \cong N_T \sim \frac{1}{2}, \tag{4.9c}$$

and therefore

$$f \sim 200 \; M. \tag{4.9d}$$

We can now distinguish two cases:

Cornell - Here the beam spill is 2 msec, and therefore from (4.3) we obtain the bound

$$M < 200 \text{ photon counts per pulse.} \tag{4.10a}$$

The corresponding number of electrons per pulse then is

$$f \sim 4 \times 10^4. \tag{4.10b}$$

SLAC - In this instance the accelerator pulse duration is 1.6 μ sec. In order to avoid pile-up and spectral distortions we ought to work at the conservative limit

$$M \sim 1 \text{ photon count per pulse;} \tag{4.11a}$$

which corresponds to a beam structure of

$$f \sim 2 \times 10^2 \; e^-/\text{pulse.} \tag{4.11b}$$

Finally if we interpret experiment (A) in the stringent terms of a comparison of the count rates only in the energy bin 5 - 5.5 keV for synchrotron radiation filtered through 50 cm of N_2 at STP [dashed line on Fig. 6(a)] and SC-radiation [dashed red line on Fig. 6(a)], we find that the synchrotron radiation count rates are given by

$$\Delta M(\text{synchr.}) \simeq 0.8 \times 10^{-2} \times \tfrac{1}{2} \times 2.2 \times 10^{-2} \times \begin{cases} 4 \times 10^4 \times 60 \text{ (Cornell)}; \\ 2 \times 10^2 \times 360 \text{ (SLAC)}; \end{cases} \tag{4.12a}$$

or

$$\Delta M(\text{synchr.}) \sim \begin{cases} 200 \text{ counts/sec (Cornell)}; \\ 6\text{-}25 \text{ counts/sec (SLAC)}. \end{cases} \tag{4.12b}$$

The × 4 SLAC enhancement is associated with a lengthening of the effective path (e) from ~ 2 cm due to the higher energy and a different H-value.

The corresponding count rates for SC-radiation at 5 keV are given by

$$\Delta M(\text{SC}) \simeq 1.6 \times 10^{-4} \times 1.1 \times 10^{-2} \times \begin{cases} 2.4 \times 10^6 \text{ (Cornell)}; \\ 7.2 \times 10^4 \text{ (SLAC)}; \end{cases} \tag{4.13a}$$

or

$$\Delta M(\text{SC}) \sim \begin{cases} 4 \text{ counts/sec (Cornell)}; \\ 0.1 - 0.4 \text{ counts/sec (SLAC)}. \end{cases} \tag{4.13b}$$

The background count-rate in an ordinary laboratory environment for an unshielded Si(Li) system, in the range 5 - 5.5 keV, is

$$\Delta M(\text{noise}) < 0.2 \text{ counts/sec}. \tag{4.14a}$$

We hope to be able to minimize the enhancement of this background in the accelerator experimental areas by installing specially machined heavimet shielding around the Si(Li) detector heads. As the blueprint indicates there will be additional radiation safeguards positioned upstream on the e^- and γ beam lines. All of these precautions should yield noise levels below the limit

$$\Delta M(\text{noise}) < 1 \text{ count/sec-channel}. \tag{4.14b}$$

In view of the conservative choice of all design parameters we consider that the sequence of estimated count rates (4.12a - 4.14b) establishes in a convincing fashion the feasibility of distinguishing the suppression of SC-radiation relative to ordinary synchrotron radiation. The corresponding beam time requirements are of the order of one hour [compare Section 5(c)]. As a final caution we note that our "canonical" example really applies to Cornell; the corresponding SLAC numbers are given *in extenso* in reference [5] and Figs. 2 and 3. Naturally the "canonical" example shows off the low SLAC duty cycle to poor advantage, e.g. in (4.13b). A slight upward adjustment of the magnetic field (see Figs. 2, 3 and 5) yields count rates at levels comfortably above the noise.

(B) *Measurement of the Synchrotron-Čerenkov Spectrum in Nitrogen at STP*:

This experiment is similar to the preceding --- however instead of measuring the photon count rate only in the bin 5.0 - 5.5 keV, it should be possible to record the entire spectrum in the range $5 \lesssim \omega \lesssim 30$ keV [see Figs. 6(a) and (b)]. The relative variations of the synchrotron spectrum filtered through N_2 and the corresponding SC spectrum are shown on Fig. 7. The minimum value (1/20 at 5 - 5.5 keV) is the ratio given in (1.1). All of the experimental design features discussed in connection with (A) above apply *mutatis mutandis* to the measurement of the entire spectrum. The only difference is that at the higher photon energies the signal/noise ratio becomes more favorable. For instance at $\omega \sim 7$ keV the SC count rates increase from (4.13b) to

$$\Delta M(SC) \sim \begin{cases} 175 \text{ counts/sec (Cornell)}; \\ 4\text{-}17 \text{ counts/sec (SLAC)}. \end{cases} \tag{4.15}$$

Verifying the relative photon count rate curve of Fig. 7 is a strong test of the SC theory because most of the calibration uncertainties cancel out in this ratio. On the other hand it is clearly desirable to sharpen the experiments to the point where some absolute calibration of radiation rates can be made. Basically this involves accurate measurements of the "alphabet" chain in (4.1). In particular the e^- beam flux can be monitored by the veto-scintillation counter sequence $A_1 S_1$ - $S_2 A_2$ shown on the blueprint. With fast scintillators

and photomultiplier assemblies, e.g. a small NE-114 plastic matched to an RCA 8575, the total counter dead time can be reduced below 10 nsec. This corresponds to a maximum count rate of

$$f \sim 2 \times 10^5 \ e^-/2 \text{ msec} \quad \text{(Cornell)}; \tag{4.16a}$$

or

$$f \sim 160 \ e^-/1.6 \ \mu\text{sec} \ \text{(SLAC)}. \tag{4.16b}$$

Clearly the rates (4.10b)-(4.16a) and (4.11b)-(4.16b) are compatible. For completeness sake we note that detector system electronics (part II of the blueprint) also provides the option of linking the e^- and γ counting chains through fast/slow coincidence logic.

The total beam time required for accumulating statistics over the entire SC spectrum adequate for $\pm 5\%$ precision is less than one hour.

(C) Variation of the Synchrotron-Čerenkov Spectrum as a Function of Nitrogen Pressure:

One of the basic features of SC radiation is its sensitive dependence on the environment; and one of the principal environmental parameters that can be conveniently controlled is density. The theory of this effect is given in [5]. It turns out in first approximation that the total emission due to Coulomb bremsstrahlung and SC-radiation can exhibit a minimum in certain spectral regions as the density is increased. This phenomenon is illustrated on Fig. 4. For experimental purposes it is of course convenient to recast this in terms of the photon number spectrum; the "dip" then turns into a shallow "dog leg". In addition one has to take into account the density dependence of the self-absorption in the scattering cells. The net effect of these competing processes for our "canonical" example --- 12 GeV electrons traversing 5 kG fields in gaseous nitrogen --- is displayed on Fig. 8. In particular the curve marked "B" indicates the following counts per second for the 6 - 6.5 keV channel:

ρ/ρ_o	≈ 0	1/2	1
Cornell	1000	160	16
SLAC	30	5	0.5

(4.17)

The standard density ρ_o corresponds to N_2 at STP. Since N_T for $\rho/\rho_o \approx 0$ is approximately 3 [compare (4.9c)] the beam intensities will have to be monitored for pile-up and possibly lowered somewhat for this run. Otherwise the count rates are satisfactory. Fig. 8 also shows the corresponding synchrotron radiation rates with sequential absorption in N_2 of variable density. Clearly the simplest way of running this experiment is to fill both the scattering cell #1 and the absorption cell #2 with N_2 at density ρ, maintain the rest of the system at vacuum, and collect the spectra with the Si(Li) detectors #1, 2. With this arrangement the 6 - 6.5 keV channel of Si(Li) #1 should yield a point on curve B, and the corresponding channel for Si(Li) #2 should read out a point on B'. The ratio variations for several spectral windows are shown on Fig. 9. Each run should take about 1/2 hour, and perhaps one might want to check 5 densities in the interval $0 \lesssim \rho \lesssim \rho_o$. The extended range $\rho_o \leqslant \rho \lesssim 3\rho_o$ is also interesting, but the feasibility of these measurements will depend on the availability of windows for the gas/vacuum partitions thin enough to minimize spectral distortions [see Fig. 10] but strong enough to withstand the pressure differentials.

(D) Measurement of the Synchrotron-Čerenkov Spectrum in Argon, Air, and Krypton:

The extension of the spectral measurements described in §§(A)-(C) to other gases at various densities is straightforward: The essential precautions are (i) that the spectral ranges have to match the Si(Li) detector efficiency [$5 \lesssim \omega \lesssim 40$ keV on Fig. 10]; (ii) the optical transmissivities have to be high enough for reasonable x-ray yields [Fig. 10]; and (iii) the photon counting rates have to fall in a range above the noise level (4.14b), and below pile-up (4.3) with a minimum of accelerator beam retuning. The set-up shown on the blueprint can then be used without modification.

We have already indicated in Section 1, §(3) that there are three gases which ought to be investigated in the initial round of experiments. These are:

(a) Argon (Z = 18) at STP because the K-edge is at 3.2 keV and the corresponding K-shell binding energy is 4.77 keV/electron.

The index of refraction can therefore not be represented by the simple asymptotic form (3.4a), and consequently the SC spectrum below 15 keV will reflect the incipient effects of absorption and strong dispersion. The modifications of (3.5) have been considered theoretically [10], but before extensive computations are carried out it would be useful to have guidance from experiment.

(b) Air at STP. Air is essentially a mixture of nitrogen and oxygen --- which are equivalent for purposes of SC-radiation. The 1% admixture of argon may however significantly affect the SC spectrum in the range below 15 keV. It will be interesting to see how the results of $\zeta(B)$ and (a) above fit together with the results for air.

(c) Krypton (Z = 36) at 0.1 bar and STP. The K-edge for krypton is at 14.3 keV and the K-shell binding energy is at 17.9 keV/electron. The L-edge is at 1.9 keV. In these cases the SC spectrum should reflect the index of refraction variations which occur between the K and L edges, in the range $5 \lesssim \omega \lesssim 40$ keV. Our preliminary design studies indicate that SC radiation from krypton in this spectral region is suitable for the construction of "magnetic" Čerenkov counters [7]. This experiment should yield values for the dispersive and absorptive components of the index of refraction pertinent to the design of the counters.

(E) The Extinction of Synchrotron-Čerenkov Radiation:

The curves shown on Figs. 2, 3, and 5 all illustrate the surprising feature that SC-radiation "turns off" exponentially under the conditions (compare (3.15a) of [5])

$$E(\text{GeV})\, H(\text{kG}) \lesssim 600\, [\rho\, Z/A]^{1/2}. \tag{4.18a}$$

For N_2 the RHS is approximately 15, and therefore the extinction region corresponds to the field strengths

$$H \sim 0.8 \text{ kG (SLAC)}; \qquad H \sim 1.3 \text{ kG (Cornell)}. \tag{4.18b}$$

Although the standard double scattering configuration shown on the blueprint is suitable for measuring the variation of the SC spectrum as a function of magnetic field strength, there are practical limits

set by the electron deflection geometry [see III(a) of the blueprint]. Specifically, the two vacuum "Y" sections, downstream from the scattering cells, will be equipped with adjustable bellows (forepump vacuum!) so that some flexibility is possible in repositioning the γ and e^- beam pipes. This arrangement is adequate for experiments of the following kind: fill the scattering cells 1 and 2 with N_2 at STP; fix the field in cell #1 at 5 kG and in cell #2 at 4.5 kG; then the SC photon count ratio (#1/#2) in the channel 6 - 6.5 keV will be ~ 2 for incident electron energies ~ 12 GeV [see Fig. 5]. The corresponding ratio for ordinary synchrotron radiation is 1.07. However larger field reductions such as 5 kG $\rightarrow$ 1 kG are not feasible with this set-up, and so we propose that at the end of the experimental series the configuration be changed to a single scattering cell positioned in ~ 4m of ~ 1 kG field: This can easily be accomplished by rearranging all the magnets around scattering cell #1 (stretched to ~ 4 m) and modifying the downstream e^- and γ beam pipes. The basic dimensions of the experimental area (2m x 25 m) would be unchanged, and we could still obtain satisfactory separation between the γ and e^- beams (~ 11 cm).

This "single arm" set-up could also be used for detecting the Ter-Mikaelian modifications of the Bethe-Heitler spectrum [Section 1 §(4a)]. In N_2 at STP these effects should appear as a quenching of the Coulomb bremsstrahlung below 12 keV; these "soft" photons should be emitted at angles of the order of 0.4 mrad with respect to the beam. Since we are assuming a nominal beam divergence of $\pm$ 0.5 mrad [the beam for E-78 at SLAC was sharpened to $\pm$ 10 μrad!] it should be possible to distinguish the γ-halo. Of course the extinction of SC radiation leads to the elegant possibility of deflecting the e^--beam away from the γ-detector without blinding it with synchrotron photons; the Ter-Mikaelian effect should then be easily discernible.

(F) Quantum Modifications of the Synchrotron Spectrum:

It has recently been shown that the classical synchrotron spectrum [see (3.2d-f)]

$$I_{Cl} \sim \varkappa(\omega/\omega_c) \tag{4.19}$$

is modified by quantum corrections for photon energies comparable to

$2\ mc^2 \sim 1$ MeV [2,8]. Schematically these corrections correspond to

$$I_Q \leftrightarrow \pi \left[\frac{\omega}{\omega_c} \left(1 + \frac{\hbar\omega}{E} \right) \left(1 - \left\{ \frac{\hbar\omega}{2\ mc^2} \right\}^2 \right)^{3/2} \right]; \quad \hbar\omega < mc^2, \quad (4.20)$$

which exhibits the surprising fact that the second order terms $(\hbar\omega/mc^2)^2$ completely dominate the first order $(\hbar\omega/E)$ corrections. Useful approximations for I_Q have been derived in [2] and [8]; numerical evaluations are now in progress [9]. Fig. 11 shows a representative comparison of the classical and quantum mechanical results for E = 12 GeV, H = 10 kG. It is clear that the divergences are large enough to be measured. The dual scattering set-up shown on the blueprint could easily be adapted for this purpose: The essential changes would be the substitution of Ge(Li) for Si(Li) detectors, and altering the magnets to provide field strengths in excess of 10 kG.

5. Experimental Design Considerations

(a) Layout of the Experiment - The plan of the complete experiment, including all principal components, is shown on the blueprint. The scale of the experimental area (2m × 25m) is determined by the electron beam energy ($\sim$ 12 - 20 GeV), the $\int H\, d\ell$ of the deflecting fields ($\sim$ 10 kG-m for each scattering cell), and the lateral clearance required downstream on the e^- and γ beams at the detectors ($\sim$ 11 cm).

Protection against background radiation and halo originating upstream from cell #1 will be provided by 20 cm thick heavimet collimators with $\lesssim$ 5 mm beam holes --- an analogous system worked well in our earlier SLAC experiments [11]. We will mate the exterior of the collimators to a lead plug which can serve as a template for a lead brick shield. A second line of defense is shown on III(a) of the blueprint: the synchrotron and SC photons incident on the Si(Li) detectors will be selected from the midregion of the scattering cells --- this yields a divergence of 11 mrad between the forward e^- beam halo and the photons of interest. The corresponding divergence of the e^- beam is 14 mrad. Finally the Si(Li) detector heads will be protected with specially machined heavimet shields for ordinary operation, and safety stoppers to prevent "burnout" by the direct e^--beam. The overall background levels under "beam on" conditions can

of course be checked with the $A_1 S_1 S_2 A_2$ - Si(Li) counting system [see §(b)].

In order to avoid soft x-ray absorption and/or spectral distortions it is necessary to run all γ-beams in $\tilde{<} 10^{-3}$ Torr (forepump) vacuum (see Fig. 10). We can also suppress the Coulomb bremsstrahlung background by running the e^--beams in forepump vacuum. The multiple scattering divergence is of the order of

$$\Delta\theta(\text{mrad}) \sim \frac{21\, \ell_{RL}^{1/2}}{E(\text{GeV})} , \qquad (5.1)$$

where ℓ_{RL} is the interposed thickness of material measured in radiation lengths. One can easily check that this is negligible ($\tilde{<}$ 0.1 mrad) in the proposed set-up. All the beam pipe plumbing is straightforward: The only points requiring care are: (i) scattering cells #1 and 2 have to be separated from the rest of the system by thin windows (mylar, Be, etc.) so that gases can be admitted and flushed out; (ii) the "Y" sections where the e^- and γ beams separate should be fitted with flexible bellows joints so that the downstream beam lines can be moved; (iii) the Be windows and flanges protecting the Si(Li) detectors should be matched to the γ-beam lines and heavimet shields so as to minimize the thickness of any air layer (< 5 mm); (iv) the e^- beam-lines must be interrupted to accommodate the scintillators S_1 and S_2; (v) the clearance between the e^- and γ beam centerlines downstream from cell #1 is about 11 cm (III(a) of the blueprint) --- this constrains the bulk of the dipole magnets installed around cell #2.

We expect to procure, fabricate, and assemble most of the subsystems required for the experiment. However it would be convenient if the accelerator laboratory could furnish the deflection magnets and power supplies: Since we do not require precise field homogeneity the 2m of transverse field for the scattering cells could be furnished simply by butting two 1m dipoles; naturally their cooling capacity should be compatible with operation at 5 kG.

(b) Detectors and Electronics - We propose to measure the γ spectra with Si(Li) detector systems [Ortec 7000 series, or equivalent]. These have a conservatively rated energy resolution of 300 eV FWHM

in the energy range of principal interest, 5 - 15 keV. Due to the fact that the magnetic fields sweep the electrons away from the synchrotron-Čerenkov photon beams, the solid state detectors will not be illuminated by e^- --- in this respect the experiment is much easier than the detection of transition radiation. Furthermore, as indicated in Section 4(A), the photon flux is sufficiently high and adjustable so that the input counting rates for the Si(Li) systems can be kept in the range 10^3 - 10^4 sec^{-1} --- this corresponds to an optimum compromise for minimizing accelerator beam time [circa 1/2 hr/spectrum; §(c) below] and maximizing the γ-energy resolution. The Si(Li) detectors will be mounted on 30 ℓ Dewars; the liquid nitrogen coolant will have to be replenished every 20 days.

The electronics associated with the Si(Li) detector system is indicated on part II of the blueprint: The specific components are:

[Si(Li)] - [bias/HV supplies] - [amplifiers/pulse shapers] - [multiplexer] - [sum amplifier] - [MCA] .

The electron beams will be monitored by conventional scintillators and fast logic. In particular S_1 and S_2 will be made with NE-114 (or equivalent) plastic with an intrinsic decay time of 4 nsec; since the e^--beams will be $\lesssim$ 1 cm in diameter, the counters can be compact and the total light decay time should be limited to ~6 nsec. If the light pulses are detected and amplified with RCA 8575 (or equivalent) PM assemblies, we can realistically expect clean pulses with dead-times below 10 nsec. The veto counters $A_{1,2}$ will be shaped in annular form to provide clearance for the e^- beams.

The detectors and fast logic associated with the four scintillators $S_{1,2}$ and $A_{1,2}$ are indicated on part II of the blueprint: The specific components are:

[scintillator] - [PM assembly (base/shield)] - [HV supply] - [discriminator] - [delay] - [coincidence] - [scaler] .

Finally, for absolute calibration of the entire set-up in terms of the synchrotron radiation rate, a fast/slow link between the e^- counters and the γ counters is essential. This is also shown on part II of the blueprint. The specific components are:

[scintillator] - [shaper/filter] - [constant fraction discriminator] - [delay] - [coincidence] - [gate/delay] .

(c) Beam Characteristics and Beam Time Requirements - The experiment has been designed to function at either 12 GeV or 20 GeV; variations of $\pm$ 1 GeV can easily be accommodated. However once an energy has been selected, it would be desirable to maintain a precision of $< \pm 0.2$ GeV throughout the entire series of experiments. We note in this connection that the double scattering set-up is effectively a spectrometer that can monitor the e^- energy to $\pm 5\%$.

The e^- beam cross-section, uniformity, and divergence enter principally in determining the effective source dimensions for synchrotron-Čerenkov emission --- these are the factors d (4.5) and e (4.6) of Section 4(A). We have assumed that the beam is cylindrical with 1 cm diameter, uniform in intensity, and has a total horizontal divergence of 1 mrad. None of these constraints is really critical as far as the success or failure of the experiment is concerned. Nevertheless we should try to achieve a beam quality matching these nominal values: For instance the total e^- beam spread at Si(Li) #1 is about 3 cm; with a generous allowance for halo this is increased to about 6 cm --- a sloppier beam would probably degrade the signal/noise by enhancing the background at detector #1. Similarly non-uniformities in lateral intensity will complicate the computer unfolding which is ultimately necessary to determine the effective radiating length e (4.6).

We can conservatively assume that the time required for set-up and test will not exceed that of the IIT megagauss experiment at SLAC which involved similar but more complicated apparatus. This implies that

beam time for set-up and test.....4 hours. (5.1)

The rest of the beam time can easily be inferred from the individual experimental descriptions given in Section 4(A)-(E). Assuming a total of 30 spectral measurements --- including cross-calibrations --- each requiring 1 hour for beam time and adequate statistics, we estimate

beam time for experiments (A)-(E)....30 hours. (5.2)

These time requirements are based on the following beam intensity parameters:

Cornell [see (4.8) and (4.10b)]

$$2 \text{ msec spill; } 4 \times 10^4 \text{ e}^-/\text{pulse} \times 60 \text{ pulses/sec} \rightarrow 2 \times 10^6 \text{ e}^-/\text{sec;} \tag{5.3}$$

SLAC [see (4.8) and (4.11b)]

$$1.6\ \mu\text{sec spill; } 2 \times 10^2 \text{ e}^-/\text{pulse} \times 360 \text{ pulses/sec} \rightarrow 10^5 \text{ e}^-/\text{sec.} \tag{5.4}$$

It would also be desirable to schedule a run at reduced intensity (peak rate of 3×10^4 e$^-$/sec) for absolute calibration of the Si(Li) system in terms of the synchrotron spectrum. One can easily check that at Cornell this would require a

reduced intensity calibration run.....2 hours. (5.5)

The lower duty cycle at SLAC would probably lengthen this by a factor of 3. If we finally allow a few hours of squandered time due to human error and equipment failure, we arrive at a total beam time estimate of circa 40 hours.

(d) Tentative Experimental Schedule - In analogy with the arrangements worked out with SLAC for the megagauss bremsstrahlung experiments [June-December 1970] we propose that most of the design, construction, assembly, and test of the experimental configuration shown on the blueprint be carried out at the IIT Magnet Laboratory. We have well equipped facilities and access to excellent supporting staff for help with mechanical and electronics problems. All of these experimental preliminaries should be complete in about 7 months. Dismantling the system at IIT and reassembling at the accelerator laboratory should take 1 1/2 months. Set-up and test on the accelerator floor, judging by our SLAC experience, should take another month. Thereafter it is a matter of scheduling the 40 hours of beam time, cf (5.2), and digesting the experimental results --- this stage could be completed in 1 - 2 months. This implies that the total time duration for occupying space in the accelerator experimental area is circa 4 months. Of course we hope that the results will be considered sufficiently significant so that additional work can be undertaken to push the

construction and test of "magnetic" Čerenkov counters and to check on the existence of the quantum modifications [Section 4(D-C), 4(F)].

The general routine of performing complex experiments at remote locations is familiar to the IIT Magnet Laboratory: During the period 1965-1970 we carried out extensive explosives experiments at our Indiana Laboratory; and in 1970-1971 took 24 tons of equipment with us to set up the megagauss bremsstrahlung experiment at SLAC.

6. References

1. T. Erber, Notices Am. Math. Soc. 22, No. 4, A472 (1975).
2. T. Erber, D. White, H. G. Latal, Acta Phys. Austriaca 44, 315-336 (1976); 45, 29-64 (1976).
3. J. Schwinger, W-Y. Tsai, T. Erber, Annals of Phys. (NY) 96, 303-332 (1976).
4. T. Erber, D. White, W-Y. Tsai, H. G. Latal, Bull. Am. Phys. Soc., Ser. II, 20, 1500 (1975).
5. T. Erber, D. White, W-Y. Tsai, H. G. Latal, Annals of Phys. (NY) [in press, 1976].
6. M. L. Ter-Mikaelian, "High Energy Electromagnetic Processes in Condensed Media", Wiley-Interscience, New York, 1972.
7. T. Rynne and T. Erber (in preparation).
8. H. G. Latal and T. Erber (in preparation).
9. G. B. Baumgartner, T. Rynne, T. Erber (in preparation).
10. Wu-Yang Tsai and T. Erber (in preparation).
11. F. Herlach et al. IEEE Trans. Nucl. Sci. NS-18, No. 13, 809-814 (1971).

7. Figures and Blueprint

Fig. 1 Graph of the bremsstrahlung function $\varkappa(z)$; compare (3.2e).

Fig. 2 Characteristics of synchrotron-Čerenkov radiation by electrons in N_2 at STP. The variation of the spectral intensity I (3.9b) is displayed as a function of ω and H for a number of illustrative cases. The divergence between synchrotron-Čerenkov radiation and the ordinary synchrotron spectrum is indicated by the dashed line marked I^S. The arrows mark the position of the spectral peak $\mathcal{E}_{max}$. The lower limits for all curves, except H = 0.7 kG, correspond

to the Coulomb bremsstrahlung break-even condition $I \tilde{>} 3.8 \times 10^{-3}$.

Fig. 3 Characteristics of synchrotron-Čerenkov radiation by electrons in N_2 at STP. The variation of the spectral intensity I (3.9b) is displayed as a function of ω and E for a number of illustrative cases. The divergence between synchrotron-Čerenkov radiation and the ordinary synchrotron spectrum is indicated by the dashed line marked I^s for the particular case E = 200 GeV. The lower limits for all curves correspond to the Coulomb bremsstrahlung break-even condition $I \tilde{>} 3.8 \times 10^{-3}$.

Fig. 4 Variation of synchrotron-Čerenkov radiation with density of N_2. The intensity I (3.9b) at ω = 5 keV and 20 keV is displayed as a function of the density ratio: vacuum = $0 \leqslant \rho \leqslant \rho_o = N_2$ at STP. The dashed lines correspond to synchrotron-Čerenkov radiation; the dash-dot portions indicate the Coulomb bremsstrahlung contribution: the solid curves represent the total spectral intensity.

Fig. 5 Synchrotron-Čerenkov photon number spectra for 12 GeV electrons radiating in N_2 at STP. The dashed curves indicate the corresponding spectra for synchrotron radiation; these diverge as $\omega^{-2/3}$ for $\omega \to 0$. The curves terminate below at the Coulomb bremsstrahlung break-even. The approximations leading to (3.5) cease to be valid for energies below $\hbar\omega_m$.

Figs. 6 (a & b) Synchrotron-Čerenkov histograms for 12 GeV electrons and 5 kG fields. ΔN^* (3.11) denotes the number of photons with energies between ω and ω + 0.5 keV radiated per electron per meter. Reading from the top the curves denote (1) synchrotron radiation; (2) synchrotron radiation filtered by 50 cm of N_2 at STP; (3) synchrotron-Čerenkov radiation and Coulomb bremsstrahlung in N_2 at STP; (4) synchrotron-Čerenkov radiation in N_2 at STP; (5) radiation (3) filtered through 50 cm of N_2 at STP; (6) radiation (4) filtered through 50 cm of N_2 at STP. The experimentally observed SC-radiation should be more intense than histogram (5)

because the nominal 50 cm absorption is actually too pessimistic by a factor ~ 2.

Fig. 7 The histogram ratio (2)/(5) of Figs. 6(a,b).

Fig. 8 This is a counterpart of Fig. 4. The curves display the photon number spectrum ΔN^* (3.11), and include Coulomb bremsstrahlung as well as self-absorption in 50 cm of N_2 at variable density. The corresponding synchrotron curves exhibit the effects of sequential filtering in N_2 of matching densities.

Fig. 9 Histogram ratios for Fig. 8. The curve $\tilde{A}$ corresponds to the ratio A/A', etc.

Fig. 10 Curves exhibiting the Si(Li) detector efficiency [Ortec data for series 7000] and nitrogen transmissivity ["Practical X-Ray Spectrometry" R. Jenkins and J. L. De Vries, Springer, New York, 1969].

Fig. 11 Quantum corrections for synchrotron radiation by 12 GeV electrons in 10 kG fields. The "classical" curve represents (3.2f); the quantum modifications correspond to (7.84c) of reference [2].

Blueprint (appended) Layout of Synchrotron-Čerenkov Experiment.

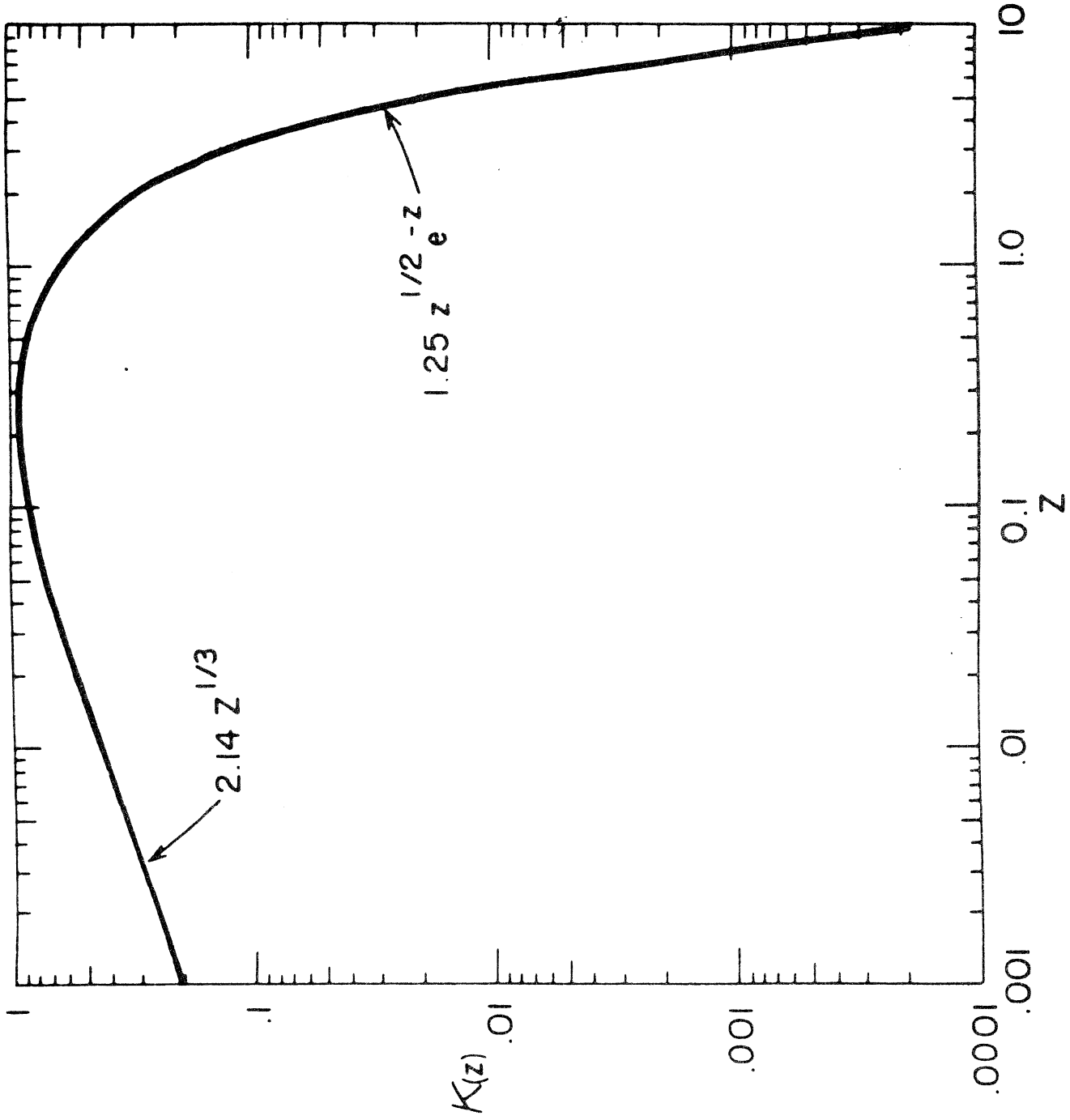

Figure 1

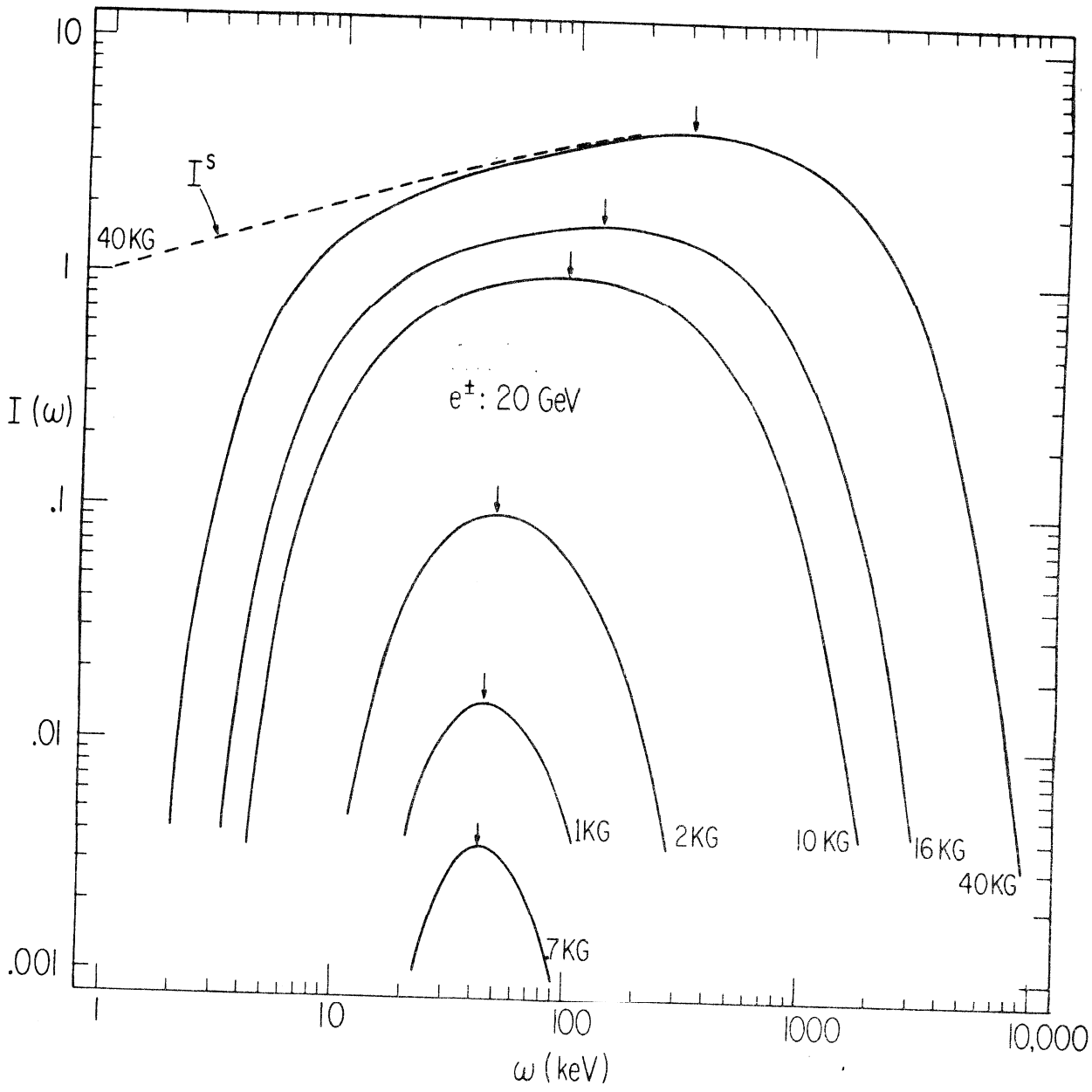
10
1
.1
.01
.001
I (ω)
I^s
40KG
e±: 20 GeV
7KG
1KG
2KG
10 KG
16 KG
40KG
1
10
100
1000
10,000
ω (keV)

Figure 2

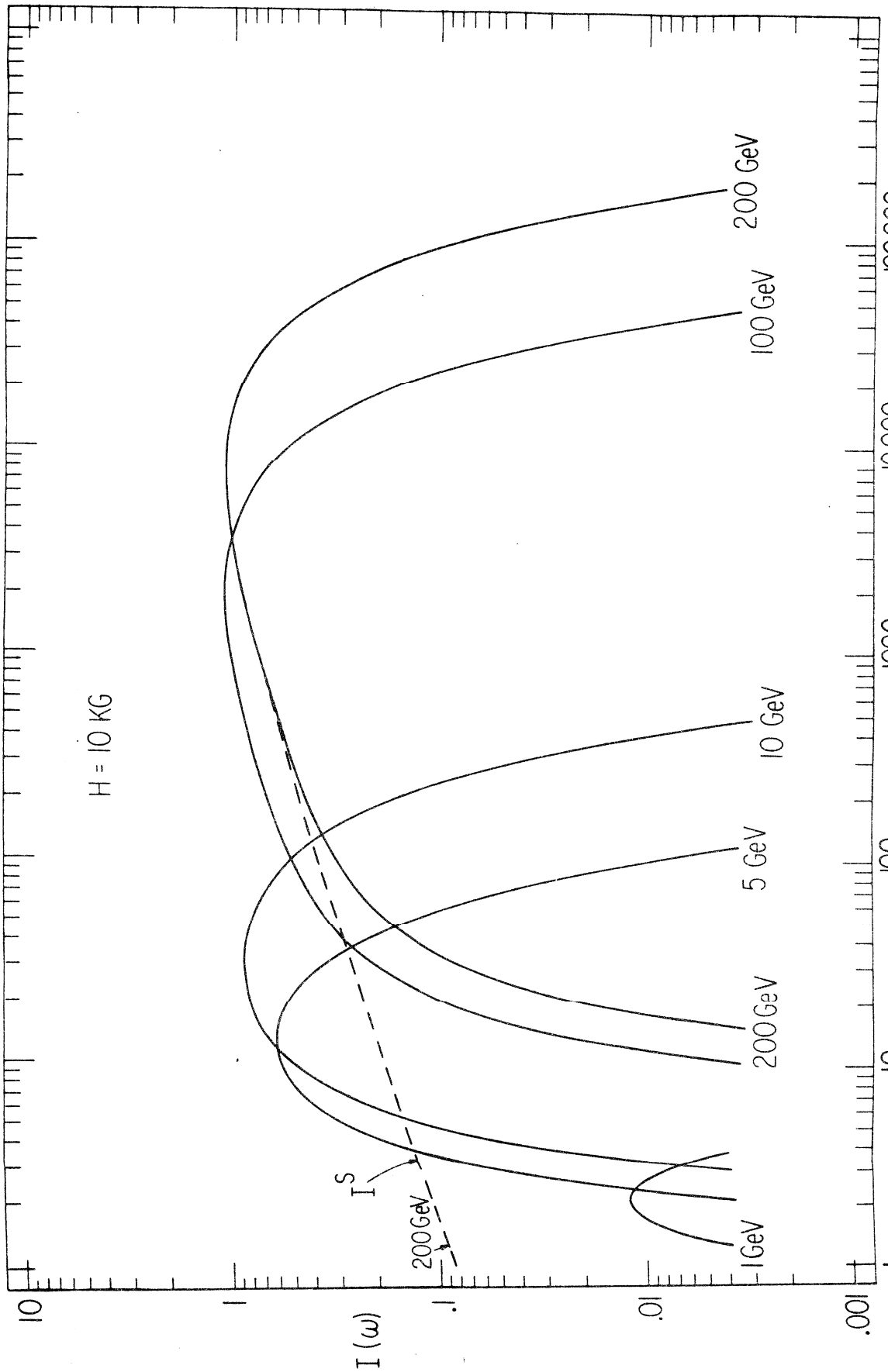
H = 10 KG
200 GeV
100 GeV
10 GeV
5 GeV
200 GeV
1 GeV
I^S
200 GeV
I (ω)
ω (keV)
10
1
.1
.01
.001
1
10
100
1000
10,000
100,000

Figure 3

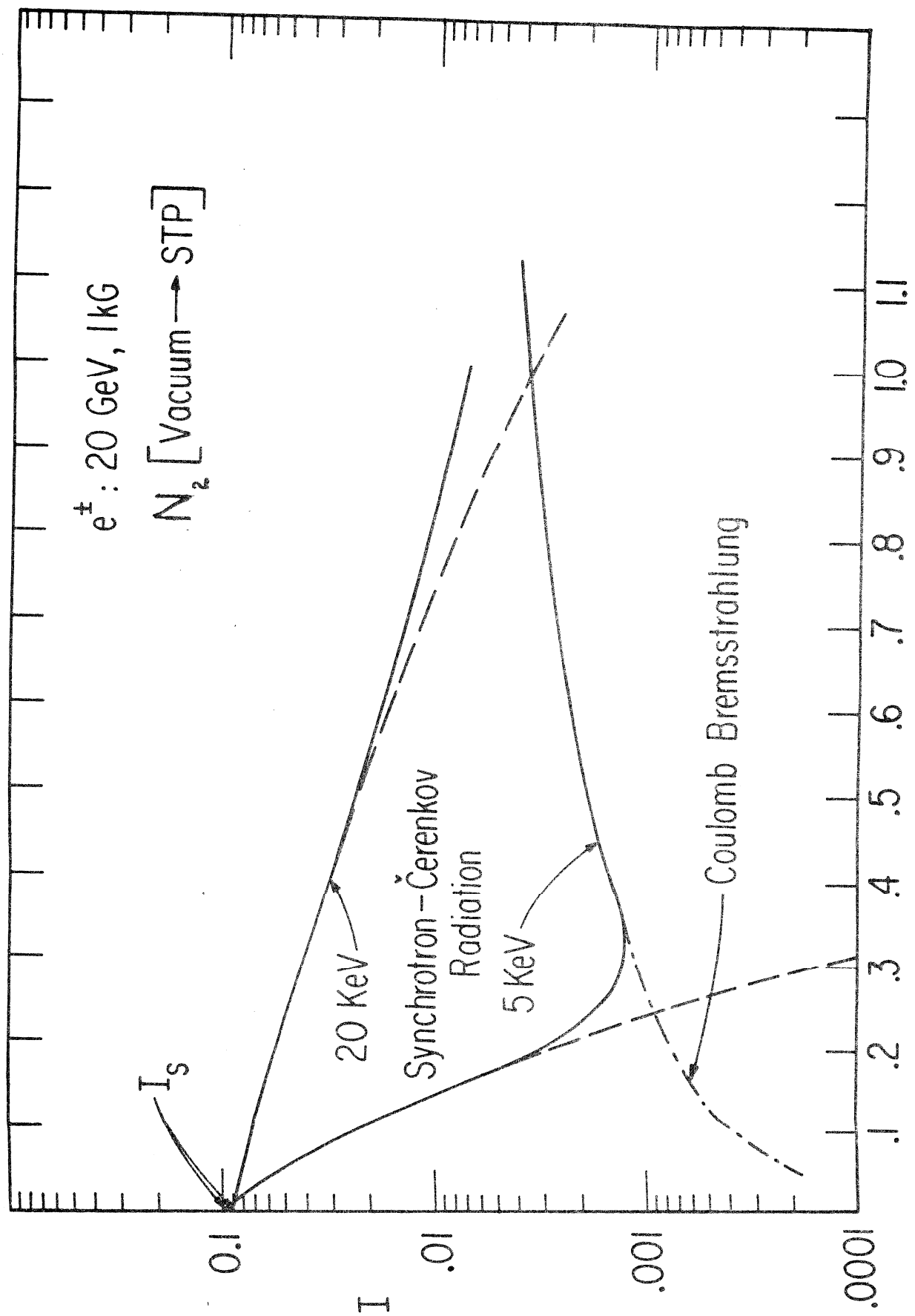
e±: 20 GeV, 1 kG
N2 [Vacuum → STP]
I
I_S
20 KeV
Synchrotron-Čerenkov Radiation
5 KeV
Coulomb Bremsstrahlung
0.1
.01
.001
.0001
.1
.2
.3
.4
.5
.6
.7
.8
.9
1.0
1.1
ρ/ρ0

Figure 4

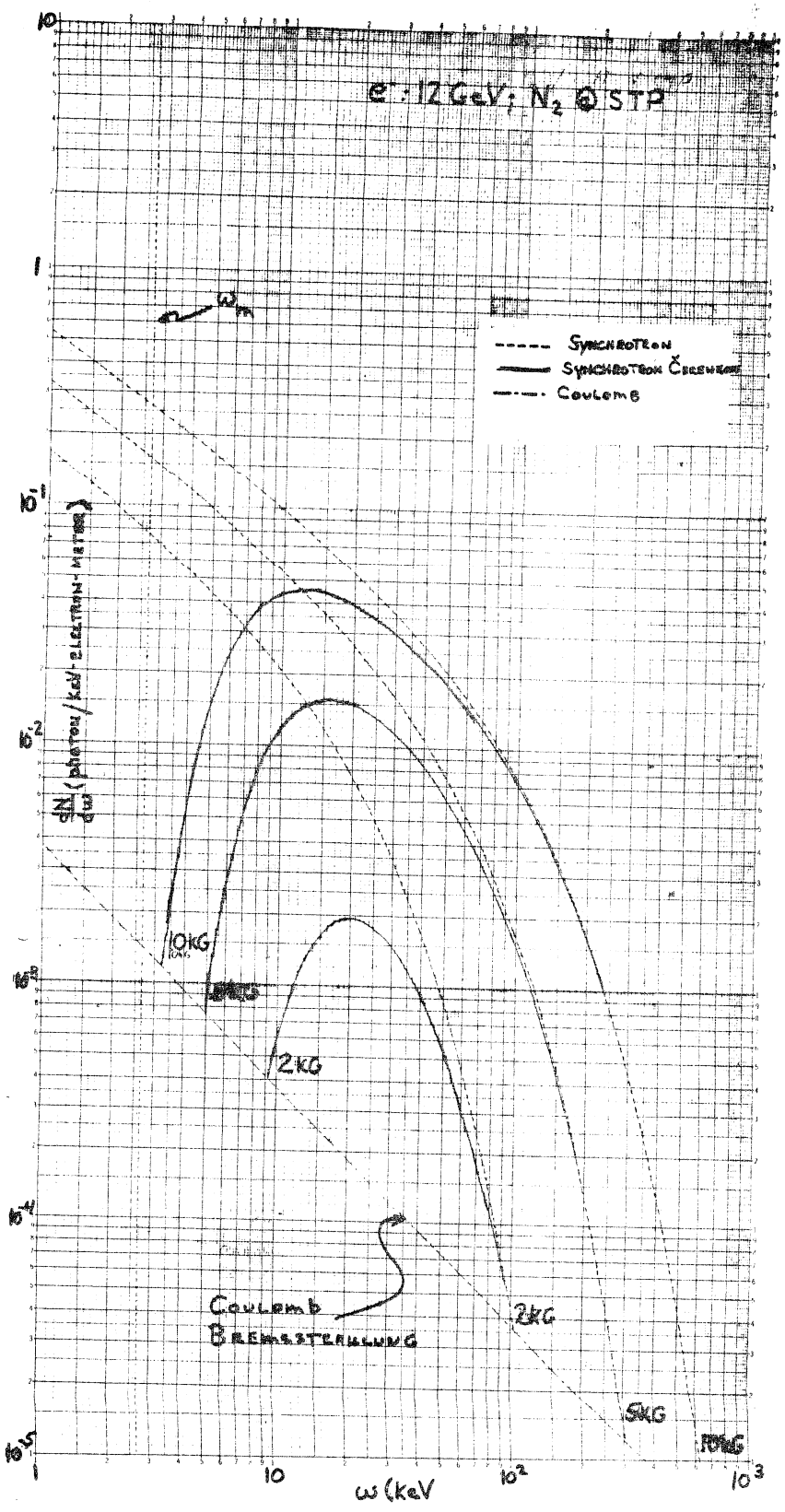
e⁻: 12 GeV; N₂ @ STP
ω_m
Synchrotron
Synchrotron Čerenkov
Coulomb
10 kG
5 kG
2 kG
1 kG
Coulomb
Bremsstrahlung
dN/dω (photons / keV / electron - meter)
ω (keV)
10
10²
10³

Figure 5

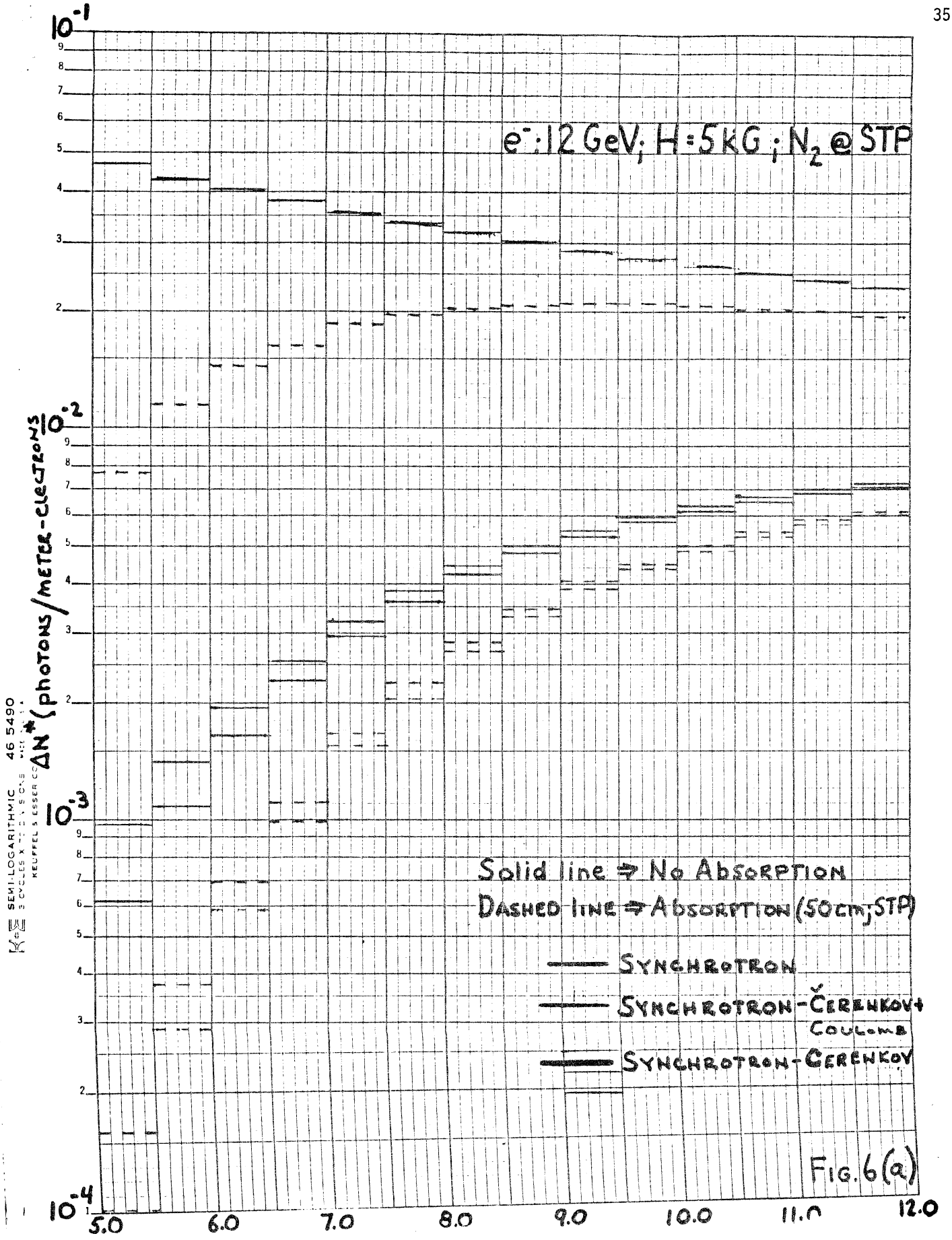
e⁻: 12 GeV; H = 5 kG; N₂ @ STP
ΔN* (photons/meter-electrons)
10⁻¹
10⁻²
10⁻³
10⁻⁴
5.0
6.0
7.0
8.0
9.0
10.0
11.0
12.0
Solid line ⇒ No Absorption
Dashed line ⇒ Absorption (50 cm; STP)
Synchrotron
Synchrotron-Čerenkov + Coulomb
Synchrotron-Cerenkov
SEMI-LOGARITHMIC 46 5490
KEUFFEL & ESSER CO.

Fig. 6(a)

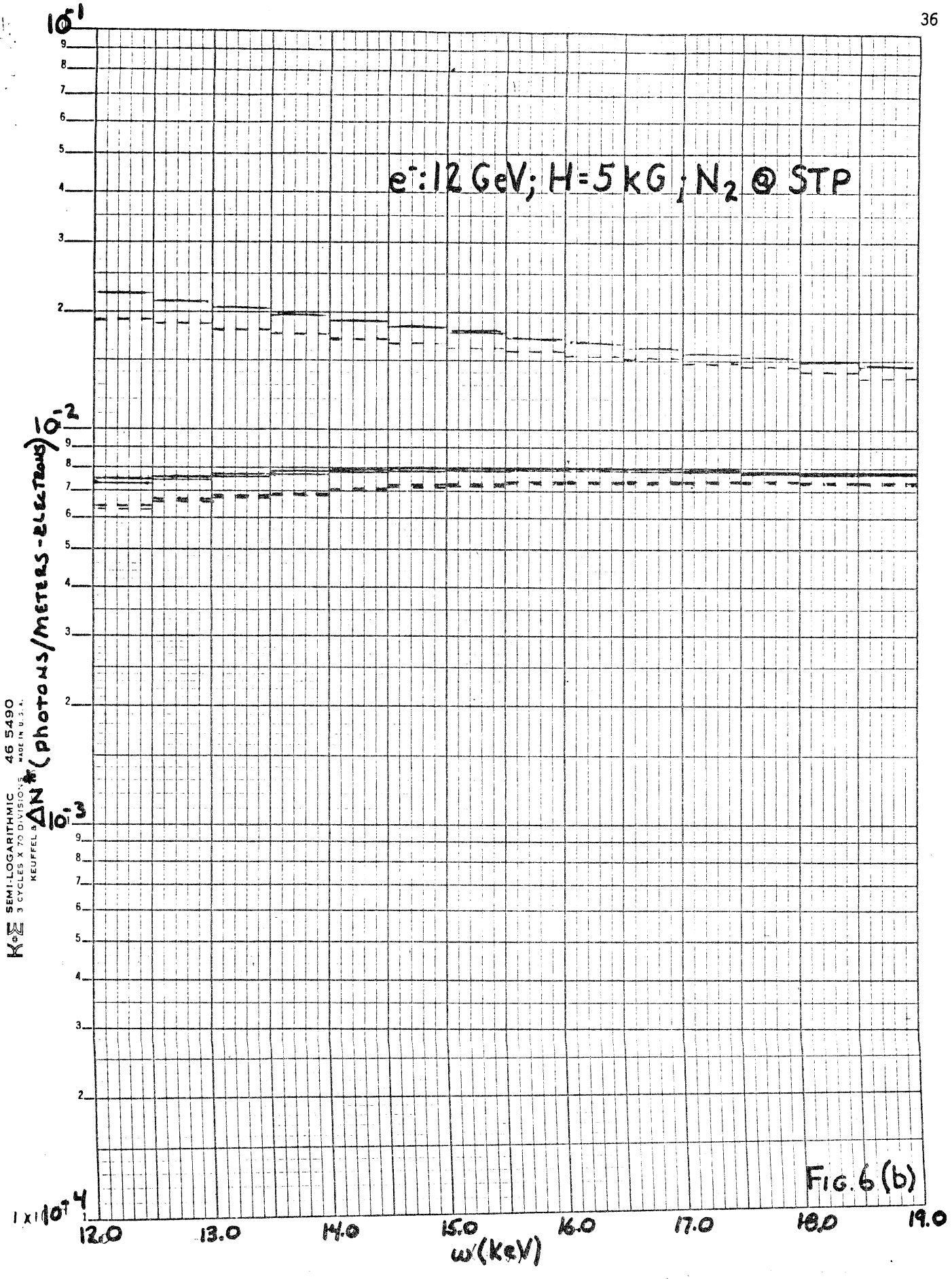
e⁻: 12 GeV; H = 5 kG; N₂ @ STP
ΔN* (photons/meters-electrons)
ω (keV)
12.0
13.0
14.0
15.0
16.0
17.0
18.0
19.0
SEMI-LOGARITHMIC
3 CYCLES X 70 DIVISIONS
KEUFFEL & ESSER
46 5490
MADE IN U.S.A.

Fig. 6 (b)

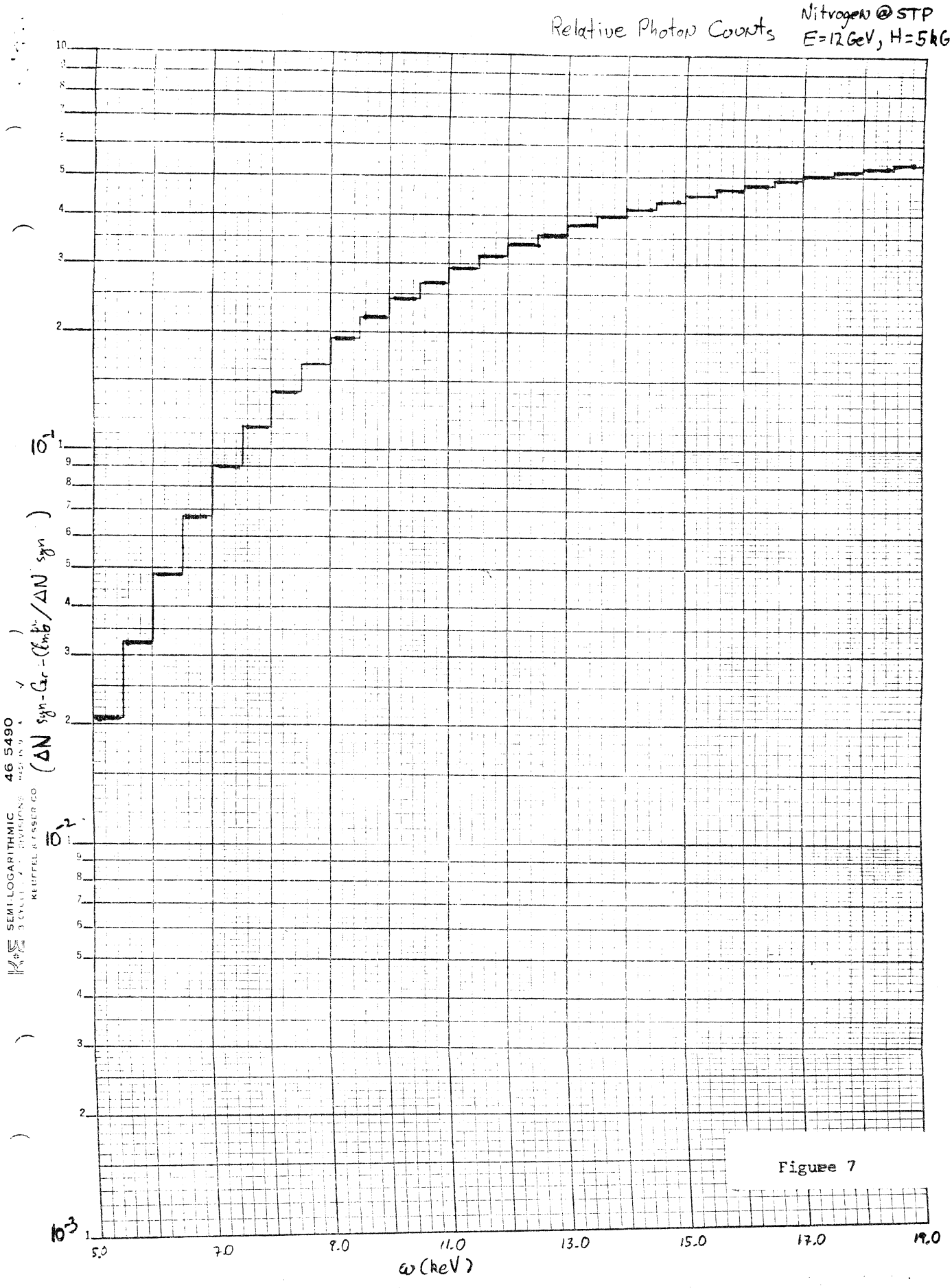
Relative Photon Counts
Nitrogen @ STP
E=12GeV, H=5kG
(ΔN syn-Cr-(ℓnb/ΔN syn)
ω (keV)
5.0
7.0
9.0
11.0
13.0
15.0
17.0
19.0
SEMILOGARITHMIC
46 5490

Figure 7

Coulomb + Synchrotron & Damped Synchrotron
A 4.0 - 4.5 keV E = 12.0 GeV
B 6.0 - 6.5 keV H = 5.0 kG
C 8.0 - 8.5 keV

MODEL DATE

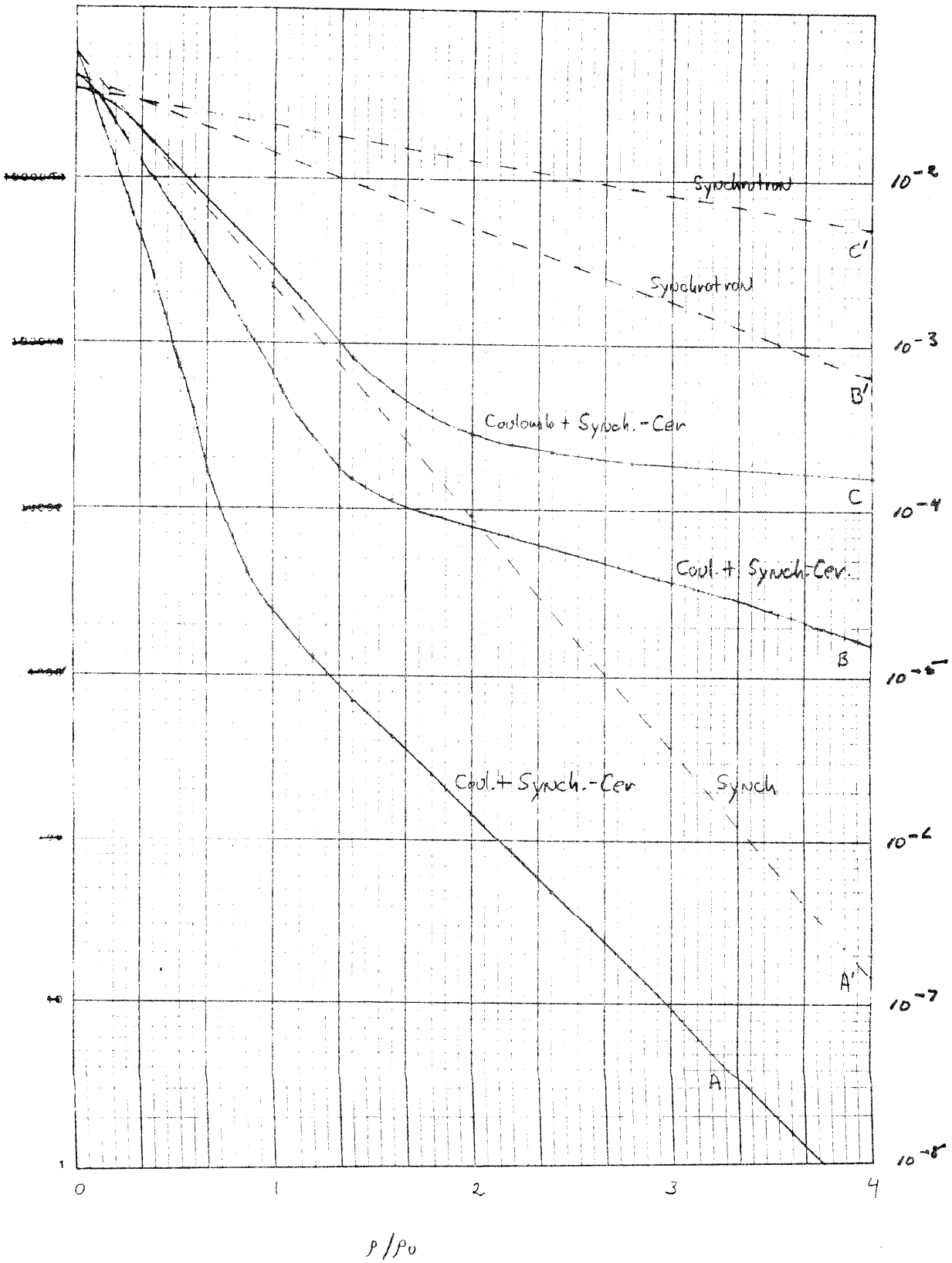

Figure 8

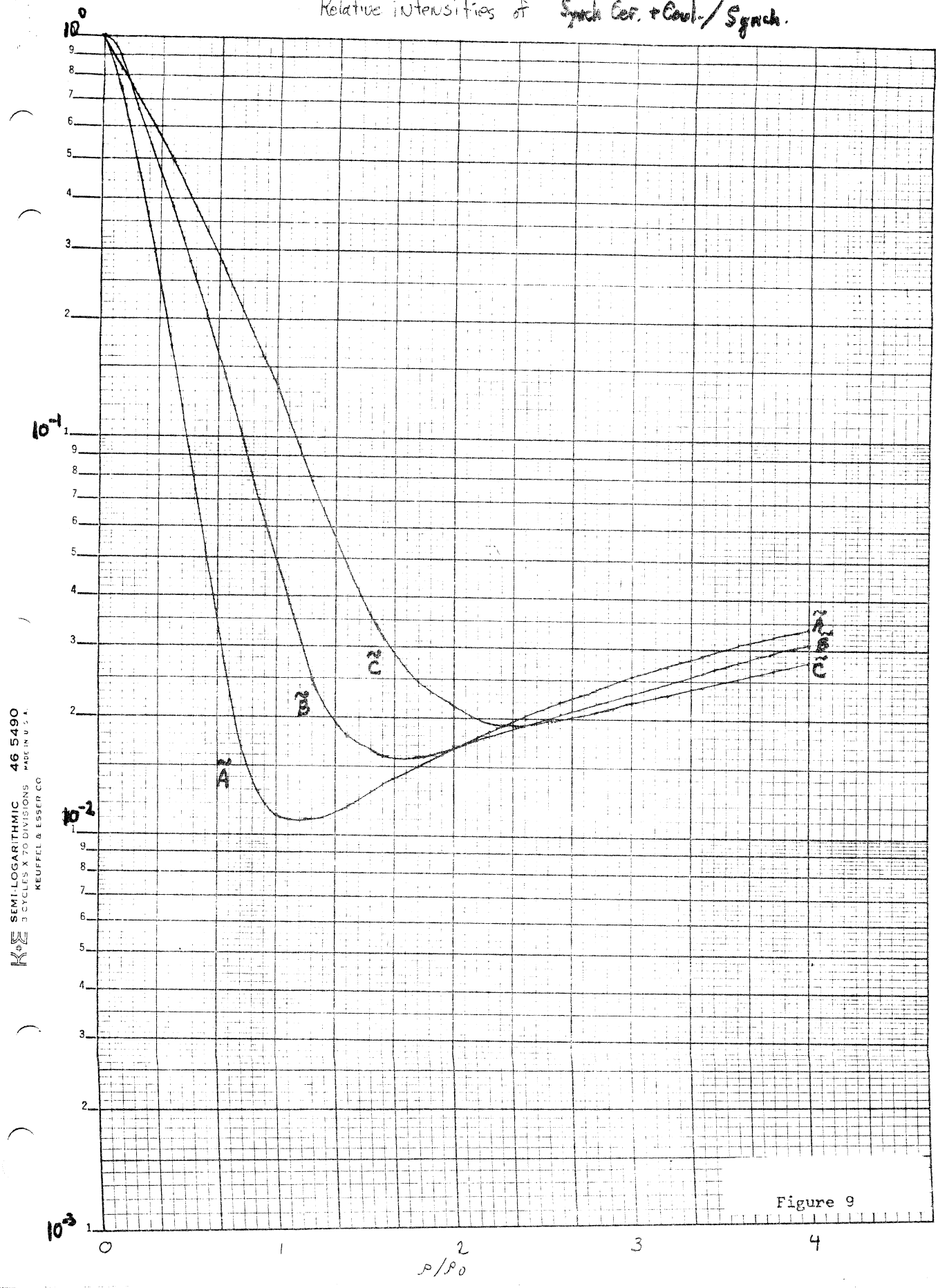
Relative intensities of Synch Cer. + Coul./Synch.
10^0
10^{-1}
10^{-2}
10^{-3}
A
B
C
0
1
2
3
4
p/p_0
SEMI-LOGARITHMIC 46 5490
3 CYCLES X 70 DIVISIONS MADE IN U.S.A.
KEUFFEL & ESSER CO

Figure 9

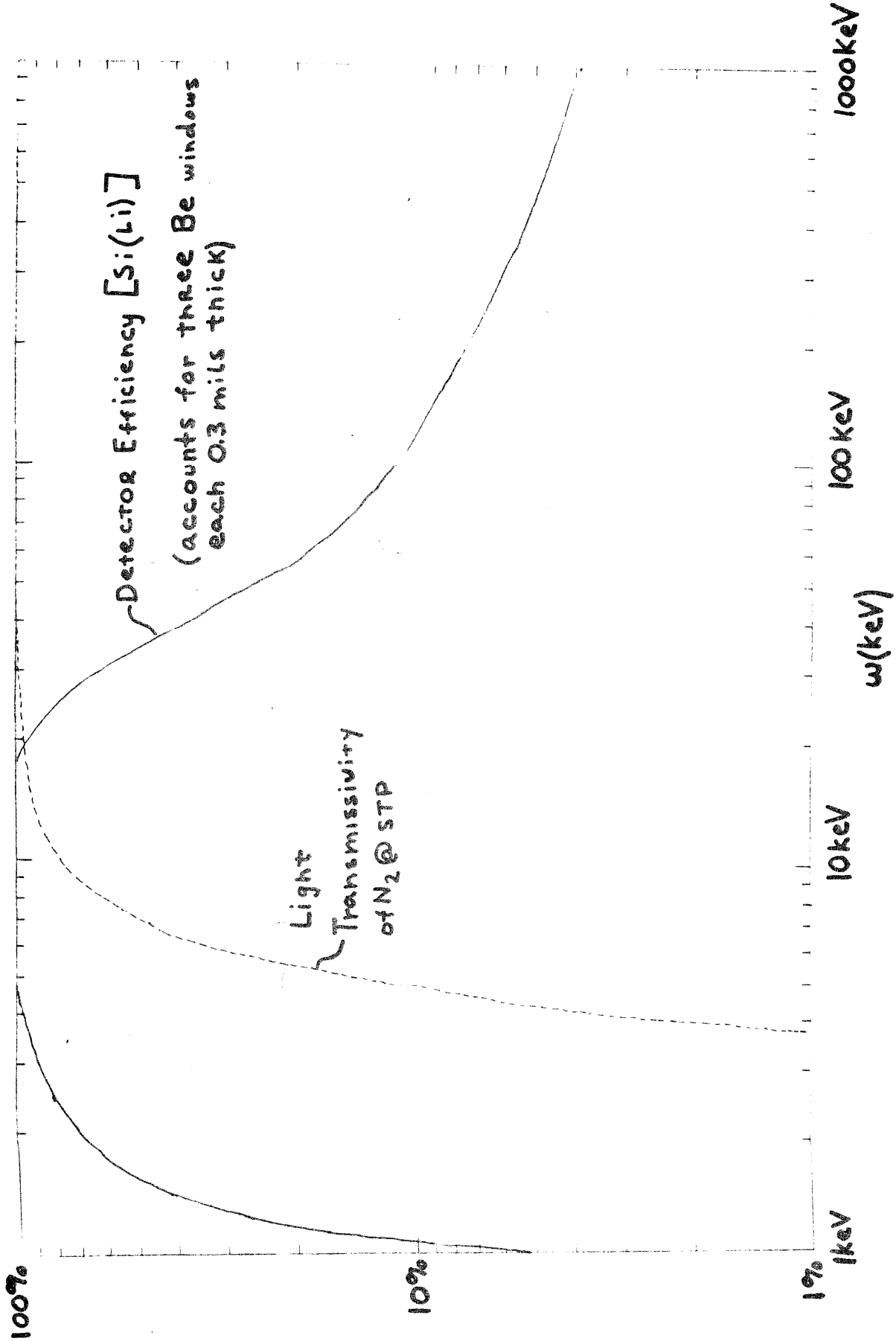
Detector Efficiency [Si(Li)]
(Accounts for three Be windows each 0.3 mils thick)
Light Transmissivity of N_2 @ STP
100%
10%
1%
1keV
10keV
100keV
1000keV
w(keV)

Figure 10

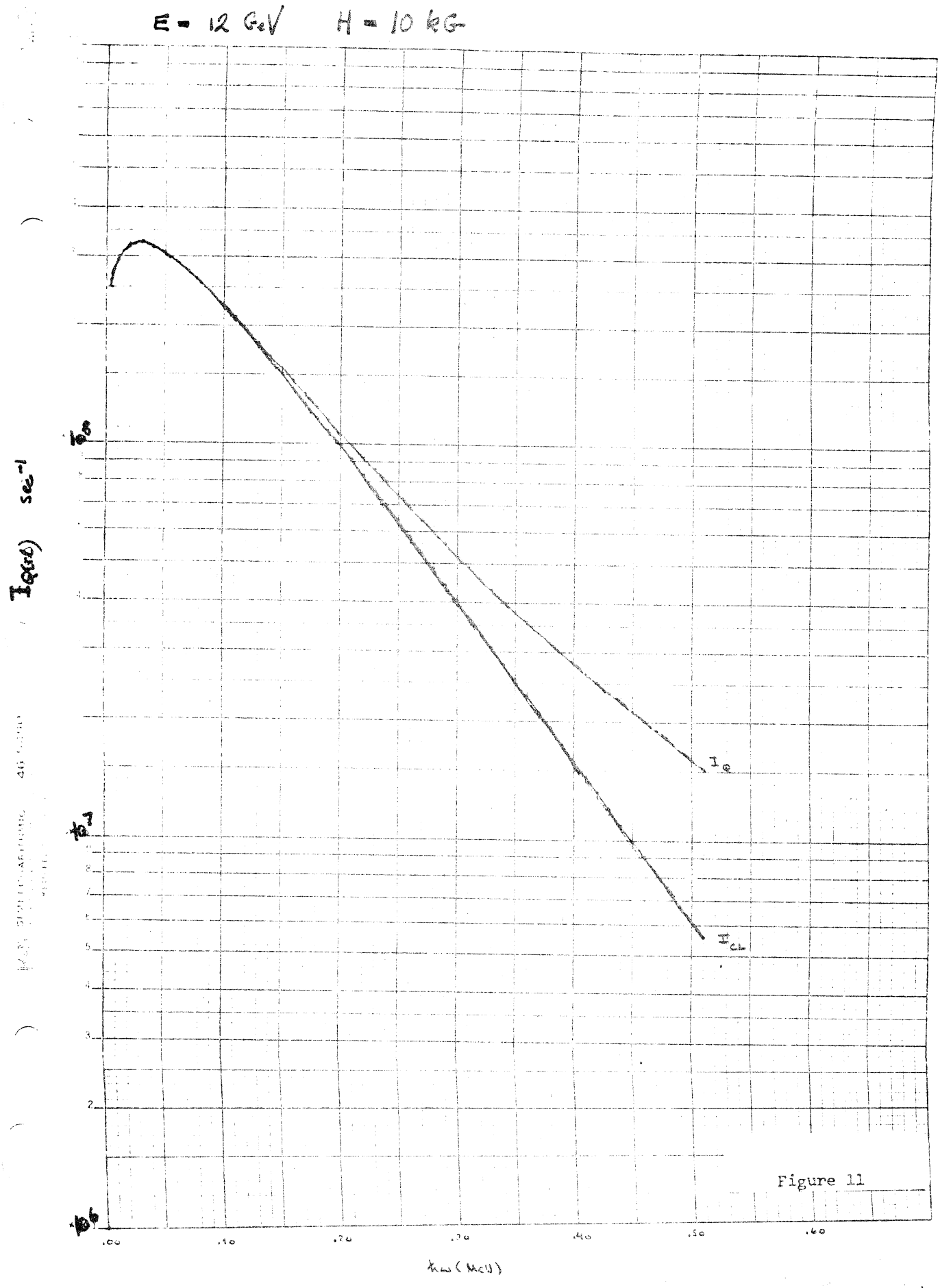
E = 12 GeV H = 10 kG
$I_{Q(E)}$ sec^{-1}
10^6
10^7
2
3
4
5
6
7
8
I_Φ
I_{CL}
.00
.10
.20
.30
.40
.50
.60
k_ω (MeV)

Figure 11

8. Summary of Arrangements with Host Laboratory

(a) Space - experimental area about 2m X 25m with access between accelerator runs (see blueprint for layout); total time for set-up, test, and running circa 4 months; counting room space ~ 5 standard instrument racks; office space for 4 people.

(b) Beam time - about 40 runs of 1 hour each at intensities 2×10^6 e^-/sec [Cornell (5.3), E ~ 12 GeV], or 10^5 e^-/sec [SLAC (5.4), E ~ 20 GeV].

(c) Laboratory services - We would appreciate some help with the beam alignment during set-up. The only equipment we would like to borrow are the magnets and their power supplies, e.g. 4 dipoles, each 1 meter long, with cooling capacity sufficient to operate at 5 kG. The Si(Li) counters will require about 70 liters of liquid N_2 every month. The dipoles will probably require access to water cooling lines. The electric power needed for the rest of the electronics is negligible --- naturally filtered and regulated AC would be preferred. Computer use will be modest; approximately the equivalent of 2 hours 1108 time.

(d) Financial - Support for the experiments will be drawn from grants (ERDA), subvention of sabbatical leaves (IIT), and U. S. Veterans Educational Benefits. Non-expendable equipment, supplies, travel, and shipping costs will be funded from grants. In addition we expect to transfer $5,000 to the host laboratory to cover the costs of minor purchases and reimbursements for technical services.

9. Research Personnel

T. Erber: Professor of Physics
Illinois Institute of Technology 1969-

Publications since 1973

1. Communications in Mathematical Physics 29, 311-17 (1973)
Mixing Transformation on Metric Spaces
(with B. Schweizer and A. Sklar)

2. Magnetism and Magnetic Materials-1972 AIP Conf. Proc. No. 10, part 2, 1710-14 (1973)
Breaking of Dilatational Symmetry of Dipole Interactions by Octupole Forces
(with M. Duda, R. Olenick, and H. G. Latal)

3. Astrophysical Journal 184, No. 1, Part 1, 301-304 (1973)
Radiative Corrections and Soft Photon Emission in Magnetic Bremsstrahlung
(with H. N. Spector)

4. American Journal of Physics 42, No. 4, 338-9 (1974)
A "λ-Transition" of Two Magnetic Dipoles
(with R. Olenick)

5. Modern Developments in Thermodynamics, edited by B. Gal-Or; J. Wiley & Sons/Israel Universities Press, New York-Jerusalem (1974); pp. 281-301
Macroscopic Irreversibility as a Manifestation of Micro-Instabilities
(with A. Sklar)

6. Nuclear Instruments and Methods, 118, 147-8 (1974)
Comments on "Separated High-Energy Electron Beams Using Synchrotron Radiation"
(with D.White)

7. Physical Review D, 10, No. 2, 492-499 (1974)
Photon Pair Creation in Intense Magnetic Fields
(with Wu-Yang Tsai)

8. Physical Review D12, No. 4, 1132-37 (1975)
Propagation of Photons in Homogeneous Magnetic Fields: Index of Refraction
(with Wu-Yang Tsai)

9. Annals of Physics 96, 303-332 (1976)
Classical and Quantum Theory of Synergic Synchrotron-Čerenkov Radiation
(with Julian Schwinger and Wu-Yang Tsai)

10. Acta Physica Austriaca 44, 315-336 (1976)
Inner Bremsstrahlung Processes: Part I
(with D. White and H. G. Latal)

11. Acta Physica Austriaca 45, 29-64 (1976)
Inner Bremsstrahlung Processes: Part II
(with D. White and H. G. Latal)

12. Acta Physica Austriaca 45, 245-254 (1976)
The Propagation of Photons in Homogeneous Magnetic Fields II: Dispersion Relations and Propagation Modes
(with Wu-Yang Tsai)

13. Physics Letters A (in press, 1976)
Magnetic Detection of Crack Initiation and Propagation
(with J. E. Nuti and S. A. Guralnick)

14. Annals of Physics (in press, 1976)
Experimental Aspects of Synchrotron-Čerenkov Radiation
(with D.White, W-Y. Tsai, and H. G. Latal)

Graduate Students

G. B. Baumgartner [BSc IIT '71; MS UI (Urbana) '73; Military Service '73-'76]

J. E. Nuti [BSc IIT '71; Military Service '73-'75]

T. Rynne [Florida Atl. U. BSc '71; MS '73]

Additional Personnel

Dr. R. W. Fetter Research Associate, Electrical Engineering, IIT

Professor H. G. Latal [U. of Graz] and Professor Wu-Yang Tsai [UCLA] will be associated with the theoretical analysis of the experiment.

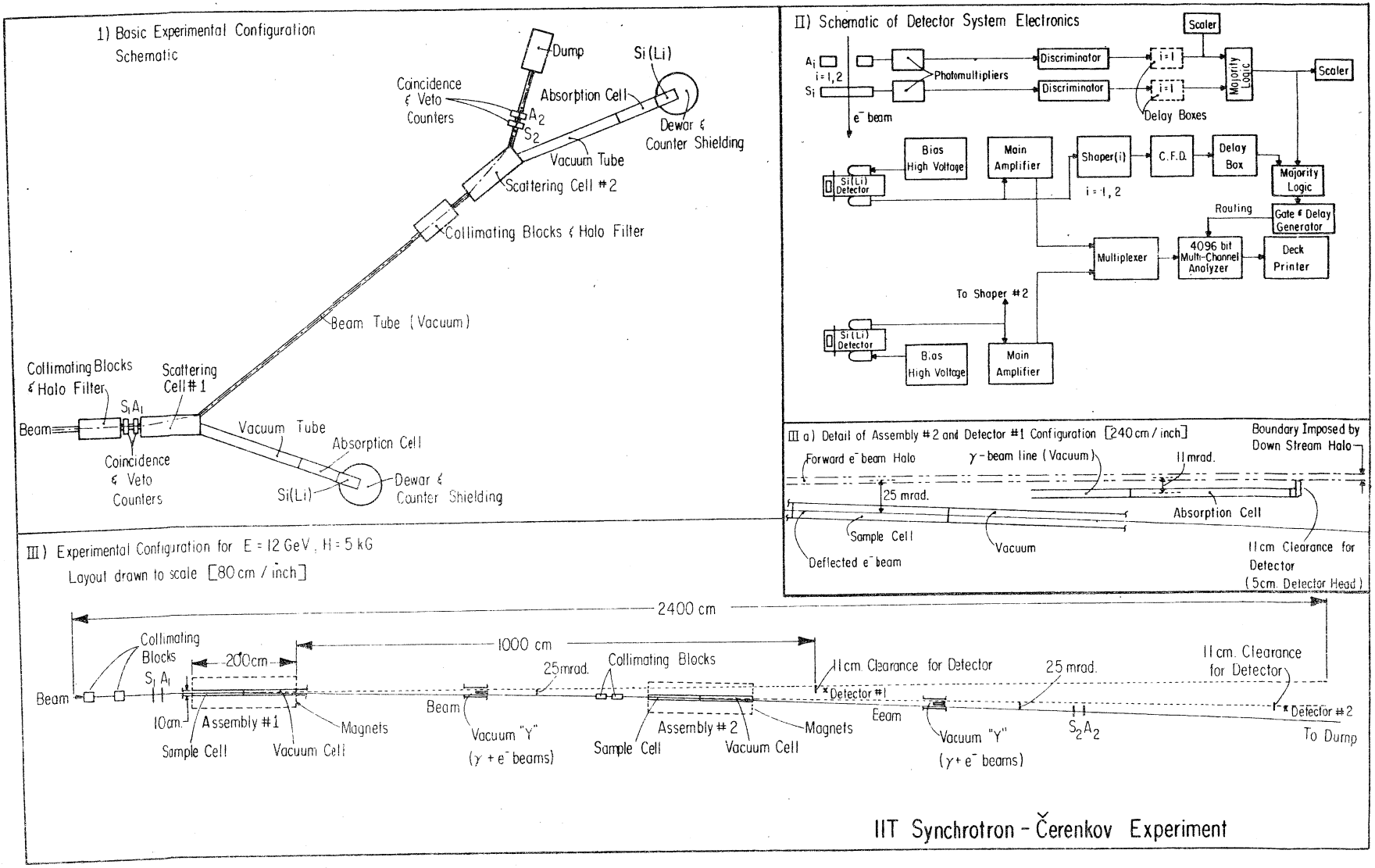
1) Basic Experimental Configuration
Schematic
Dump
Si(Li)
Coincidence & Veto Counters
Absorption Cell
A_2
S_2
Dewar & Counter Shielding
Vacuum Tube
Scattering Cell #2
Collimating Blocks & Halo Filter
Beam Tube (Vacuum)
Collimating Blocks & Halo Filter
Scattering Cell #1
$S_1 A_1$
Beam
Vacuum Tube
Absorption Cell
Coincidence & Veto Counters
Si(Li)
Dewar & Counter Shielding
II) Schematic of Detector System Electronics
Scaler
A_i i=1,2
S_i
Photomultipliers
Discriminator
Discriminator
i=1
i=1
Majority Logic
Scaler
e⁻ beam
Delay Boxes
Bias High Voltage
Main Amplifier
Shaper(i)
C.F.D.
Delay Box
Majority Logic
Si(Li) Detector
i=1,2
Routing
Gate & Delay Generator
Multiplexer
4096 bit Multi-Channel Analyzer
Deck Printer
To Shaper #2
Si(Li) Detector
Bias High Voltage
Main Amplifier
III a) Detail of Assembly #2 and Detector #1 Configuration [240 cm / inch]
Boundary Imposed by Down Stream Halo
Forward e⁻ beam Halo
γ-beam line (Vacuum)
11 mrad.
25 mrad.
Absorption Cell
Sample Cell
Vacuum
Deflected e⁻ beam
11cm Clearance for Detector (5cm. Detector Head)
III) Experimental Configuration for E = 12 GeV, H = 5 kG
Layout drawn to scale [80 cm / inch]
2400 cm
Collimating Blocks
S_1 A_1
200cm
1000 cm
25mrad.
Collimating Blocks
11cm Clearance for Detector
25 mrad.
11cm. Clearance for Detector
Beam
10cm.
Assembly #1
Magnets
Beam
Detector #1
Beam
Detector #2
Sample Cell
Vacuum Cell
Vacuum "γ" (γ + e⁻ beams)
Assembly #2
Sample Cell
Vacuum Cell
Magnets
Vacuum "γ" (γ + e⁻ beams)
S_2 A_2
To Dump
IIT Synchrotron - Čerenkov Experiment